Ocean waves in a multi-layer shallow water system with bathymetry

Ocean waves in a multi-layer shallow water system with bathymetry

By Afroja Parvin,

A Thesis Submitted to the School of Graduate Studies in the Partial Fulfillment of the Requirements for the Degree Masters of Science

McMaster University © Copyright by Afroja Parvin June 22, 2018

McMaster University

Masters of Science (2018)

Hamilton, Ontario (School of Computational Science and engineering)

TITLE: Ocean waves in a multi-layer shallow water system with bathymetry

AUTHOR: Afroja Parvin (McMaster University)

SUPERVISOR: Dr. Nicholas Kevlahan

NUMBER OF PAGES: xiv, 134

Abstract

Mathematical modeling of ocean waves is based on the formulation and solution of the appropriate equations of continuity, momentum and the choice of proper initial and boundary conditions. Under the influence of gravity, many free surface water waves can be modeled by the shallow water equations (SWE) with the assumption that the horizontal length scale of the wave is much greater than the depth scale and the wave height is much less than the fluid's mean depth. Furthermore, to describe three dimensional flows in the hydrostatic and Boussinesq limits, the multilayer SWE model is used, where the fluid is discretized horizontally into a set of vertical layers, each having its own height, density, horizontal velocity and geopotential. In this study, we used an explicit staggered finite volume method to solve single and multilayer SWE, with and without density stratification and bathymetry, to understand the dynamic of surface waves and internal waves.

We implemented a two-dimensional version of the incompressible DYNAMICO method and compare it with a one-dimensional SWE. For multilayer SWE, we considered both two layer and a linear stratification of density, with very small density gradient, consistent with Boussinesq approximation ($\frac{\Delta\rho}{\rho} \ll 1$). We used Lagrangian vertical coordinate which doesn't allow mass to flow across vertical layers. Numerical examples are presented to verify multilayer SWE model against single layer SWE, in terms of the phase speed and the steepness criteria of wave profile. In addition, the phase speed of the barotropic and baroclinic mode of two-layer SWE also verified our multilayer SWE model. We found that, **for multilayer SWE, waves move slower than single layer SWE and get steeper than**

normal when they flow across bathymetry. A series of numerical experiment were carried out to compare 1-D shallow water solutions to 2-D solutions with and without density as well as to explain the dynamics of surface wave and internal wave. We found that, a positive fluctuations on free surface causes water to rise above surface level, gravity pulls it back and the forces that acquired during the falling movement causes the water to penetrate beneath it's equilibrium level, influences the generation of internal waves. Internal waves travel considerably more slowly than surface waves. On the other hand, **a bumpy or a slicky formation of surface waves is associated with the propagation of internal waves**. The interaction between these two waves is therefore demonstrated and discussed.

Acknowledgements

First and foremost, I would like to thank my supervisor Dr. Nicholas Kevlahan, for his continuous support during the completion of this research. The door to Prof. Kevlahan office was always open whenever I ran into a trouble or had a question about my research or writing. And most importantly, during the writing of this thesis, he gave me the moral support and the freedom I needed to move on. I would like to thank my committee members Walter Craig, Tom Hurd and Zahra Keshavarz Motamed for their constructive feedback about this thesis. I would like to give special thanks to Paolo Cudrano, Lorena Aguirre, Dewan Ferdous Wahid and Alexander Chernyavsky for helping me in every way and for all the fun we have had together in last two years. And last but not the least, I must express my gratitude to my parents for providing me unfailing support and continuous encouragement throughout my years of study. This accomplishment would not have been possible without them.

Contents

List of Figures

Declaration of Authorship

I, Afroja Parvin, declare that this thesis titled, "Ocean waves in a multi-layer shallow water system with bathymetry" and the work presented in it are my own.

Chapter 1

Introduction

The Oceans have a significant influence on Earth's weather and climate. They cover roughly 70% of the Earth's surface and provide a large reservoir for heat and other constituents of the Earth's climate system. This great reservoir continuously exchanges heat, moisture, and carbon with the atmosphere and driving our weather patterns. Due to it's buffering abilities, the ocean represents the flywheel of the Earth's climate system [1]. Thus the scientific understanding of the ocean's time mean state, as well as it's variability and it's stability to various forms of perturbations, represents a key goal of physical oceanography. Our inability to perform controlled experiments on large- scale systems, leads to computer model as a critical tool for justifying climate phenomena. Mainly, computer models are becoming primary tool for predicting physical and biological characteristics of the ocean fluid. But the study of these geophysical phenomena involves complex geometries. Numerical simulations of such flows are still very demanding and challenging.

In the past decades, significant advances have been realized in terms of mathematical modeling to reduce the complexity of the original primitive equations , leading to the importance of shallow water systems [2]. Shallow water systems are the usual model to describe the flow in rivers and channels. Apart from these, they also describe the oceanic and atmospheric circulations at very large horizontal scales. In physical oceanography, the **shallow water equations (SWE)** are mainly used for simulating Tsunami wave propagation. The main assumptions of the SWE are that the horizontal length scale is much greater than the depth scale and the wave height is much less than the fluid's mean depth. Under this assumption, conservation of mass implies that the vertical velocity of the fluid is small. But ocean dynamics is not as simple as we think. The temperature and salinity variations of ocean leads to the variation of density, which profoundly affects the dynamics of oceanic flow. Considering these aspects has led to the **multi-layer shallow water** system.

The multi-layer shallow water model is used to describe three dimensional compressible or incompressible flows in the hydrostatic limit, where the fluid is discretized horizontally into a set of layers, each with its own height, density, velocity, temperature and geopotential. The hydrostatic approximation is valid provided horizontal fluid accelerations are much less than gravitational acceleration g. This approximation breaks down at small scales, or when convection is important. Moreover, by including Coriolis term, this model can also describes large scale atmospheric and oceanic flows. Beside this, Bathymetry is one of the most important parameters for an ocean model because it is one of the most important keys to understand the vertical mixing mechanisms in the ocean. Dense bottom water can

spill through the fracture zones and other deep-sea passages at very high velocity and experience strong mixing as they surge over rough bathymetry. On the other hand, mid-ocean tidal velocities are too weak to generate turbulence on its own. Thus, when they flow over rough bathymetry, they interact with bathymetry to produce internal waves. These waves propagate into the water column above and produce turbulence to $1000 - 2000$ m above the bottom [3]. These all mechanisms involve with bathymetry, points to the necessity of improving the knowledge of bathymetry, to better understand the deep and intermediate ocean circulation.

In the last few years, several numerical methods have been developed to solve the single layer shallow water system. Andreas et al. [4] used the finite volume scheme to solve the one dimensional shallow water equations based on a continuous, piecewise linear discretization of the bathymetry. Their main idea was to design special reconstruction of water level at wet/dry fronts, in the framework of the second-order semi-discrete central-upwind scheme to preserve the positivity of water height as well as to handle friction forces with wetting and drying. Nikolos et al. [5] formulated and validated a node-centered finite volume numerical scheme for unstructured triangular meshes in order to investigate the potential to compute flow regimes modeled by the non-linear shallow water equations. Burguete et al. [6] and Cea et al. [7] dealt with the robust treatment of friction forces term which was included in the momentum equation of the 1D shallow-water model with drying and wetting. The work in [6] shows that pointwise discretization of the friction term unbalances this term with the rest of the terms in the equation in steady state while an upwind discretization of the friction term ensures the correct discrete balance. On the other hand, in [7], their work involves the finite

volume discretisation of the bed friction term in the two-dimensional shallow water equations. They analysed that the discretisation improves the accuracy of the model where the bed friction is a relevant force in the momentum equation, and it guarantees a perfect balance between gravity and bed friction under uniform flow conditions.

Yulong and Xiangxiong [8], explored the extension of high order discontinuous Galerkin methods for the shallow water equations on unstructured triangular meshes. They confirmed that the resulting scheme guarantees the positivity of the water depth. Their numerical example also verified the positivity-preserving property, higher order accuracy and well balanced property for smooth and discontinuous solutions.

Emmanuel et al. [9] found that for single layer shallow water system, a well balanced scheme with local hydrostatic reconstruction is more stable than a finite volume scheme. Moreover, this simple and fast well balanced scheme preserves the nonnegativity of the water height and satisfies a semidiscrete entropy inequality.

Kevlahan and Dubos [10] developed a conservative adaptive wavelet method for solving the shallow water equations on a staggered hexagonal C-grid. This method was implemented for regular planar geometry in Matlab and demonstrated the potential of this method for simulating multiscale geophysical flows. They ensured that there is no numerical generation of vorticity when solving the SWE and also mass is conserved. In the following year, they extended the adaptive wavelet approach to the sphere and reimplements the algorithm in Fortran 95 and message passing interface [11]. Their goal was to achieve high computational

efficiency and good parallel scaling.

Apart from the single layer shallow water equations, several techniques have been developed to solve the two layer shallow water equations, where the bottom layer is comparatively denser than the top layer. The Q-scheme [12], relaxation approach [13] and central-upwind scheme [14] are the most popular schemes to solve two layers approximations. Kyle proposed high-resolution f-wave-propagation finite volume methods to solve two layer shallow water equations with variable bathymetry [15].

Finally, several numerical scheme have been proposed for solving one dimensional multilayer shallow water equations with mass transfer, without density stratification [16] and within density stratifications [17]. In [16], the authors proposed a multi-layer model to simulate free surface density-stratified flows over variable bathymetry. They showed that multilayer system admits a kinetic interpretation, and they used this to formulate a robust finite volume scheme for its numerical approximation. Couderc et al. [2] presented an explicit Froude scheme for solving multilayer shallow water model with density stratifications. They highlighted the stability and efficiency of the scheme and ensured robustness and well-balanced properties for motionless steady states. Francois and Vladimir proposed a robust well-balanced scheme for multi-layer shallow water equations [18]. They introduced a variant of splitting scheme which ensured the conservation of total momentum and dealt with the restriction of complex eigenvalues. In [19], Parisot and Vila introduced a multi-dimensional numerical scheme approximating the solutions of the multilayer shallow water model in the low Froude number regime. They showed that their numerical solutions satisfied the dissipation of energy and other physical

properties required for oceanic flows. Andrew and Paul derived Multilayer shallow water equations with complete Coriolis force on a non-traditional beta-plane [20].

Dubos et al. [21] presented the design of the icosahedral dynamical core DYNAMICO where DYNAMICO solves the multi-layer rotating shallow-water equations. In their model, the horizontal mesh is a quasi-uniform icosahedral C-grid and the vertical discretization is obtained from the three-dimensional Hamiltonian formulation. They used Explicit Runge–Kutta time integration for dynamics and forward-in-time integration with horizontal/vertical splitting is used for tracers.

The choice of vertical coordinate is one of the most important aspects of ocean model's design. There are several vertical coordinate systems in use, such as z-coordinates, σ-coordinates, layered and isopycnal coordinate systems. In z-coordinate system, the vertical coordinate is depth. This coordinate system is useful in the areas that are well mixed because they can provide very fine resolution which is needed to represent three-dimensional turbulent processes. But in the region of sloping bathymetry, the levels of this coordinate system intersect with bathymetry and generate unrealistic velocities near the bottom. On the other hand, sigma coordinate is the vertical coordinate system that follows the bathymetry and free surface and keeps the same number of vertical grid points everywhere in the domain. A large number of hydrostatic and non-hydrostatic models use pressure based terrain-following sigma coordinates as the vertical coordinate ([22],[23], [24], [25]). This coordinate system is appropriate for the continental shelf and coastal regions. But the model, that use sigma coordinate systems, has difficulty for handling sharp topographic changes from one grid point to other. Because pressure gradient error can give rise to unrealistic flows. In Isopycnal

coordinate system, models use potential density referenced to a given pressure as the vertical coordinate. This system divides the water column into distinct homogeneous layers and the thickness of these layers can vary from place to place and time to time. This coordinate system is good for lateral transfer process and they also can have complex bathymetry.

Another well developed vertical coordinate system is Lagrangian vertical coordinate system. It was first formulated in [26], and was reviewed and discussed in [24]. A floating mass coordinate that does not allow mass to flow across vertical layers, is called Lagrangian vertical coordinate. One of the major advantage to apply this coordinate system is that it reformulates 3D motion into pure horizontal 2D flow within the floating Lagrangian layers and the resulting system closely resembles that of shallow water system [27]. The Lagrangian coordinate system requires periodic remapping in order to avoid severe deformation of the vertical mesh that might occur when vertical layers pinch together or move too far apart.

Waves in the free surface of the ocean are mainly generated by wind. These wind driven waves or surface waves are mainly created due to the friction between air and surface water. They can also form as a result of geological effects. Tsunami are one of the most common examples of surface waves. These waves can form when a rapid shift in water is caused by underwater earthquakes or landslides. On the other hand, internal waves form in the interior of the ocean. Similar in many aspects to surface waves which travel along the sharp density interface between air and water, internal waves propagate along the density gradients within the ocean. Perturbations to these density gradients are restored by gravity, generating a propagating wave. Kelvin waves are one of the most common examples of internal

waves.

Internal waves are triggered when the interface between the layers of different densities is perturbed. The trigger can be the momentum generated by a ship or could be due to tidal motions [28]. In 1893, a Norwegian oceanographer, Fridtjof Nansen reported a mysterious phenomenon, called **dead water**. He wrote that, a boat may experience strong resistance to forward motion in apparently calm conditions [29]. The water directly below his ship was less salty because fresh water had been added at the ocean surface because of melting sea ice. The interface between two layers of different density supported internal waves which stole energy from ship and resisted the forward motion of the ship.

The main goal of this thesis is to implement a two-dimensional version of the incompressible DYNAMICO method with bathymetry and density stratification and compare it with a one-dimensional SWE. We verify our multilayer model by comparing the phase speed and wave behavior with that of single layer SWE and by verifying correct behaviour of internal waves. In addition, one of the most important goal of this study is to understand the dynamics and the interaction between surface waves and internal waves . Regarding this, a series of numerical experiments have been evaluated to predict the reason behind this interaction, in the presence of bathymetry.

The outline of this thesis is as follows: In Chapter 2 the preliminaries of this study are described. We introduce Single layer and multilayer shallow water equations and their derivation from the Euler equation, as well as the principles of conservation of mass and momentum. We discuss the approximations we made

for our system such as hydrostatic and geostrophic balance. We mathematically derive the Boussinesq approximations which we considered only when density is multiplied by gravity. We also look at the different forms of wave solution and the computations of dispersion relations between wave number and frequency have been included too.

In Chapter 3, the numerical scheme to solve our system are introduced. We use second order finite difference- finite volume scheme on a staggered grid, to solve both single layer and multi layer shallow water equations. For single layer SWE, water height η is discretized at the center of each cell and velocity u is discretized at the edge of each cell. In multilayer case we introduce Lorenz staggering for vertical discretization. For the horizontal discretization, we calculate the velocity (u) at the edge of each cell and inertial mass (μ) and mass weighted density distribution (Θ) has been calculated at the center of each cell. The Lagrange multiplier (i.e. pressure) is discretized at the center of each cell for all full vertical levels where as geopotential is discretized at the interfaces of each vertical layer. For the time integration, we use third-order four stage Runge-Kutta scheme. We also discuss the stability of our solver, challenges we face to solve our system and the necessity of meeting CFL condition to get stable solutions.

The technique for the validation of multilayer SWE model, and a series of numerical experiments which helps to explain the phenomena of surface waves and internal waves, is described in chapter 4. The former includes two sections: one include the comparison of single and multilayer SWE model for the phase speed and wave profile of surface waves and the other one is for the internal waves. In other words, the characteristics of barotropic and baroclinics mode of

the two-layer SWE has been presented. In the later sections, the following three numerical experiments were conducted. Firstly, we consider a positive fluctuations to the free surface of ocean in a two layer stratified fluid with a very small density differences, consistent with Boussinesq approximation, to observe the generation of both surface waves and internal waves. The initial set up of second experiments is the same as the previous case, apart from the fact that now we consider a linear stratified density. In our last experiment, we consider a small perturbation of density at the interface between two layers of different densities, to observe the generation of internal waves as well as, how that influences the propagation of waves at the free surface of ocean. All of these experiments have been done with and without the consideration of bathymetry.

The final chapter summarizes the main results of this thesis and outlines possible future work, that were not included in this study.

Chapter 2

Basic Theory

2.1 Introduction

The **shallow water equations (SWE)** describe the motion of a thin layer of constant density fluid which are kept in hydrostatic balance. It is bounded from below by a rigid surface and from above by a free surface and the horizontal length scale is much larger than the vertical one. Above this free surface, we consider the inertia of any other fluid is negligible. This same configuration can be considered for the generalization of multilayer fluid where one fluid lie on the top of others, forming a stacked shallow water system. Basically, the Shallow water equations is derived from the conservation of mass and momentum in the case where the scale of horizontal motion is much greater than that of vertical motion and the wave height is much less than the fluid's mean depth. Under these assumptions, conservation of mass implies that the vertical velocity of the fluid is small. From

the momentum equation, it also can be shown that vertical pressure gradients are nearly hydrostatic, i.e vertical accleration is much less than gravity. Beside this, vertical integration allows to remove vertical velocity from the equations. Thus the Shallow water equations are derived.

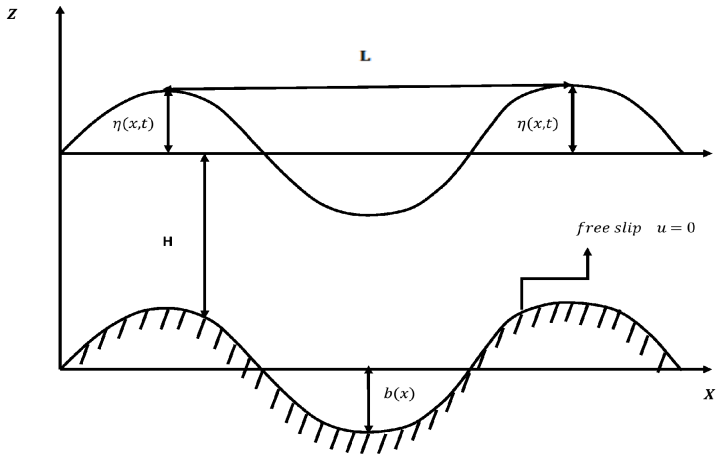

FIGURE 2.1: A Single layer Shallow water system, $h(x,t) = H + \eta(x,t) - b(x)$ is the thickness of fluid layer. Vertical fluid particle velocity is given by material derivative of the free surface position $\eta(x,t)$. Also $\frac{L}{H} \gg 1$ and $\frac{\eta}{H} \ll 1$.

.

The major application of the shallow water equations are in marine flow prediction, particularly the interest is connected to tsunamis, where a tsunami is defined as a seismically induced wave that propagates in the region of the continental shallows and shelf. Moreover, tsunamis also propagates in the open ocean.

Figure 2.1 represents the single layer of fluid where $\eta(x,t)$ is the displacement of free surface, $h(x,t) = H + \eta(x,t) - b(x)$ is the total thickness and H is the mean height from the flat bottom.

To derive the SWE, we start with the Euler equations. These equations describe how the velocity, pressure and density of moving fluid are related. The Euler equations neglect the viscosity of the fluid which is included in the Navier-Stokes equations. The mass and momentum equations are:

$$\frac{\partial \rho}{\partial t} + \nabla \cdot (\rho \mathbf{u}) = 0, \tag{2.1}$$

$$\frac{D\mathbf{u}}{Dt} + \mathbf{f} \times \mathbf{u} + \frac{1}{\rho}\nabla p = 0. \tag{2.2}$$

where $\mathbf{u}(x, y, z, t)$ is the velocity of the fluid particles, ρ is the density of the fluid, p is the pressure and $\mathbf{f} = 2\Omega \sin \Phi$ is called Coriolis parameter. Here Ω is the angular velocity of Earth's rotation and Φ is the latitude. But for this thesis, we will focus on only horizontal and vertical slice which means the velocity of the fluid particles would be function of $x, z,$ and t.

So to derive shallow water equation for single layer of fluid from Euler's mass and momentum equations, we are using the following assumptions:

1. The horizontal length scale is much greater than the vertical length scale $\left(\frac{L}{H} \gg 1\right)$,
2. The wave height is much less than the fluid's mean depth $\left(\frac{\eta}{H} \ll 1\right)$,
3. Vertical pressure gradient are in hydrostatic balance $\left(\frac{\partial p}{\partial z} = -\rho g\right)$. This means that vertical acceleration is much less than gravity $\left(\frac{du_z}{dt} \ll g\right)$

In this chapter, first we will discuss the assumptions based on hydrostatic and geostrophic balance. Then we will derive the SWE. We will also introduce Boussinesq approximation, which gives us a more general set of equations utilizing the fact that density variation in the oceans is very small and so density variations enter only via buoyancy . Then we will introduce the SWE for multilayers of fluid. Finally, we will end with a discussion on the different wave solutions of the Shallow water equation. For completeness, we will discuss gravity wave, Kelvin waves and Rossby waves for two dimensional SWE and Internal gravity waves for one dimensional shallow water equation.

2.2 Hydrostatic and Geostrophic Balance

2.2.1 Hydrostatic Balance

The ocean is in hydrostatic equilibrium when the pressure gradient force drawing parcel upwards from higher pressure near the surface to lower pressure aloft, is balanced by the force of gravity pulling the parcel back down to the surface. In the derivation of SWE, we assumed that the system was in hydrostatic balance because the definition of shallow water states that horizontal scale of flow is much greater than the vertical scale of flow.

Consider the momentum equation in Z-direction.

$$\frac{Dw}{Dt} = -\frac{1}{\rho}\frac{\partial p}{\partial z} - g. \tag{2.3}$$

Using dimensionless quantity, the non-dimensional form of (2.3) is;

$$\frac{U^2 H}{L^2} = \frac{p}{\rho H} \quad g. \tag{2.4}$$

where the order of magnitude of horizontal velocity $U = 10\text{ms}^{-1}$, horizontal length $L = 10^6\text{m}$, the order of magnitude of the vertical scale $H = 10^4\text{m}$, pressure $p = 10^5\text{hPa}$, density $\rho = 1\text{Kgm}^{-3}$ and gravity $g = 10\text{ms}^{-2}$. Using these we get from (2.4);

$$\frac{U^2 H}{L^2} = \frac{p}{\rho H} \quad g$$

$$10^{-6} \ll 10 \quad 10$$

Comparing these components we can see that the order of magnitude on the left hand side are much smaller than compared to those on the right hand side. So by neglecting the left hand side of equation (2.3) finally we get the equation for hydrostatic balance

$$\frac{\partial p}{\partial z} = -\rho g. \tag{2.5}$$

Also if we consider the aspect ratio of horizontal-vertical scale, we should start with continuity equation. So $\nabla \cdot u$ gives $\frac{U}{L} \sim \frac{W}{H}$. Thus the order of magnitude of horizontal advective terms of the vertical momentum equation becomes $\frac{Dw}{Dt} \sim \frac{UW}{L} = \frac{U^2 H}{L^2}$. So the ratio,

$$\frac{\left|\frac{Dw}{Dt}\right|}{\left|\frac{\partial p}{\rho dz}\right|} \sim \frac{\frac{U^2 H}{L^2}}{\frac{\Phi}{H}} \sim \frac{\frac{U^2 H}{L^2}}{\frac{U^2}{H}} = \frac{H^2}{L}.$$

where Φ is the change in $\phi = \frac{\partial p}{\rho}$ and for $\lambda - h$ scale, by considering the horizontal non-rotating Boussinesq momentum equation, we have $\frac{D\mathbf{u}}{Dt} = -\nabla\phi$, which implies that $\phi \sim U^2$. For hydrostatic balance the magnitude of the pressure gradient is greater than the material derivative of the fluid flow for large scale motions, so we can say that $\frac{H^2}{L} \ll 1$. so we have justified that $H \ll L$.

2.2.2 Geostrophic Balance

Sea water naturally tends to move from region of high pressure to a region of low pressure. The force pushing the water towards the low pressure region is called pressure gradient force. In a geostrophic flow, instead of water moving from high pressure region to low pressure, it moves along the lines of equal pressure (isobars). This occurs because of the rotation of earth, resulting a force felt by the water moving from high to low, known as Coriolis force. The Coriolis force is at right angles to the flow and when it balances the pressure gradient force, the resulting flow is known as *geostrophic*.

In other words, a flow is in geostrophic balance if the relation $\Phi \sim fUL$ holds. Where U is the magnitude of horizontal velocity, L is the horizontal scale over which it varies, f is the Coriolis parameter and Φ is the pressure deviation. so we have

$$\frac{\left|\frac{Dw}{Dt}\right|}{\left|\frac{\partial p}{\rho dz}\right|} \sim \frac{\frac{UW}{L}}{\frac{fUL}{H}} \sim \frac{U}{fL}\frac{WH}{UL} = R_0\frac{H}{L}.$$

where $R_0 = \frac{U}{FL}$ is called the **Rossby number**. If $R_0 \ll 1$ we say that the Coriolis force is balanced by the horizontal pressure gradient and the flow is in geostrophic balance.

The geostrophic equations are the simplified form of the Navier Stokes equations in a rotating frame. In particular, it is assumed that there is no acceleration, no

viscosity and the pressure is hydrostatic. The resulting balance is;

$$\begin{aligned} fv =& \frac{1}{\rho}\frac{\partial p}{\partial x}, \\ fu =& -\frac{1}{\rho}\frac{\partial p}{\partial y}, \\ 0 =& -\frac{\partial p}{\partial z} - \rho g. \end{aligned}$$

For the Shallow water system the horizontal momentum equations are reduced in the form;

$$-fv = -g\frac{\partial \eta}{\partial x}, \tag{2.6}$$

$$fu = -g\frac{\partial \eta}{\partial y}. \tag{2.7}$$

2.3 Single layer SWE

The single-layer SWE model is one of the simplest and useful model in Geophysical fluid dynamics because it allows to consider the Coriolis effect due to the rotation of earth in a simple framework rather than using complicated effects of stratifications. By the definition of Shallow water dynamics, horizontal scale of flow is much greater than the depth of the water and the height of wave is much smaller than the mean depth of fluid. Thus the fluid motion is fully determined by the mass continuity and momentum equations. In the following section we derive the SWE for a vertical slice (x,z) using mass and momentum conservation and the appropriate approximations introduced earlier.

2.3.1 Mass Conservation equation

Consider two dimensional (x-z) motions on a non-rotating shallow body of water with uniform density. To derive SWE, the first step is to consider mass conservation. We integrate the continuity equation $\nabla \cdot \mathbf{u} = 0$, vertically as follows,

$$
\begin{aligned}
&\int_{-(H-b)}^{\eta} (\nabla \cdot \mathbf{u})\, dz = 0, \\
&\Rightarrow \int_{-(H-b)}^{\eta} \left[\frac{\partial u}{\partial x} + \frac{\partial w}{\partial z}\right] dz = 0, \\
&\Rightarrow \frac{\partial}{\partial x}\int_{-(H-b)}^{\eta} u dz - u|_{z=\eta}\frac{\partial \eta}{\partial x} + u|_{z=-(H-b)} \\
&\frac{\partial\left[-(H-b)\right]}{\partial x} + w|_{z=\eta} - w|_{z=-(H-b)} = 0, \\
&\Rightarrow \frac{\partial}{\partial x}\int_{-(H-b)}^{\eta} u dz - u|_{z=\eta}\frac{\partial \eta}{\partial x} + w|_{z=\eta} = 0, \\
&\Rightarrow \frac{\partial \eta}{\partial t} + \frac{\partial}{\partial x}\int_{-(H-b)}^{\eta} u dz = 0, \\
&\Rightarrow \frac{\partial \eta}{\partial t} + \frac{\partial}{\partial x}\left[(\eta + H - b)\,\mathbf{u}\right] = 0.
\end{aligned}
$$

For a flat bottom $b = 0$, so the continuity equation is;

$$\frac{\partial \eta}{\partial t} + \frac{\partial}{\partial x}\left[(H + \eta)\,\mathbf{u}\right] = 0.$$

In vector form :

$$\frac{\partial \eta}{\partial t} + \nabla \cdot (\eta \mathbf{u}) = 0. \tag{2.8}$$

2.3.2 Momentum equation

Now in the similar way, consider the momentum balance of water in volume. We shall need to know the distribution of pressure P within water. For doing this we use the principle of hydrostatic balance, which states that the pressure increases with depth according to overhead mass per unit area. So the hydrostatic pressure is,

$$\frac{\partial p}{\partial z} = -\rho g,$$

and then by integrating with respect to z we get,

$$p = p_0 - \rho g z. \tag{2.9}$$

At the top of the fluid the pressure is determined by the weight of the overlying fluid and this is assumed negligible, thus $p = 0$ on free surface $z = h = \eta(x,t)$ gives $p_0 = \rho g \eta$. Substituting the value of p_0 to equation (2.9) gives

$$\begin{aligned} p =& \rho g \eta - \rho g z; \\ =& \rho g(\eta - z); \\ =& \rho g(h(x,t) - z). \end{aligned}$$

The consequence of this is that the horizontal gradient of pressure is independent of height. That is $\nabla p = \rho g \nabla \eta$ Substituting the value in our momentum equation (2.2) by neglecting Coriolis effect, gives

$$\frac{D\mathbf{u}}{Dt} = -\frac{1}{\rho}\nabla\,(p) = -g\nabla\eta \tag{2.10}$$

Thus combining the momentum and conservation of mass, we get the **SWE**

$$\frac{\partial \eta}{\partial t} + \nabla \cdot (\eta \mathbf{u}) = 0, \tag{2.11a}$$

$$\frac{D\mathbf{u}}{Dt} + g\nabla\eta = 0. \tag{2.11b}$$

When $\frac{\eta}{H} \ll 1$ and $u \ll 1$ then we get the ***linear*** form of **SWE** for the perturbations $\eta(x,t)$ and $u(x,t)$:

$$\frac{\partial \eta}{\partial t} + \frac{\partial u}{\partial x} = 0, \tag{2.12}$$

$$\frac{\partial u}{\partial t} + g\frac{\partial \eta}{\partial x} = 0. \tag{2.13}$$

2.4 One Dimensional Boussinesq Approximation

The SWE model is an efficient numerical tool for the simulation of large scale long waves and for shallow water flows. But when it is applied to relatively short waves or weekly nonlinear dispersive waves such as solitary waves, the errors could be unbearable. The reason behind this is as follows; in SWE model, the wave dispersion is completely neglected if we exclude Coriolis force in the momentum equation, as noted in section 2.7.1. Moreover, to model a dispersive wave, nonhydrostatic pressure approximation is required. Because dispersion is a characteristic of nonlinear or nonhydrostatic waves, occurs when the wave speed is a non-constant function of the wave amplitude or wave frequency [30].

First depth-averaged model including weakly dispersive and non-linear effects was derived by Boussinesq, where the non-hydrostatic pressure was approximated and included in the momentum equation [31]. Later, Peregrine used the depth-averaged velocity and presumed that vertical velocity varied linearly over depth [32].

Thus the Boussinesq equations model water waves in shallow water, including the first order effects of nonlinearity and dispersion, while shallow water equations neglect frequency dispersion effects on wave propagation. The Boussinesq equations are derived from the incompressible, irrotational Euler equations.

The following are the one-dimensional Boussinesq equations for depth averaged velocity: [4]

$$\frac{\partial u}{\partial t} + u\frac{\partial u}{\partial x} + g\frac{\partial \eta}{\partial x} - \frac{H^3}{3}\frac{\partial^3 u}{\partial x^2 \partial t} = 0, \tag{2.14}$$

$$\frac{\partial \eta}{\partial t} + \frac{\partial}{\partial x}\left(H + \eta\right) u = 0. \tag{2.15}$$

Under the same conditions, the difference between shallow water equation and Boussinesq momentum equation is the term $\frac{H^3}{3}\frac{\partial^3 u}{\partial x^2 \partial t}$, which is neglected in shallow water equation, but on the other hand this term is retained in Boussinesq momentum equation. To understand the reason behind this, let us look at the scaled non-dimensionalised form of the momentum equation.

Non - dimensionalisation:

To non-dimensionalise the system variables, the following parameters ρ, g and H were chosen, where H is the average depth. This choice are useful but not unique. Thus we have,

$$\tilde{x} = \frac{x}{H}, \tilde{z} = \frac{z}{H}, \tilde{h} = \frac{h}{H}, \tilde{\eta} = \frac{\eta}{H},$$
$$\tilde{t} = \sqrt{\frac{x}{H}}t, \tilde{U} = \frac{U}{\sqrt{gH}}, \tilde{p} = \frac{p}{\rho g H}$$

Scaling:

To examine each part of the equations, it is necessary to scale the individual variables so that every aspect of the problem has variation of O(1). The nonlinearity

and dispersion of the system are parameterized by the ratios ϵ and σ respectively.

$$\epsilon = \frac{a}{H}, \tag{2.16}$$

$$\sigma = \frac{H}{\lambda} \tag{2.17}$$

where H is typical water depth, a is the typical wave amplitude and λ is the typical wave length. The Ursell number is defined as the ratio between these two parameters that predicts which wave theory will be applicable. Thus we have $U_r = \frac{\epsilon}{\sigma^2} = \frac{a\lambda^2}{H^3}$. The coordinates are scaled as;

$$\hat{x} = \sigma\tilde{x}, \hat{t} = \sigma\tilde{t}, \hat{\eta} = \frac{\tilde{\eta}}{\epsilon}. \tag{2.18}$$

Substituting these scales in free surface boundary conditions and in continuity equation gives the scales of velocity.

$$\hat{U} = \frac{\tilde{U}}{\epsilon}, \hat{W} = \frac{\tilde{W}}{\epsilon\sigma}. \tag{2.19}$$

So finally, we have the scaled non - dimensional form of momentum equation is;

$$\frac{\partial\hat{U}}{\partial\hat{t}} + \epsilon\hat{U}\frac{\partial\hat{U}}{\partial\hat{x}} + \frac{\partial\hat{\eta}}{\partial\hat{x}} + \sigma^2\left(\frac{\tilde{h}^2}{6}\frac{\partial^2}{\partial\hat{x}^2}\left(\frac{\partial\hat{U}}{\partial\hat{t}}\right) - \frac{\tilde{h}}{2}\frac{\partial^2}{\partial\hat{x}^2}\left(\tilde{h}\frac{\partial\hat{U}}{\partial\hat{t}}\right)\right) = O(\epsilon\sigma^2, \sigma^4). \tag{2.20}$$

The Boussinesq wave theory is valid in the distinguished limit $\epsilon \ll 1$, $\sigma \ll 1$ and $U_r = O(1)$. That's why in momentum equation, terms up to $O(\epsilon, \sigma^2)$ are retained.

For SWE, we need to discard the term with $O(\sigma^2)$, and in order to it, we need the scale ϵ to be larger than σ^2. Thus for SWE we need, $U_r \gg 1$, while for Boussinesq approximation $U_r = 1$. Therefore, if we have $\sigma^2 \ll \epsilon$, the SWE is a better choice,

otherwise if their magnitude is of $O(1)$ then Boussinesq approximation is the best option to apply.

2.4.1 Physical dispersion

It is very common to compare the dispersion characteristics of the Boussinesq equations with those of linear water wave theory [33], [34].
The phase velocity for a wave with frequency ω and wave number k is defined as $c = \frac{\omega}{k}$. For linear wave theory, the phase speed is defined by [35],

$$c^2 = \frac{\omega^2}{k^2} = gH\frac{\tanh(kH)}{kH}. \tag{2.21}$$

In the limit, $\sigma \ll 1$, the ratio in (2.21) approach to 1 and so $c^2 \sim gH$. The resulting waves are nearly non-dispersive.
Therefore, this approximation can impose severe restrictions on the range of water depth, for the problem of propagating water wave in a general domain. But the main goal of the derivation of Boussinesq model is to obtain an approximation of the ratio in (2.21), in order to extend it outside of the limit $\sigma \ll 1$ [36].

Furthermore, the linearized form of weakly nonlinear Boussinesq equations (2.14), gives the following dispersion relation,

$$c^2 = \frac{\omega^2}{k^2} = \frac{gH}{1 + \frac{(kH)^2}{3}}. \tag{2.22}$$

Without dispersion, equation (2.22) shows that, this dispersion relation reduces to that of the shallow water equations with phase speed $c^2 \sim gH$.

2.4.2 Applications of the Boussinesq equations

Interesting wave phenomena have been found when both nonlinearity and dispersion occur together. Under this situations, nonlinear steepening balances dispersive spreading, and the propagation of waves is known as *solitary waves*. Boussinesq equations are one of those equation that satisfies this balanced motion [37].

The nonlinear shallow water equations and Boussinesq equations are most often used for analyzing the solitary wave phenomenon. [38] have compared these two approaches for Predicting Solitary Wave runup on plane beaches. They found that, when solitary waves are close to the slope, the two approaches produce almost identical results for non-breaking waves. But for breaking waves, the Boussinesq equations give a better result of the wave evolution before to the breaking point. On the other hand, nonlinear SWE cannot generally provide a realistic prediction of the actual location of wave breaking. Since no frequency dispersion is included in these equations, they are restricted to shallow water region and they are mainly suitable for describing the propagation and run-up of bores in the inner surf zone after wave breaking has been fully developed.

In addition, [39] examines the run-up of the flood wave on the downstream dam wall, and its dependence on the bed slope. They found that the Boussinesq model gives better agreement with the measurements, since it is capable of capturing the short undulations at the front of the flood bore.

2.5 Shallow water equation in Dissipative form

2.5.1 Rotating Flow

In our derivation of the momentum equation in the section 2.3.2, we neglected the effects of Earth's rotation, i.e. the Coriolis force was ignored. However, when we consider rotating flow, we need to include the Coriolis force in our momentum equation. The effect of the Coriolis force is an apparent deflection of the path of an object that moves within a rotating coordinate system, as mentioned in section 2.2.2. The object does not actually deviate from its path, but it appears to do so because of the motion of the coordinate system. On the Earth an object that moves along a north-south path, will undergo apparent deflection to the right in the Northern Hemisphere and to the left in the Southern Hemisphere. Thus the Coriolis deflection is related to the motion of the object, the motion of the Earth, and the latitude. If $\mathbf{u}$ is the velocity of the fluid, $\vec{\omega}$ is the angular velocity of Earth rotation and ϕ is the latitude then the Coriolis Force is $-2\vec{\omega}\sin\phi\times\vec{u}$, where $\mathbf{f} = -2\vec{\omega}\sin\phi$ is called Coriolis Parameter. By taking into account the Coriolis force, the momentum equation (2.10) can be written as

$$\frac{D\mathbf{u}}{Dt} + \mathbf{f}\times\mathbf{u} = -\frac{1}{\rho}\nabla p. \tag{2.23}$$

So the Shallow water equation (2.11a) and (2.11b) can be written as

$$\frac{\partial\eta}{\partial t} + \nabla\cdot(\eta\mathbf{u}) = 0, \tag{2.24}$$

$$\frac{D\mathbf{u}}{Dt} + \mathbf{f}\times\mathbf{u} + g\nabla\eta = 0. \tag{2.25}$$

In conservation form,

$$\frac{\partial \eta}{\partial t} + u\frac{\partial \eta}{\partial x} = 0, \tag{2.26}$$

$$\frac{\partial u}{\partial t} + \frac{\partial}{\partial x}\left(\frac{1}{2}u^2 + g\eta\right) + 2\Omega \times \mathbf{u} = 0. \tag{2.27}$$

2.5.2 Boussinesq approximation for multilayer

The Boussinesq approximation is one of the popular way to solve non-isothermal flow, such as natural convection flows without having to solve for the full compressible formulation of the Navier-Stokes equations. This is not the same Boussinesq approximation used for the surface waves. We know the governing equation for inviscid, non-rotating fluid are;

$$\rho\frac{D\mathbf{u}}{dt} + 2\Omega \times \mathbf{u} = -\nabla p - \rho g\hat{z}, \tag{2.28}$$

$$\frac{\partial \rho}{\partial t} + \nabla \cdot (\rho \mathbf{u}) = 0, \tag{2.29}$$

$$\frac{d\rho}{dt} = 0. \tag{2.30}$$

This approximation is accurate when density variations are small as this reduces the nonlinearity of the problem. So in the inertial terms and in the continuity equation we substitute $\rho \to \rho_0$ is constant. It assumes that variations in density have no effect on the flow field, except when they give rise to buoyancy forces in the vertical equation of motions. Buoyancy is defined as $b = g\left(\rho_0 - \rho\right)/\rho_0$. Also we define reference pressure $p_0 = -g\rho_o z + constant$ in hydrostatic balance with the reference density, and then introduce reference pressure $p_0 = -g\rho_0 z + const.$

Also introduce $\tilde{p} = p - p_0(z)$. Then we have;

$$\begin{aligned} -\frac{\partial p}{\partial x} &= -\frac{\partial \tilde{p}}{\partial x}, \\ -\frac{\partial p}{\partial y} &= -\frac{\partial \tilde{p}}{\partial y}, \\ -\frac{\partial p}{\partial z} - \rho g &= -\frac{\partial \tilde{p}}{\partial z} + g\rho_0 - g\rho. \end{aligned} \tag{2.31}$$

Thus (2.31) can be written as;

$$-\nabla p - g\rho\hat{z} = -\nabla\tilde{p} + \rho_0 b\hat{z} \tag{2.32}$$

Considering $\Phi = \frac{\tilde{p}}{\rho_0}$ (analogous to geopotential on pressure coordinates), the resulting set of Boussinesq equations for a non-rotating system are;

$$\begin{aligned} \frac{D\mathbf{u}}{dt} + 2\Omega \times \mathbf{u} &= -\nabla\Phi + b\hat{z}, \\ \nabla \cdot \mathbf{u} &= 0, \\ \frac{db}{dt} &= 0. \end{aligned} \tag{2.33}$$

where $\frac{D}{Dt} = \frac{\partial}{\partial t} + \mathbf{u} \cdot \nabla$ is the material derivative for the velocity and Ω is the rotation vector.

2.6 Multi layer Shallow water equation

In this section we will consider the dynamics of multilayer of fluid which are stacked on top of each other, where each layer may have different thicknesses, velocities and densities. This is a very powerful model to solve various aspects of hydrodynamical flows such as rivers, estuaries, bays and other near-shore regions where water flows interact with the bed geometry and wind shear stresses. The pressure is continuous along the interface but density jumps discontinuously which makes the horizontal velocity to have corresponding discontinuity too. The pressure in each layer is assumed to be in hydrostatic balance so we can find pressure in any interface by integrating from down to bottom. Thus in the first layer we have,

$$p_1 = \rho_1 g(\eta_0 - z)$$

In the second layer we have,

$$\begin{aligned} p_2 &= \rho_1 g(\eta_0 - \eta_1) + \rho_2 g(\eta_1 - z); \\ &= \rho_1 g\eta_0 - \rho_1 g\eta_1 + \rho_2 g\eta_1 - \rho_2 gz; \\ &= \rho_1 g\eta_0 + g\eta_1(\rho_2 - \rho_1)\rho_2 gz; \\ &= \rho_1 g\eta_0 + \rho_1 g_1'\eta_1 - \rho_2 gz. \end{aligned}$$

where $g_1' = g\frac{(\rho_2-\rho_1)}{\rho_1}$ and so on. Thus for nth layer the dynamical pressure is given by ;

$$p_n = \rho_1 \sum_{i=0}^{n-1} g_i'\eta_i$$

where $g_i' = g\frac{(\rho_{i+1}-\rho_i)}{\rho_1}$. Thus the momentum equation for each layer is given by;

$$\frac{D\mathbf{u}_n}{Dt} = -\frac{1}{\rho_n}\nabla p_n. \tag{2.34}$$

and the mass conservation for each layer is given by;

$$\frac{\partial \eta_n}{\partial t} + \nabla \cdot (h_n \mathbf{u}_n) = 0. \tag{2.35}$$

We will develop and analyze the results of a numerical discretized multilayer Boussinesq model in Chapter 4.

2.7 Wave Solutions of SWE

Depending on different parameters, such as the effects of rotation or vorticity, there are different wave solutions for the SWE. These waves are classified as Gravity waves, Rossby waves and Kelvin waves. The two-dimensional SWE with Coriolis force are;

$$\begin{aligned} \frac{\partial u}{\partial t} + u\frac{\partial u}{\partial x} + v\frac{\partial u}{\partial y} - fv &= -g\frac{\partial \eta}{\partial x}, \\ \frac{\partial v}{\partial t} + u\frac{\partial v}{\partial x} + v\frac{\partial v}{\partial y} + fu &= -g\frac{\partial \eta}{\partial y}, \\ \frac{\partial \eta}{\partial t} + \frac{\partial u\eta}{\partial x} + \frac{\partial v\eta}{\partial y} &= 0. \end{aligned} \tag{2.36}$$

For the analysis of shallow water wave solutions [40], we linearize the equations around a state of rest, i.e. a state with zero velocity and zero surface elevation. The idea of linearization is that all variables are assumed to have infinitesimal small amplitude and we retain only terms that are linear in these small perturbation

variables. Thus the advection term in the momentum equations may be neglected. By doing this, we arrive at the following set of equations;

$$\begin{aligned} \frac{\partial u}{\partial t} - fv &= -g\frac{\partial \eta}{\partial x}, \\ \frac{\partial v}{\partial t} + fu &= -g\frac{\partial \eta}{\partial y}. \end{aligned} \tag{2.37}$$

$$\frac{\partial \eta}{\partial t} + H\left(\frac{\partial u}{\partial x} + \frac{\partial v}{\partial y}\right) = 0. \tag{2.38}$$

where we have considered $\eta(x, y, t) = h(x, y, t) = H + O(\epsilon)$ in the continuity equation since we have assumed flat bottom of ocean.

2.7.1 Gravity Waves

The wave we get by neglecting Coriolis force in the SWE is called shallow water gravity waves. It can exit only if the fluid has a free surface or an internal density discontinuity. In shallow water gravity waves the restoring force is in the vertical direction so that it is transverse to the direction of propagation. Now to find the dispersion relation for shallow-water gravity waves in the absence of a mean flow, with constant H, and ignoring Coriolis, we start with (2.37) and (2.38). Assuming a sinusoidal disturbance such as;

$$\begin{aligned} u &= Ae^{i(kx+ly-\omega t)}, \\ v &= Be^{i(kx+ly-\omega t)}, \\ \eta &= Ce^{i(kx+ly-\omega t)}. \end{aligned} \tag{2.39}$$

and substituting back to (2.37) and (2.38) we get the following matrix equation;

$$\begin{bmatrix} \omega & 0 & -gk \\ 0 & \omega & -gl \\ kH & lH & -\omega \end{bmatrix} \begin{bmatrix} A \\ B \\ C \end{bmatrix} = \begin{bmatrix} 0 \\ 0 \\ 0 \end{bmatrix}$$

Since A and C can not be zero, so we have

$$\begin{vmatrix} \omega & 0 & -gk \\ 0 & \omega & -gl \\ kH & lH & -\omega \end{vmatrix} = 0$$

Solving this for ω gives $\omega = \sqrt{(k^2 + l^2)gH}$, where k is the zonal wavenumber, ω is the wave frequency. The total wave number in the direction of propagation is $K = \sqrt{(k^2 + l^2)}$. Thus we get the following dispersion relation

$$\boxed{\omega = K\sqrt{gH}}. \tag{2.40}$$

The waves that obey this dispersion relation are known as shallow water gravity waves since the restoring force for the wave motion is gravity. The phase speed for shallow water gravity waves is

$$\boxed{c = \frac{\omega}{K} = \sqrt{gH}}. \tag{2.41}$$

which shows that the phase speed is independent of wavenumber and depends only on the depth of the fluid layer, H. Therefore, all wavenumbers travel at the same phase speed and thus the waves are non-dispersive. But we will get dispersive wave

only if we consider the Coriolis force in SWE. We will consider it in the following section on Rossby waves.

2.7.2 Rossby Waves

Rossby waves are also known as planetary waves and they occur in rotating fluids. These waves form as the result of the rotation of the planet. There are different shapes and size of oceanic waves. Among them slow-moving Rossby waves are different from surface waves. Unlike waves breaking along the shore, Rossby waves are huge and massive. It's undulating movement of the ocean can stress horizontally across the planet for hundreds of kilometers in a westward direction. These waves are so massive that they can change earth's climate conditions. They are responsible for coastal flooding in some regions of the world.

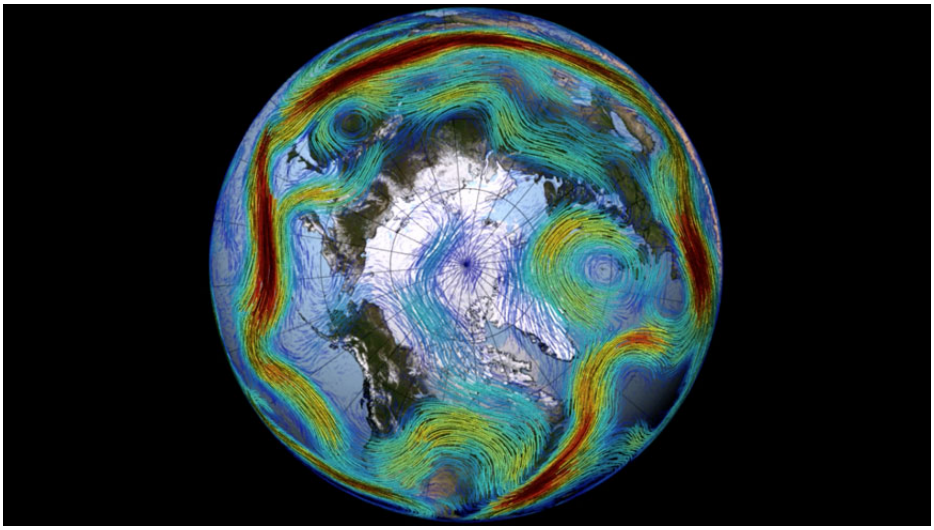

FIGURE 2.2: This picture from NASA's Goddard Space Flight Center shows both long and short atmospheric waves as indicated by the jet stream. And this jet stream is an example of atmospheric Rossby waves. The colors represent the speed of the wind ranging from slowest (light blue colors) to fastest (dark red). [41].

The movement of Rossby wave is complex. The driving mechanism of Rossby waves is the interaction of the flow with meridional variations of the Coriolis parameter f. Where f depends on the latitude with $f = 2\Omega \sin\phi$; Ω is the Earth's angular velocity, ϕ is the latitude on the Earth. If the y coordinate is directed northward and measured from a reference latitude ϕ_0, then $\phi = \phi_0 + \frac{y}{a}$, where a is the radius of the Earth. Using Taylor expansion around $y = 0$, we have $f \approx f_0 + \beta_0 y$, where $f_0 = 2\Omega \sin\phi_0$ is the reference Coriolis parameter and $\beta_0 = 2\Omega/a \cos\phi_0$ is the beta parameter.

Now substituting the expansion of $f \approx f_0 + \beta_0 y$ in (2.37) and (2.38), we get;

$$\frac{\partial u}{\partial t} - (f_0 + \beta_0 y)v = -g\frac{\partial \eta}{\partial x}. \tag{2.42}$$

$$\frac{\partial v}{\partial t} + (f_0 + \beta_0 y)u = -g\frac{\partial \eta}{\partial y}. \tag{2.43}$$

$$\frac{\partial \eta}{\partial t} + H\left(\frac{\partial u}{\partial x} + \frac{\partial v}{\partial y}\right) = 0. \tag{2.44}$$

In order to solve these equations, we use the first order geostrophic balance in equations (2.42) and (2.43) which reads for;

$$\begin{aligned} u &\simeq -\frac{g}{f_0}\frac{\partial \eta}{\partial y}, \\ v &\simeq +\frac{g}{f_0}\frac{\partial \eta}{\partial x}. \end{aligned} \tag{2.45}$$

Using (2.7.2) for the momentum equations yields,

$$-\frac{g}{f_0}\frac{\partial^2\eta}{\partial y\partial t} - f_0 v - \frac{\beta_0 g}{f_0} y\frac{\partial \eta}{\partial x} = -g\frac{\partial \eta}{\partial x},$$
$$+\frac{g}{f_0}\frac{\partial^2\eta}{\partial x\partial t} + f_0 u - \frac{\beta_0 g}{f_0} y\frac{\partial \eta}{\partial y} = -g\frac{\partial \eta}{\partial y}.$$

which can be solved to

$$u = -\frac{g}{f_0}\frac{\partial \eta}{\partial y} - \frac{g}{f_0^2}\frac{\partial^2\eta}{\partial x\partial t} + \frac{\beta_0 g}{f_0^2} y\frac{\partial \eta}{\partial y},$$
$$v = +\frac{g}{f_0}\frac{\partial \eta}{\partial x} - \frac{g}{f_0^2}\frac{\partial^2\eta}{\partial y\partial t} - \frac{\beta_0 g}{f_0^2} y\frac{\partial \eta}{\partial x}.$$

Finally, substituting in the continuity equation (2.44) leads the the equation for the surface interface displacement;

$$\frac{1}{R_D^2}\frac{\partial \eta}{\partial t} - \frac{\partial}{\partial t}\nabla^2\eta - \beta_0\frac{\partial \eta}{\partial x} = 0. \tag{2.46}$$

where $R_D = \frac{\sqrt{gH}}{f_0}$ is called Rossby radius of deformation. Equation (2.46) can be expressed as a function of stream function ψ in the following form;

$$\frac{\partial}{\partial t}\left(\nabla^2\psi - \frac{1}{R_D^2}\psi\right) + \beta\frac{\partial \psi}{\partial x} = 0. \tag{2.47}$$

Seeking solution of the form $\psi = \psi_0 e^{i(kx+ly-\omega t)}$ and substituting back to (2.47) gives the dispersion relation for Rossby waves;

$$\boxed{\omega = -\frac{\beta k}{k^2 + l^2 + \frac{1}{R_D^2}}} \tag{2.48}$$

we have seen that the dispersion relation is always negative, which means that

these waves always propagate westward with respect to the zonal flow. Thus, the SWE equations support dispersive wave solutions only if the Coriolis force is included.

2.7.3 Kelvin Waves

Kelvin waves are some of the most important oceanic waves. The solution of Kelvin waves in SWE regimes requires the support of a lateral boundary and it occurs in the ocean where it can travel along coastlines or in the equator where Coriolis force is zero. To find the dispersion relation, we start with linearized shallow water equations.

Suppose the meridional ridge is present at $x = 0$, with the fluid is eastward of the ridge [40]. Since the zonal velocity has to be zero at the meridional ridge, we will seek for the solution in which $u = 0$ everywhere. Thus substituting $u = 0$ in the linearized SWE (2.38) with constant depth, we get;

$$\begin{aligned} -fv &= -g\frac{\partial \eta}{\partial x}, \\ \frac{\partial v}{\partial t} &= -g\frac{\partial \eta}{\partial y}, \end{aligned} \tag{2.49}$$

$$\frac{\partial \eta}{\partial t} + H\frac{\partial v}{\partial y} = 0. \tag{2.50}$$

We assume the wave is traveling in the meridional (north-south) direction, i.e

$$\begin{aligned} v &= v_0(x)e^{i(ly-\omega t)}, \\ \eta &= \eta_0(x)e^{i(ly-\omega t)}. \end{aligned} \tag{2.51}$$

Using (2.51) in (2.49)and (2.50) gives;

$$\begin{aligned} -fv_0 &= -g\frac{\partial \eta_0}{\partial x}, \\ -\omega v_0 &= -gl\eta_0, \\ -\omega\eta_0 + Hlv_0 &= 0. \end{aligned} \tag{2.52}$$

Solving this system for ω gives two possible dispersion relations for Kelvin waves;

$$\boxed{\omega = \pm l\sqrt{gH}} \tag{2.53}$$

The sign is determined by the geostrophic relation in zonal direction. Since the velocity doesn't depend on l, the wave is non-dispersive. The equation for the zonal structure of η

$$\frac{\partial \eta_0}{\partial x} = -\frac{fl}{\omega}\eta_0 \tag{2.54}$$

this can be solved as,

$$\eta_0 = Ae^{(\frac{fl}{\omega})x}$$

At northern hemisphere, the positive sign of dispersion relation gives exponentially growing solution for large x and the solution is unphysical. So we neglect them. And the other way is around for southern hemisphere. Finally, the Kelvin wave solution is,

$$\eta = A\cos(ly - \omega t)e^{-\frac{x}{R_D}}, \tag{2.55}$$

$$v = -A\sqrt{\frac{g}{H}}\cos(ly - \omega t)e^{-\frac{x}{R_D}}. \tag{2.56}$$

where $R_D = \frac{\sqrt{gH}}{f}$ is called Rossby deformation radius.

The interesting feature of Kelvin wave is, they travel along ridges to their right, in the Northern hemisphere. While, on the Southern hemisphere, they travel along ridges to their left. And the reason of these two different travel direction is Coriolis force. In addition, the wave is in geostrophic balance in zonal direction meaning that Coriolis force in the westward direction is balanced by the pressure gradient towards the eastward direction and similarly the other way around.

There is another kind of Kelvin waves which plays an important role in the equatorial dynamics and these waves are called equatorial kelvin wave. In this case the meridional velocity vanishes everywhere identically ($v = 0$) i.e. no flow along y direction [42]. Thus the linearized SWE (2.38) reduces to,

$$\begin{aligned} \frac{\partial u}{\partial t} + g\frac{\partial \eta}{\partial x} &= 0, \\ fu + g\frac{\partial \eta}{\partial y} &= 0, \end{aligned} \tag{2.57}$$

$$\frac{\partial \eta}{\partial t} + H\frac{\partial v}{\partial x} = 0. \tag{2.58}$$

Since the wave is traveling in the zonal direction, we look for the wave solutions of (2.57)-(2.58) in the form.

$$\begin{aligned} u &= u_0(y)e^{i(kx-\omega t)}, \\ \eta &= \eta_0(y)e^{i(kx-\omega t)}. \end{aligned} \tag{2.59}$$

we obtain the dispersion relation for wave frequency ω

$$\omega^2 = gHk^2 \tag{2.60}$$

and the equation for the meridional structure of η

$$\frac{\partial \eta_0}{\partial y} = -\frac{fk}{\omega}\eta_0 \tag{2.61}$$

The only solution for (2.60) and (2.61) that decays for large y is,

$$\eta = \eta_0 e^{(-\frac{fk}{2\omega})y} e^{i(kx-\omega t)}$$

which is called Kelvin wave solution. Here η_0 is an arbitary amplitude. Kelvin waves propagate eastward for $(\frac{\omega}{k}) > 0$ and non-dispersive. For the other solution of (2.60) and (2.61), the wave that propagate westward would grow exponentially for large value of y and gives unphysical solutions. So we discard them.

These Kelvin waves are essential for equatorial thermocline adjustment. They play vital role in the ENSO (El Nino Southern Oscillation) cycle.

2.7.4 Internal waves

A stable stratified (i.e. density decreasing with height) atmosphere or ocean can support Internal wave. They are generally slower because they depend on a weaker density difference and can propagate both on horizontally and vertically. A practical example of stratified fluid system is a thermally stratified lake water of summertime. At this time, temperature variation is observed between the bottom and the surface of the lake. Because temperature increases form the bottom (coldest part) to top (warmest part) of the lake. On the other hand, density increases in the opposite way. This means that we expect less dense water at the surface of the lake whereas dense water should be expected at the bottom of the lake with buoyant waters floating on top of denser water. Thus internal gravity waves are generated whenever a source of energy displaces fluid vertically in the presence of density stratification.

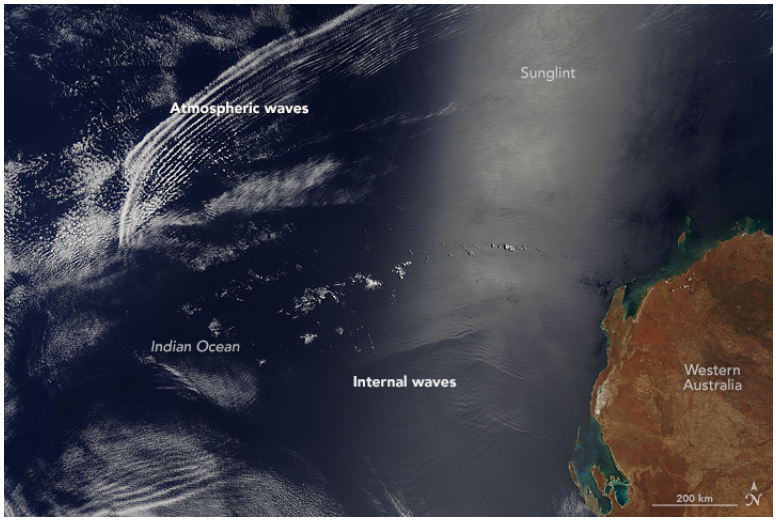

FIGURE 2.3: *Wave patterns off the coast of Western Australia. The presence of sunlight makes it possible to see the faint ripples of internal waves; that is, large waves that propagate below the water surface, within the depths of the sea.* [43].

Although temperature variations create changes in density, the actual density differences remain modest, and a linear relation between density and temperature is $\rho = \rho_0[1 - \alpha(T - T_0)]$ where ρ_0 is the reference density at reference temperature T_0 and α is the coefficient of thermal expansion. As we discussed earlier in section, this means that the Boussinesq approximation is valid. In 2D, the continuity equation $\nabla \cdot \mathbf{u}$ reduces to

$$\frac{\partial u}{\partial x} + \frac{\partial w}{\partial z} = 0. \tag{2.62}$$

and momentum equation can be written as;

$$\frac{\partial u}{\partial t} = -\frac{1}{\rho_0}\frac{\partial \rho}{\partial x}. \tag{2.63}$$

$$\frac{\partial w}{\partial t} = -\frac{1}{\rho_0}\frac{\partial \rho}{\partial z} - g[1 - \alpha(T - T_0)]. \tag{2.64}$$

The linearized form of energy equation is;

$$\frac{\partial T'}{\partial t} + w\frac{\partial \bar{T}}{\partial z} = 0. \tag{2.65}$$

Subtracting the z–derivative of (2.63) from the x–derivative of (2.64) gives;

$$\frac{\partial}{\partial t}\left(\frac{\partial w}{\partial x} - \frac{\partial u}{\partial z}\right) = \alpha g\frac{\partial T'}{\partial x}. \tag{2.66}$$

now to eliminate T' using (2.65) yields;

$$\begin{aligned} &\frac{\partial^2}{\partial t^2}\left(\frac{\partial w}{\partial x}-\frac{\partial u}{\partial z}\right)+\alpha g\frac{\partial \bar{T}}{\partial z}\frac{\partial w}{\partial x}=0,\\ &\Rightarrow \frac{\partial^2}{\partial t^2}\left(\frac{\partial w}{\partial x}-\frac{\partial u}{\partial z}\right)+N^2\frac{\partial w}{\partial x}=0. \end{aligned} \tag{2.67}$$

where $N^2=\alpha g\frac{\partial \bar{T}}{\partial z}$ and N is the Brunt-Vaisala buoyancy frequency.

For example consider an incompressible, stratified non-rotating fluid at rest and in hydrostatic equilibrium. The fluid experiences small amplitude perturbations around the basic state, so the linearized equation of motion in 2D can be used.

$$\rho_0\frac{\partial u}{\partial t}=-\frac{\partial p}{\partial x},$$

$$\rho_0\frac{\partial w}{\partial t}=-\frac{\partial p}{\partial z}-\rho g,$$

$$\frac{\partial w}{\partial t}+w\frac{\partial \rho_0}{\partial z}=0.$$

where $\rho_{total}=\rho_0+\rho$, $p_{total}=p_0+p$, $\rho=$ Perturbation density

$p=$ perturbed pressure. If $u=0$ and $p=0$, we have the special form of solution;

$$\begin{aligned} &\rho_0\frac{\partial w}{\partial t}=-\rho g,\\ &\Rightarrow \rho_0\frac{\partial^2 w}{\partial t^2}=-g\frac{\partial \rho}{\partial t}=wg\frac{\partial \rho_0}{\partial z},\\ &\Rightarrow \frac{\partial^2 w}{\partial t^2}=\left(-\frac{g}{\rho}\frac{\partial \rho_0}{\partial z}\right)w=0,\\ &\Rightarrow \frac{\partial^2 w}{\partial t^2}+N^2w=0. \end{aligned}$$

where $N^2 = -\frac{g}{\rho}\frac{\partial \rho_0}{\partial z}$ Now to solve the system (2.67)and (2.62) we seek a solution of the form;

$$\begin{aligned} u &= U\sin(kx + lz - \omega t), \\ w &= W\sin(kx + lz - \omega t). \end{aligned} \tag{2.68}$$

Substituting (2.68) back to the system yields;

$$\begin{aligned} kU + lW &= 0, \\ l\omega^2 U + k(N^2 - \omega^2)W &= 0. \end{aligned} \tag{2.69}$$

Solving this system (2.69) gives the dispersion relation for Internal Gravity waves;

$$\boxed{\omega = \pm N\sqrt{\frac{k^2}{(k^2 + l^2)}}}. \tag{2.70}$$

The term $\frac{k^2}{(k^2+l^2)}$ is less than or equal to one, so ω must be less than or equal to one.

Now let's consider the two-dimensional propagation of the wave relative to excitation vector ω. If the horizontal excitation vector is $\vec{\omega} = \omega\hat{i}$ then the angle between ω and the two dimensional wave number $\mathbf{K} = k\hat{i} + l\hat{j}$ is [44],

$$\begin{aligned} \cos\theta &= \frac{\vec{K}\cdot\vec{\omega}}{\left|\vec{K}\right||\vec{\omega}|}, \\ &= \sqrt{\frac{k^2}{(k^2 + l^2)}}, \\ &= \pm\frac{\omega}{N} \\ \therefore \omega &= \pm N\cos\theta. \end{aligned}$$

Now if the frequency of excitation is less than the frequency of the buoyancy oscillation, i.e. $\omega \ll N$ and $\cos\theta \approx 0$, then the wave propagation is perpendicular to the direction of excitation.

If $\omega = N$ and $\cos\theta \approx 1$, then the direction of the wave propagation is the same as the direction of excitation.

On the other hand, if $\omega > N$ then no wave forms and $\cos\theta$ doesn't exit. Because $\omega > N$ means that we force the system to swing faster than it's threshold frequency, which is not possible and as a result, no wave forms.

In chapter 4, we will present the numerical results for Internal waves propagation.

Chapter 3

An explicit staggered finite volume scheme for single and multi layer SWE

3.1 Introduction

In the introduction section, it is mentioned that shallow water equations are a model to describe fluid flow in rivers, channels and oceans. In the one-dimensional case, for flat bottom of ocean, the conservation form of shallow water equations is:

$$\frac{\partial \eta}{\partial t} + \frac{\partial}{\partial x}\left(\left(H + \eta\right) u\right) = 0, \tag{3.1a}$$

$$\frac{\partial u}{\partial t} + \frac{\partial}{\partial x}\left(\frac{1}{2}u^2 + g\eta\right) = 0. \tag{3.1b}$$

where typical initial conditions for η and u at time $t = 0$ are of the form:

$$\eta(x,0) = 10e^{\frac{-\frac{1}{4}(x-0.2L_x)^2}{\delta^2}}, \quad u(x,0) = 0.$$

and the boundary conditions are

$$\eta(t,0) = \eta(t,L), \quad u(t,0) = u(t,L).$$

where t is the time variable, x is the space variable, u is the velocity, η is the displacement of water from the free surface, H is the average height from the flat bottom of ocean, L_x is the length scale of horizontal motion and g is the gravitational constant.

In the presence of bathymetry, (3.1a)-(3.1b) can be written as;

$$\frac{\partial \eta}{\partial t} + \frac{\partial}{\partial x}\left((H + \eta - \beta)\, u\right) = 0, \tag{3.3a}$$

$$\frac{\partial u}{\partial t} + \frac{\partial}{\partial x}\left(\frac{1}{2}u^2 + g\eta\right) = 0. \tag{3.3b}$$

with initial conditions for η and u is of the following form:

$$\eta(x,0) = 10e^{\frac{-\frac{1}{6}(x-0.2L_x)^2}{\delta^2}}, \quad u(x,0) = 0. \tag{3.4}$$

and the following Gaussian function has been chosen for bottom bathymetry:

$$\beta(x) = 70e^{\frac{-\frac{1}{4}(x-0.7L_x)^2}{\delta^2}} \tag{3.5}$$

We can normalize by taking $g = H = 1$ and the normalized one dimensional shallow water system is:

$$\frac{\partial \eta}{\partial t} + \frac{\partial}{\partial x}\left((1+\eta)\,u\right) = 0, \tag{3.6}$$

$$\frac{\partial u}{\partial t} + \frac{\partial}{\partial x}\left(\frac{1}{2}u^2 + \eta\right) = 0. \tag{3.7}$$

The wave speed for shallow water system is $c = \sqrt{gH}$ which is constant for constant mean depth H. And by putting $g = H = 1$, we get $c = 1$ for normalized shallow water equations.

The shallow water equations are non-linear hyperbolic system of conservation laws. To solve this type of problem, finite volume methods have proved to be very effective. Staggered finite volume discretizations for solving nonlinear hyperbolic system of conservation laws have been investigated by [45].

In this chapter, we review an explicit finite volume scheme for the discritization of single and multi layer shallow water equations. The different unknown variables of the system are approximated on staggered meshes with average height at cell centres (nodes) and velocities at cell edges (interfaces). The cells are uniform in size and form the control volumes for the finite volume scheme. The numerical fluxes are computed with centered discretizations. The method is second order accurate in space. The chapter is organized as follows: Section 3.2 describes one dimensional staggered scheme for single layer shallow water equations. Section 3.3 describes the discretization of multilayer shallow water equations. Section 3.4 describes four stage third order Runge - Kutta time integration scheme. Section 3.5 describes the stability analysis of the system.

3.2 Description of one dimensional staggered scheme for single layer SWE

3.2.1 Nonlinear Shallow water system

We begin with the non dimensional shallow water equations (3.1a)-(3.1b) on the space domain $\Omega := (0, L_x)$ and the time interval $(0, T)$. We impose periodic boundary conditions. The time interval is divided into N_t time steps of length Δt and the space domain is divided into N_x cells of length Δx. The left end, the center and the right end of the i-th cell are denoted by x_e, x_i and x_{e+1} respectively. We discretize η at the center of the cells whereas we discretize velocity u at the interfaces between the cells. The approximation of η at point x_i and at time t^n is denoted by η_i^n and the approximation of u at point x_e and at time t^n is denoted by u_e^n. This grid set up is shown in Figure 3.1. Typical initial conditions for η and u at time $t = 0$ are of the form:

$$\eta(x, 0) = 10e^{\frac{-\frac{1}{6}(x-0.2L_x)^2}{\delta^2}}, \quad u(x, 0) = 0.$$

where $\eta(x, 0)$ is a Gaussian curve centred at zero and δ is the standard deviation parameter, $\delta \ll L$. The periodic boundary conditions are applied as;

$$\eta_o^n = \eta_{N_x}^n, \quad u_1^n = u_{N_x+1}^n.$$

The space discretization is represented as follows:

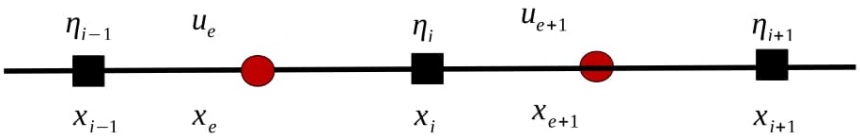

FIGURE 3.1: One-dimensional staggered grid. velocity (u) is discretized at the interfaces between each cell and η is discritized at the centre of each cell.

In order to discretize (3.1a)-(3.1b) we first need to approximate the height (mass) flux through the edges. For example, at edge x_{e+1} the flux is $u_{e+1}\eta_{e+1}$ and at edge x_e the flux is $u_e\eta_e$. We approximate η_{e+1} from the cell centre values using linear interpolation. Thus we have,

$$\eta_{e+1} = \frac{1}{2}\left(\eta_{i+1} + \eta_i\right), \tag{3.8}$$

$$\eta_e = \frac{1}{2}\left(\eta_i + \eta_{i-1}\right). \tag{3.9}$$

The divergence of the height flux is then approximated at the cell centre x_i using second order central finite difference method.

$$\frac{\partial}{\partial x}\left[\left(H+\eta\right)u\right]_i = \frac{(H+\eta_{e+1})u_{e+1} - (H+\eta_e)u_e}{\Delta x}.$$

Thus the discretized form of (3.1a) at control volume center is;

$$\begin{aligned} \frac{\partial \eta_i}{\partial t} &= -\frac{\partial}{\partial x}\left[\left(H+\eta\right)u\right]_i, \\ \Rightarrow \frac{\partial \eta_i}{\partial t} &= -\frac{(H+\eta_{e+1})u_{e+1} - (H+\eta_e)u_e}{\Delta x}. \end{aligned}$$

In a similar way, we can derive the approximation for $(\frac{\partial u}{\partial t})_{e+1}$ at interface x_{e+1}. First we interpolate the velocities to the cell centres using linear interpolation. Thus we have,

$$u_i = \frac{1}{2}\left(u_{e+1} + u_e\right), \tag{3.10}$$

$$u_{i+1} = \frac{1}{2}\left(u_{e+2} + u_{e+1}\right). \tag{3.11}$$

The gradient at the cell edge x_{e+1} is then approximated using the second order central finite difference approximation as

$$\begin{aligned}
\left(\frac{\partial u}{\partial t}\right)_{e+1} &= -\frac{\partial}{\partial x}\left(\frac{1}{2}u^2 + g\eta\right)_i, \\
&\approx -\frac{1}{\Delta x}\left[\left(\frac{1}{2}u^2 + g\eta\right)_{i+1} - \left(\frac{1}{2}u^2 + g\eta\right)_i\right], \\
&= -\frac{1}{\Delta x}\left[\frac{1}{2}\left((u_{i+1})^2 - (u_i)^2\right) + g\left(\eta_{i+1} - \eta_i\right)\right], \\
&= -\frac{1}{\Delta x}\left[\frac{1}{2}\left(\left(\frac{1}{2}\left(u_{e+2} + u_{e+1}\right)\right)^2 - \left(\frac{1}{2}\left(u_{e+1} + u_e\right)\right)^2\right) + g\left(\eta_{i+1} - \eta_i\right)\right].
\end{aligned}$$

3.2.2 Linearised Shallow water system

In this section, we discretize the linearised form of shallow water equations. The system is linearised about the average water depth H and with the zero velocity u. Thus we have $h(x,t) = H + \eta(x,t)$ where $\eta \ll 1$ is the elevation of water from free surface. Thus we have

$$\begin{aligned} &\frac{\partial h}{\partial t} + \frac{\partial}{\partial x}(hu) = 0, \\ \Rightarrow\ &\frac{\partial (H+\eta)}{\partial t} + \frac{\partial}{\partial x}((H+\eta)u) = 0, \\ \Rightarrow\ &\frac{\partial \eta}{\partial t} + \frac{\partial}{\partial x}(\eta u) = 0. \end{aligned}$$

Similarly we have,

$$\frac{\partial u}{\partial t} = -\frac{\partial}{\partial x}\left(\frac{1}{2}u^2 + g\eta\right) = -\frac{\partial}{\partial x}(g\eta)\,.$$

Then we non-dimensionalise by taking $g = 1$ and $H = 1$ and finally we get the following linearised form of shallow water equation;

$$\frac{\partial \eta}{\partial t} = -\frac{\partial u}{\partial x}, \tag{3.12}$$

$$\frac{\partial u}{\partial t} = -\frac{\partial \eta}{\partial x}. \tag{3.13}$$

By discritizing in space as before, our approximation for linear system becomes;

$$\left(\frac{\partial \eta}{\partial t}\right)_i = -\frac{1}{\Delta x}(u_{e+1} - u_e)\,, \tag{3.14}$$

$$\left(\frac{\partial u}{\partial t}\right)_{e+1} = -\frac{1}{\Delta x}(\eta_{i+1} - \eta_i)\,. \tag{3.15}$$

3.3 Staggered scheme for Multilayer Shallow water equations

3.3.1 Multi-Layer Shallow water equations

Multi layer shallow water equation can be extended to three dimensions layer-wise using the hydrostatic approximation for pressure as in Dubus et al.[21]. The multi-layer shallow water model is used to describe incompressible flows in the shallow water region, in the situation where several layers with different densities can be identified. For setting up this model, we used the following assumptions: Shallowness of layers with respect to horizontal scales, small viscosity, hydrostatic balance, almost uniform velocity in each layer and stratification of density. Denoting $\partial_\alpha = \frac{\partial}{\partial \alpha}$ for $\alpha = x, t$, the one dimensional multilayer shallow water system can be written as:

$$\partial_t \mu + \partial_x(\mu u) = 0, \tag{3.16a}$$

$$\partial_t \Theta + \partial_x(\theta U) = 0, \tag{3.16b}$$

$$\partial_t u + \partial_x(\frac{1}{2}u^2 + \frac{\lambda}{\rho} + \Phi) + \theta \partial_x(-\Phi) = 0. \tag{3.16c}$$

Here,

$$\text{Pseudo-density:} \qquad \mu = \rho_r \Delta z; \quad \Delta z = \frac{(H+\eta)}{N_z}; \tag{3.18a}$$

$$\text{Horizontal mass flux vector} \quad U = \mu u; \tag{3.18b}$$

$$\text{Inertial mass weighted density perturbation:} \quad \Theta = \mu\theta; \tag{3.18c}$$

$$\text{Geopotential at interfaces:} \qquad \phi_l = \phi_s + \frac{g\mu}{\rho_r}. \tag{3.18d}$$

Here it's important to mention that, for compressible fluid θ is potential temperature but for incompressible case, θ acts as a buoyancy.

Also,

N_z is the number of the layer,

N_x is the number of cells in space domain,

dt is the time step,

H is the vertical length of ocean,

η is the elevation of inertial mass from free surface,

λ is the Lagrange multiplier to enforce incompressibility,

ρ_r is the reference density and

geopotential at ocean surface, $\phi_s = 0$.

But in the presence of bathymetry,

$$\text{Layer Thickness:} \qquad \Delta z = \frac{(H+\eta-\beta(x))}{N_z}; \tag{3.19a}$$

$$\text{Geopotential at ocean surface:} \qquad \phi_s = 0 + g\beta(x). \tag{3.19b}$$

where $\beta(x)$ is the bottom bathymetry, defined by equation (3.5).

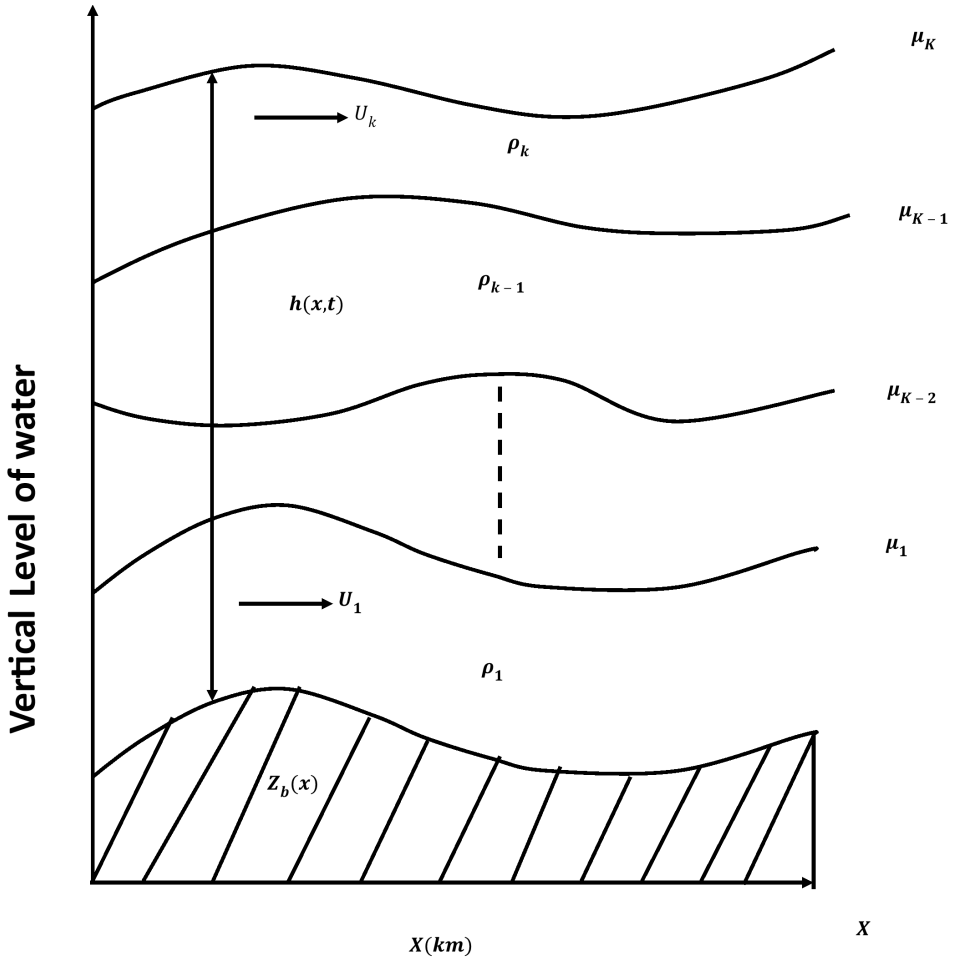

FIGURE 3.2: Multi-Layer Shallow water system,where $b(x)$ represents bathymetry. Density (ρ_i), inertial mass (μ_i), mass weighted density distribution (Θ_i) and velocity (u_i) are defined on each vertical level. The thickness of each vertical level is $\Delta z_i = \frac{\mu_i}{\rho_r}$, where $i = 1, 2, 3.....K$.

Here figure (3.2) represents the model for multi-layer Shallow water equations. Density is stratified vertically and meets the condition of boussinesq approximation $((\frac{\Delta\rho}{\rho_r} \ll 1); i = 1, 2, 3....K.)$. Velocity, Inertial mass and mass weighted density distribution is defined at each vertical level. Using hydrostatic balance, the thickness of vertical level is defined as $\Delta z = \frac{\mu}{\rho_r}$.

3.3.2 Discretization of Inertial Mass and Mass weighted density distribution equation

In this section we will describe how to discritize the transport of mass and mass weighted density distribution equations using explicit finite volume scheme. Like single layer SWE, we begin with the one dimensional multi layer shallow water equations (3.16a)-(3.16c) on the space domain $\Omega := (0, L_x)$ and the time interval $(0, T)$. We applied periodic boundary conditions. The time interval is divided into N_t time steps of length Δt and the space domain is divided into N_x cells of length Δx. The center of each cell is denoted by i and the edge of the cell is denoted by e. For vertical discritization, Lorenz staggering is used. And this full vertical levels are indexed by $k = 1, 2.....K$ and interfaces between full levels are indexed by $l = 1/2, 3/2...L = K + 1/2$. Thus the fluids are labeled from bottom to top. Scalar densities μ and Θ is discritized at the center of each cell and we describe them by μ_{ik}, Θ_{ik} whereas the velocity is descritized at the edge of each cell for all k-th vertical level and we denote them by u_{ek}. Lagrange multiplier λ is discritized at the center of each cell at k-th vertical level and the geopotential Φ lies at the interfaces of vertical level. The situation is represented in Figure (3.3). In absence of bathymetry, the geopotential at the bottom of the ocean is considered as zero. Beside this the layer thickness is discretized as $\Delta z_k = \frac{(H+\eta(x_i))}{N_z}$.

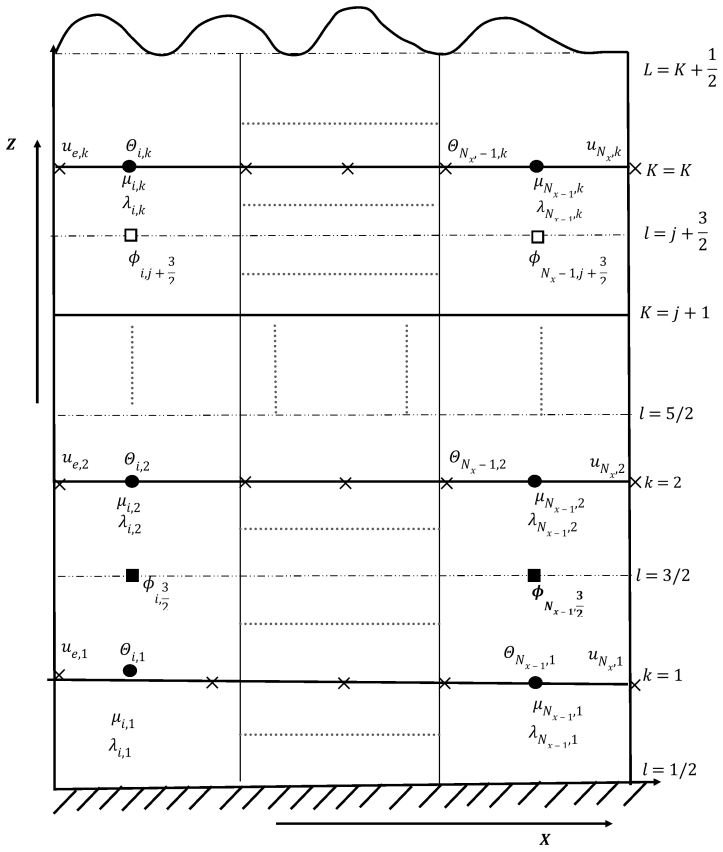

FIGURE 3.3: Staggered scheme for Multi-Layer Shallow water system. μ_{ik}, Θ_{ik} and λ_{ik} are discritized at the center of each cell at k-th vertical level where $i = 1, 2....N_{x-1}, k = 1, 2, ...K$. u_{ek} is discritized at the edge of each cell where $e = 1, 2, ...N_x$. Geopotential Φ_{il} is discritized at the interface of vertical level where $l = 1/2, 3/2, ...K + 1/2$.

On the other hand, with bottom bathymetry,the layer thickness is discretized as $\Delta z_k = \frac{(H+\eta(x_i)-\beta(x_i))}{N_z}$. And the discretization of geopotential at the bottom of the ocean is given as, $\phi_s = 0 + g\beta(x_i)$.

For non-flat bottom of ocean, we use $\sigma - z$ coordinate system where vertical coordinate is depth. At interface,

$$z_l = z_s + \Delta z(l-1) \tag{3.20}$$

where $z_s = 0 + \beta(x)$, while on the other hand, for flat bottom of ocean we use uniform z coordinate with $z_s = 0$ in equation (3.20).

Figure 3.4 and Figure 3.5 represents these two coordinate system.

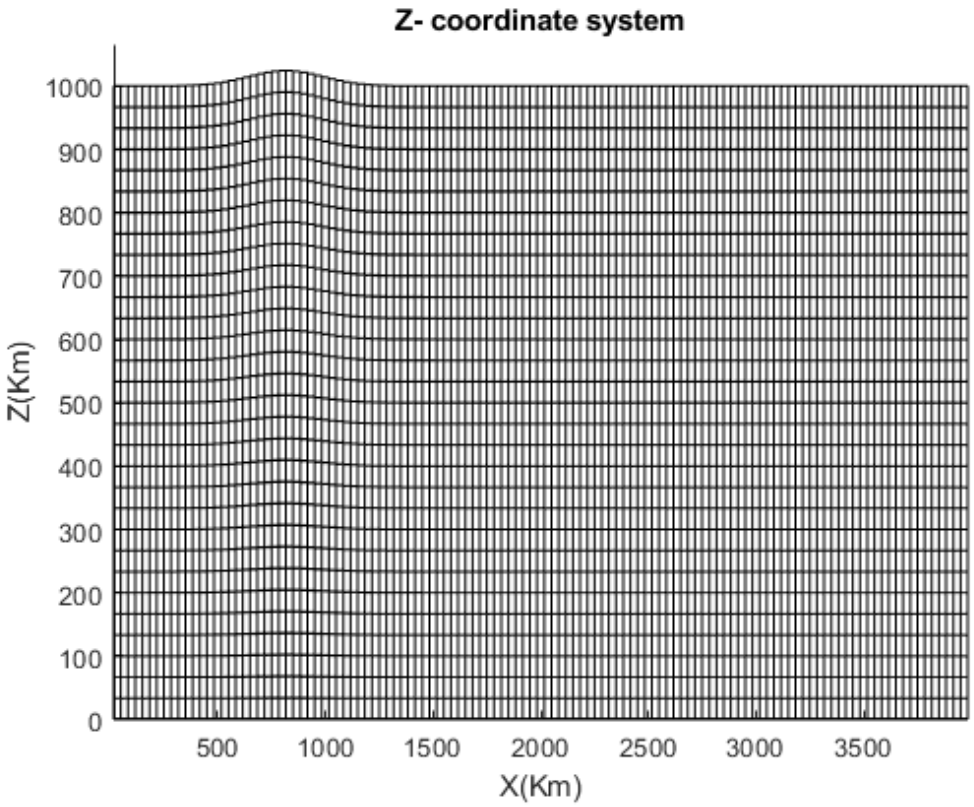

FIGURE 3.4: Coordinate system with uniform layer thickness $\Delta z = \frac{(H+\eta(x))}{N_z}$. where $\eta(x)$ is the elevation of inertial mass from free surface of ocean.

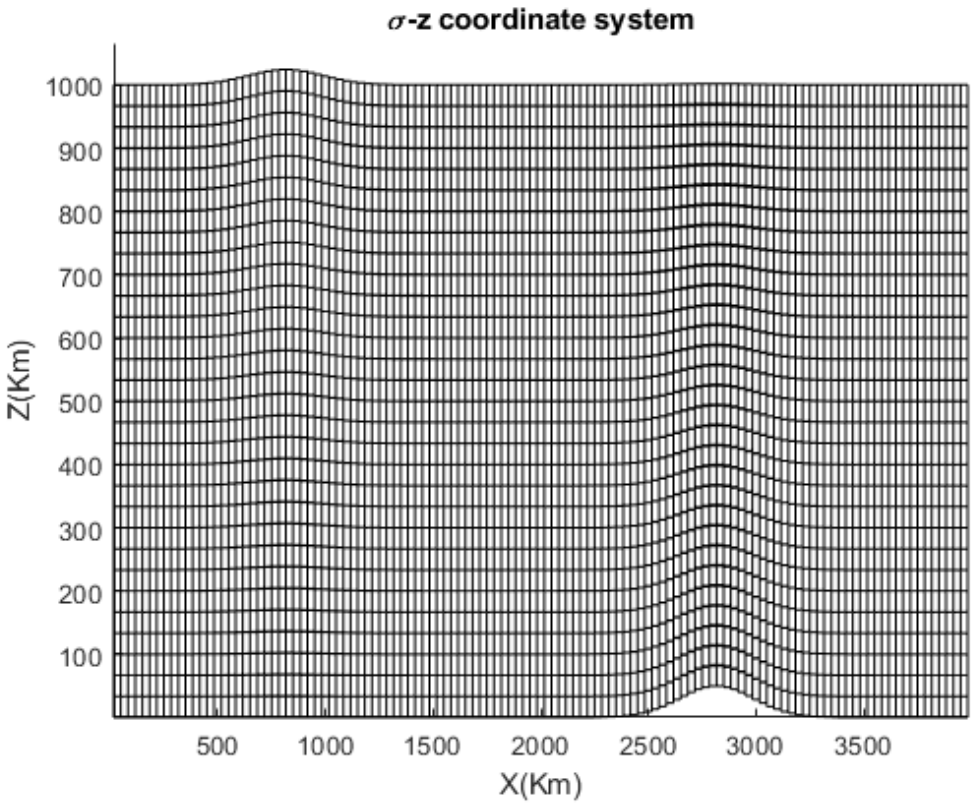

FIGURE 3.5: Coordinate system with vertical layer thickness $\Delta z = \frac{(H+\eta(x)-\beta(x))}{N_z}$. where $\eta(x)$ is the elevation of inertial mass from free surface and $\beta(x)$ is the bottom bathymetry of ocean.

Using those above mentioned notation, the discritised inertial mass and mass weighted density distribution budget can be written in the form;

$$\partial_t \mu_{ik} + \partial_i(\mu_{ek} u_{ek}) = 0, \tag{3.21}$$

$$\partial_t \Theta_{ik} + \partial_i(\theta^{\star}_{ek} \mu_{ek} u_{ek}) = 0. \tag{3.22}$$

where we have $\theta_{ik} = \frac{\Theta_{ik}}{\mu_{ik}}$ and $\theta^{\star}_{ek}$ is reconstructed at interfaces between control volumes as in the one dimensional case, using linear interpolation.

3.4 Discritization of equation of motion

We want to write the equations of motion corresponding to the discrete Hamiltonians (H). In [21] T. Dubos et al. showed that the approximations of H for incompressible fluid can be done by introducing Boussinesq approximations. Thus the horizontally discretized form of Hamiltonian is;

$$H = \frac{1}{2}\sum_{ik}\mu_{ik}u_{ek}^2 + \sum_{ik}\left[\mu_{ik}\left(1-\frac{\Theta_{ik}}{\mu_{ik}}\right)\bar{\Phi}_{ik} + \lambda_{ik}\left(\frac{\mu_{ik}}{\rho_r} - \frac{\partial_k\Phi_i}{g}\right)\right] + \frac{p_\infty\sum\Phi_{iL}}{g}. \tag{3.23}$$

For incompressible Hamiltonian, the geopotential is obtained by enforcing $\frac{\partial H}{\partial\lambda_{ik}} = 0$, which gives;

$$\begin{aligned}
&\frac{\partial_k\Phi_i}{g} = \frac{\mu_{ik}}{\rho_r},\\
&\Rightarrow \frac{\Phi_l - \Phi_{l-1}}{\Delta z} = \frac{g\mu_{ik}}{\rho_r},\\
&\Rightarrow \Phi_l = \Phi_{l-1} + \frac{g\mu_{ik}\Delta z}{\rho_r},\\
&\Rightarrow \Phi_l = \Phi_s + \frac{g\mu_{ik}\Delta z}{\rho_r}.
\end{aligned}$$

The hydrostatic balance is expressed as $\frac{\partial H}{\partial\Phi_{il}} = 0$ which gives $\overline{(1-\theta_{ik})\,\mu_{ik}}^{\,l} + g^{-1}\delta_l\lambda_{ik} = 0$ with the upper boundary conditions $\lambda_{iK} = p_\infty + \frac{g}{2}(1-\theta_{iK})\,\mu_{iK}$. Therefore λ_{ik} can be determined starting from the top level and can be interpreted as the pressure at full model levels, where as geopotential lies at the interfaces. Pressure at free surface, i.e $p_\infty = 0$

Finally, the horizontal momentum balance is written as follows;

$$\partial_t u_{ek} + \partial_e B_{ik} + \theta^\star_{ek}\partial_e\Pi_{ik} = 0. \tag{3.24}$$

where in equation (3.23) $\frac{\partial H}{\partial \mu_{ik}}$ gives $B_{ik} = \frac{\partial H}{\partial \mu_{ik}} = \frac{1}{2}u_{ek}^2 + \bar{\Phi}_{ik} + \frac{\lambda_{ik}}{\rho_r}$ and $\Pi_{ik} = \frac{\partial H}{\partial \Theta_{ik}} = -\bar{\Phi}_{ik}$.

3.5 Runge Kutta Time integration Scheme

To solve our nonlinear system numerically; we used third order fourth stage Runge -Kutta scheme to approximate the trend in time for inertial mass, mass weighted density distribution and velocity. We approximate the solutions at each time step between initial time t_0 and final time t_T. The solution at $n+1$ -th time step is calculated as follows;

$$
\begin{aligned}
U_0 &= y_n, \\
U_1 &= U_0 + \Delta t \frac{1}{2} f\left(t, U_0, \frac{\partial y}{\partial x}\right), \\
U_2 &= U_1 + \Delta t \frac{1}{2} f\left(t, U_1, \frac{\partial y}{\partial x}\right), \\
U_3 &= \frac{2}{3}U_0 + \frac{1}{2}U_2 + \Delta t \frac{1}{6} f\left(t, U_2, \frac{\partial y}{\partial x}\right), \\
U_4 &= U_3 + \Delta t \frac{1}{2} f\left(t, U_3, \frac{\partial y}{\partial x}\right), \\
y_{n+1} &= U_4, \\
t_{n+1} &= t_n + \Delta t.
\end{aligned}
$$

Where y_n represents the solution at time $t = n$, the initial condition for inertial mass, mass weighted density distribution and velocity is defined by y_1 at time t_0 and $f\left(t, U, \frac{\partial y}{\partial x}\right)$ is the approximation of the right hand side of the equation in space. Now using finite difference - finite volume discritization with Runge -Kutta

approximations, we can solve our system in forward time from $t = 0$ to $t = T$. And by doing this we obtained our final solutions for $\mu(x,t)$, $\Theta(x,t)$ and $u(x,t)$.

3.6 Stability and Courant-Friedrichs-Lewy Condition

Generally, a numerical scheme is stable in time if it does not amplify numerical errors. A lack of stability in our scheme can cause exponential growth of numerical errors. The Courant-Friedrichs-Lewy (CFL) criterion is what ensures stability for hyperbolic problems. For discrete hyperbolic equations, CFL condition expresses that the distance that any information travels during the timestep length within the mesh must be lower than the distance between mesh elements. It means that the time step must be less than a certain value. If the time step is too large, then it might happen that this value could be larger than the time taken for our information to travel to adjacent grid points in space where the solution is calculated.

For one-dimensional case, the form of CFL is the followings;

$$\frac{c\Delta t}{\Delta x} \leq c_{max} = 1. \tag{3.25}$$

Where the quotient $\frac{c\Delta t}{\Delta x}$ is called the CFL number.

Here, $c = \sqrt{gH}$ is the wave speed,

Δt is the time step,

Δx is the length interval .

Thus to meet the CFL criterion for the single layer, the time step should be $\Delta t \leq \frac{\Delta x}{c}$. But for our multi-layer model, the condition for choosing the time step is different from a single layer. In our model, the horizontal interfaces may steepen due to nonlinearity and this can cause the computation to break down because the gradient cannot be resolved. We deal with this by adding viscous diffusion to the equations (3.21) and (3.24). Since we have added diffusion terms in our system, so the required time step for obtaining stable solutions is the following;

$$\Delta t < \min\left(\frac{C_1 \Delta x}{\sqrt{gH}}, \frac{C_2 \Delta x^2}{\nu}\right). \tag{3.26}$$

where ν is the smallest viscosity parameter, which is added to stabilized the numerical instability of our system.

In addition, since the horizontal interfaces are Lagrangian (i.e. they move with the vertical velocity of the fluid) a layer may collapse, or layers may become too thick. In the multilayer shallow water model, these issues with the Lagrangian vertical coordinate were controlled by periodically remapping the vertical coordinates back to the original coordinates.

Figure 3.6 shows the physical demonstration of remapping. For each cell, the shifted variable μ, Θ and u are remapped onto uniform vertical grid, i.e. we interpolated these integrated quantities to preserve mass, momentum heat in each layer.

The remapping algorithm is as follows;

- From the shifted mass density, find the current z coordinates of vertical interfaces.

- Find new uniformly spaced z coordinates of vertical interfaces.
- Calculate inertial mass at horizontal edges and then interpolate integrated variables (μ and Θ) onto uniform vertical grid.
- Update mass density at horizontal cell edges.
- Interpolate velocity onto uniform vertical grid.
- Return interpolated μ, Θ and u .

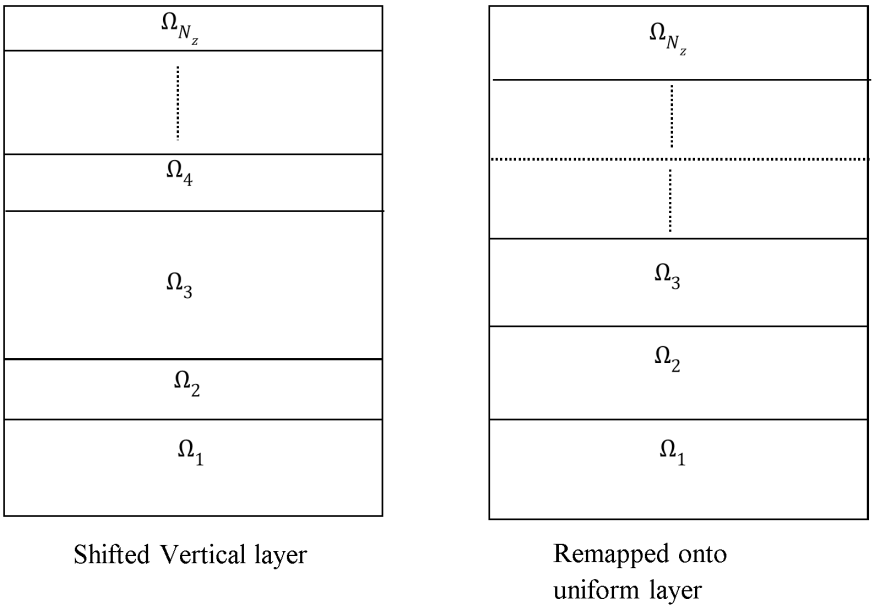

FIGURE 3.6: Physical demonstration of remapping. Variables μ_{ik}, Θ_{ik} and u_{ek} are remapped onto uniform vertical grid point for each cell Ω_i where $i = 1, 2, ...N_z$. Here the top most right figure represents the uniform grid where variables are remapped.

To solve the shallow water and multilayer shallow water system numerically, second order finite difference-finite volume method have been implemented in **Matlab**.

Chapter 4

Results and discussion

4.1 Introduction

We began our analysis of the staggered scheme (second order finite difference-finite volume) on single layer ((3.1) and(3.3)) and multi-layer shallow water equations (3.16). We chose a total time period from 0 to 350 and the spatial domain $[0, 4000]$km. The space domain is divided into $N_x = 400$ cells of length $\Delta x = 10$. We consider vertical length 1000km which we divided into 100 layers. The time step Δt is chosen by (3.26). The time interval for remapping is chosen for 5s. The set up of horizontal and vertical domain will be the same for all of our numerical experiments.

For flat bottom of ocean, the typical initial conditions for the perturbation to the free surface η and velocity u at time $t = 0$ is,

$$\eta(x,0) = 10e^{\frac{-\frac{1}{6}(x-0.2L_x)^2}{\delta^2}}, \quad u(x,0) = 0. \tag{4.1}$$

On the other hand, in the presence of bottom bathymetry, the typical initial conditions for the perturbation to the free surface η is,

$$\eta(x,0) = 10e^{\frac{-\frac{1}{6}(x-0.2L_x)^2}{\delta^2}}. \tag{4.2}$$

and for both cases, the boundary conditions are

$$\eta(t,0) = \eta(t,L), \quad u(t,0) = u(t,L). \tag{4.3}$$

The following function has been chosen for bottom bathymetry:

$$\beta(x) = 70e^{\frac{-\frac{1}{4}(x-0.7L_x)^2}{\delta^2}} \tag{4.4}$$

The mean density function is given as:

$$\rho = \rho_r \left(1 - \frac{\Delta\rho}{2}\left(1 - \tanh\left(\frac{-z + H/2}{0.05H}\right)\right)\right) \tag{4.5}$$

On the other hand, for linear density stratification, the density function is

$$\rho = \rho_r \left(1 - \Delta\rho\frac{z}{H}\right) \tag{4.6}$$

The aim of this chapter is to validate multilayer SWE (3.16) and to explore numerically the effect of density gradients on surface wave propagation, both in the presence and absence of bottom bathymetry. We will also explore the interaction of barotropic and baroclinic waves generated by the interaction of surface and internal waves.

The first part of this chapter presents some numerical simulations to validate our multilayer shallow water model, such as the comparison of surface wave propagation for single layer and multilayer shallow water model with and without density gradient as well as bathymetry. In addition, we also validate our model by looking at internal wave propagation along a strong density gradient. The later section of this chapter presents the results of a set of numerical experiments. We consider two cases of stably stratified density gradients: two layers and linearly density gradient, including the effects of bathymetry. Finally, in the last section, we summarize and discuss the results from the numerical experiments.

4.2 Validation of Multi-layer SWE model

4.2.1 Comparison of single layer and multi-layer Shallow water model for surface waves

We begin our validation of the model by comparing the surface wave propagation of single layer and multilayer SWE. In order to do this, we consider four numerical test cases:

1. Zero Density gradient without bathymetry,
2. Small Density gradient without bathymetry,
3. Zero Density gradient with bathymetry.
4. Small Density gradient with bathymetry,

For all of these test cases, we chose a total time period from 0 to 150 s.

4.2.1.1 Zero Density gradient without bathymetry

In this section, we examine the surface wave propagation for single layer and multilayer SWE with flat bottom. For the multilayer model, we consider the case of zero density gradient. The horizontal and vertical domain of the model is introduced in the introduction section of this chapter. The initial condition for the perturbation to the free surface η is given by (4.2) and the density stratification function is given by (4.5).

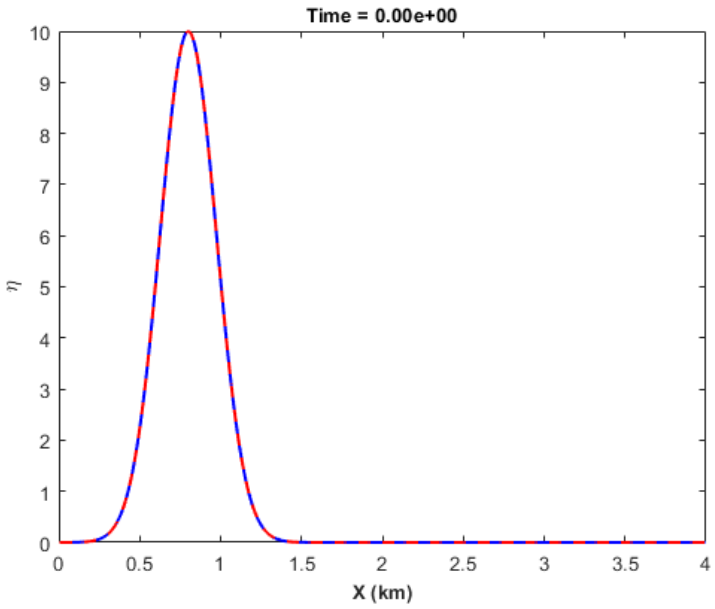

FIGURE 4.1: Initial elevation of inertial mass from free surface $\eta(m)$. The spatial domain X is rescaled as $\frac{L_x}{H}$.

Figure 4.1 represents the initial perturbation of water mass to the free surface both for single layer and multi layer shallow water equations, which is of the form $\eta(x,0) = 10e^{\frac{-\frac{1}{6}(x-0.2L_x)^2}{\delta^2}}$.

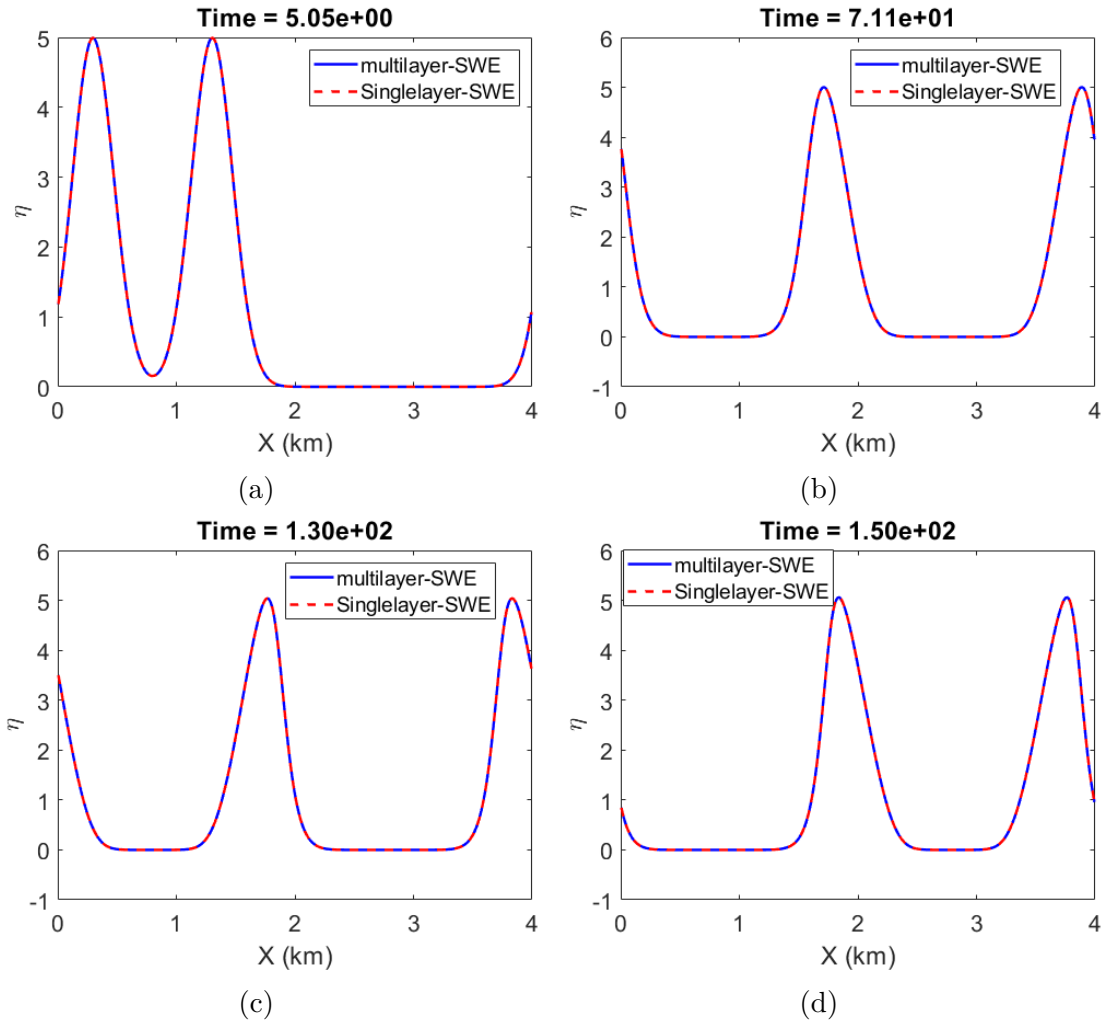

FIGURE 4.2: Comparison of surface wave ($\eta(m)$) propagation for single layer and multi layer shallow water equation. (a) Wave breaks into two parts at t = 5.05 s; (b) Wave approaches towards boundary at t = 71 s; (c) Wave hits boundary at t = 130 s; (d) Position of waves at t = 150 s. The behaviour of multilayer model is exactly same as Single layer SWE.

Figure 4.2 shows the propagation of the surface wave at different time steps. Since density is constant so there are no internal wave and the single and multilayer SWE models should generate the same surface waves. This is verified in figure, which shows exactly the same surface wave evolution for both the single

and multilayer SWE numerical models.

4.2.1.2 Small Density gradient without bathymetry

In this simulation, we examine the surface wave propagation for single layer and multilayer SWE with flat bottom. The horizontal and vertical domain, the initial perturbation to the free surface and the boundary conditions are the same as 4.2.1.1. The layer thickness and geopotential is defined by 3.18a and 3.18d. The density stratification function is given by (4.5) where we consider very small density gradient $\Delta\rho = 0.1$, consistent with Boussinesq approximation ($\frac{\Delta\rho}{\rho_r} \ll 1$).

Figure 4.3 shows the propagation of the surface wave at different times. It is noted that our choice of initial conditions and parameters ensure that our case satisfies all the validity conditions for the multilayer SWE model (i. e. $\frac{\eta}{H} \ll 1$ and $\frac{Lx}{H} \gg 1, \Delta\rho/\rho_r \ll 1$). We have seen that the waves are very similar, but that the single layer SWE wave travels a bit faster. We just presented few snapshot to explain the phenomena. If we look at the peak of wave both for single and multilayer SWE, we can see that, the peak of single layer SWE reaches to the boundary at $t = 48$s, while for multilayer, it reaches at $t = 50$s. Here, we observed the phase speed for single layer is $c_{numerical} = \frac{700}{(48.1-41.1)} = 100$, which is approximately identical to the phase speed for SWE, $c = \sqrt{gH} = \sqrt{9.81 * 1000} \approx 99.0\text{ms}^{-1}$ what we know theoretically. On the other hand, we observed the phase speed for the multilayer case is $c_{numerical} = \frac{700}{(50.1-41.1)} \approx 77.7\text{ms}^{-1}$. So we can say that the results are qualitatively correct (i.e. the multilayer SW wave moves slower). The reason for this behavior will explain in the section 4.2.2. At $t = 130$

s, we also observe a slight bump in the middle which forms due to the transfer of energy to internal waves.

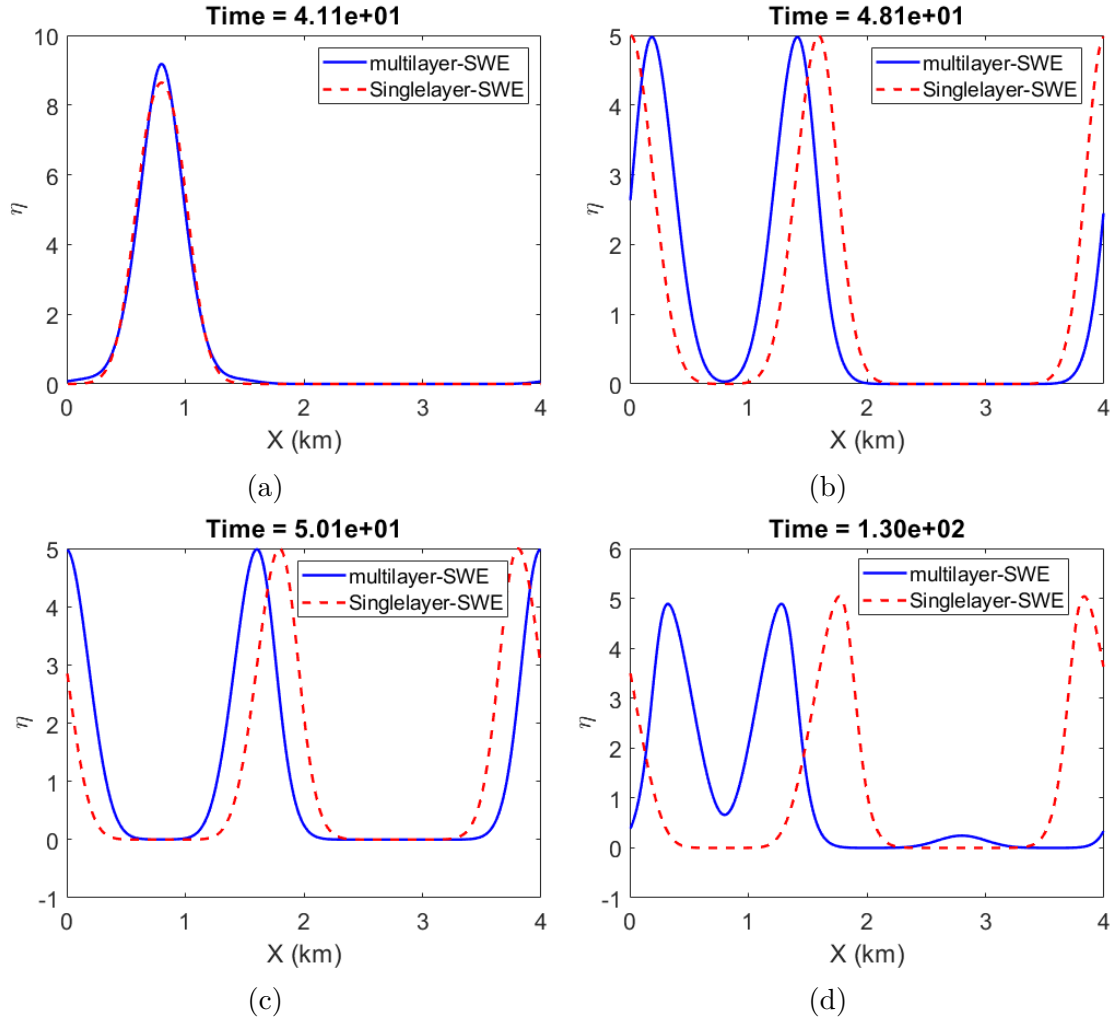

FIGURE 4.3: Comparison of surface wave ($\eta(m)$) propagation for single layer and multi layer shallow water equation. (a)Wave in their initial position at t = 41.1 s; (b) Surface wave hits the boundary at t = 48 s; (c) internal wave hits boundary at t = 50 s; (d) Position of waves at t = 130 s. Compare to SWE, a slight difference in terms of wave's position is observed in multilayer SW model.

4.2.1.3 Zero Density gradient with bathymetry

In this test case, we examine surface wave propagation for single layer and multilayer SWE model, in the presence of bathymetry, with no density gradient. The layer thickness and the geopotential are given by (3.19a) and (3.19b) respectively. The initial condition for η and the function for bathymetry is given by (4.2) and (4.4) respectively.

Figure 4.4 shows the propagation of surface wave at different time steps. As expected, the multi layer SWE model behaves the same as the single layer shallow water model, apart from the fact that multilayer SW wave move slightly slower than the single layer. Because for single layer SWE, bathymetry is just a parameter, so it does not affect the wave speed. But for multilayer SWE, the equation we are solving is different and we used $\sigma - z$ coordinate system, where the layers closest to bathymetry, follows the terrain (Figure 3.5). As a result, when the wave reaches to bathymetry, it tries to cross the obstacle and feels the effect of decreasing depth. Thus multilayer SW waves slow down with decreasing water depth even when we assume zero density gradient. So the results are qualitatively correct, which verifies our numerical multilayer SWE model.

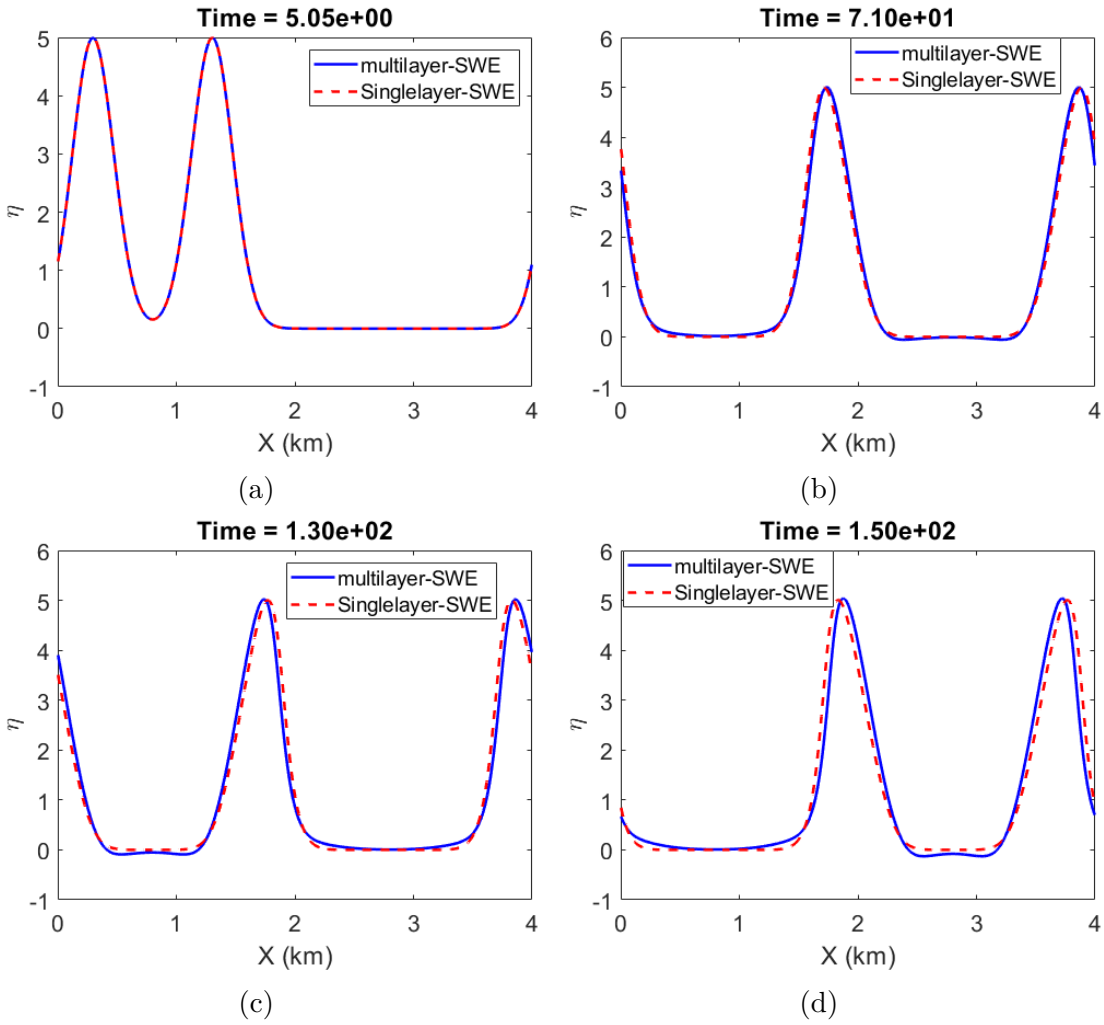

FIGURE 4.4: Comparison of surface wave ($\eta(m)$) propagation for single layer and multi layer shallow water equation. (a) Wave breaks into two parts at t = 5.05 s; (b) Wave hits boundary at t = 71.01 s; (c) Wave approaches to original position at t = 130 s; (d) Position of waves at t = 150 s The behaviour of multilayer model is exactly same as Single layer SWE.

4.2.1.4 Small Density gradient with bathymetry

The aim of this simulation is to examine surface wave propagation for single layer and multilayer SWE model in the presence of bathymetry. The horizontal space domain, vertical layer, initial perturbation to the free surface and the function for bathymetry have been chosen the same as the test case 4.2.1.3. But now, for this test case, we consider two layers of stratified densities with very small density difference (to satisfy the Boussinesq approximation). The stratification of mean density function is given by (4.5) with density gradient $\Delta\rho = 0.1$.

Figure 4.5 shows the propagation of the surface wave at different time steps, in the presence of bathymetry. From the figure we observe that multilayer SWE wave move slower than the single layer SWE wave, as outlined in test case 4.2.1.2. In addition, by looking the peak of the multilayer wave, we observe that, in the presence of bathymetry, the wave speed is slightly slower as well and the wave profile is steeper compared to case of a flat bottom. This is since,when such a wave approaches regions with shallower depth (i.e. the area around the bathymetry where the mean height, H is small, compare to that of other area), the the higher wave which propagate faster, overtake the shallower parts of the wave.

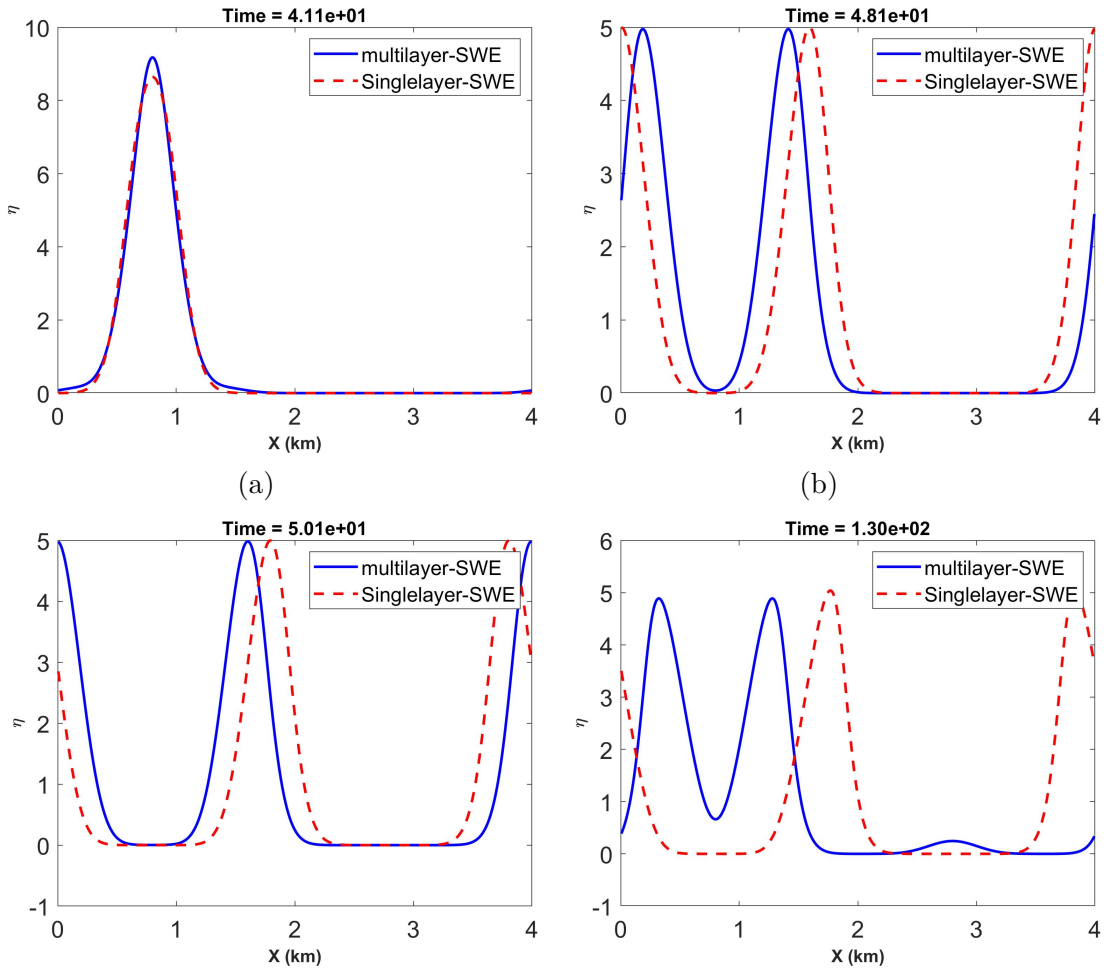

FIGURE 4.5: Comparison of surface wave ($\eta(m)$)propagation for single layer and multi layer shallow water equation. (a) Wave in their initial position at t = 41.1 s; (b) Surface waves hits the boundary at t = 48.1 s; (c) internal waves hits the boundary at t = 50.1 s; (d) Position of waves at t = 130 s. Compare to SWE, a slight difference in terms of waves position is observed in multilayer SW model.

4.2.2 Comparison of single layer and multi-layer Shallow water model for Internal waves

To study the validity of our multilayer shallow water model, here we investigate the propagation of an internal wave in the multilayer SWE model with two stably stratified densities. The horizontal space domain is $\Omega := [0, L_x]$ where ($L_x = 4H \quad$ and $\quad H = 1000 \quad$ km), the vertical domain is divided into two layers, the initial velocity is zero and the water height from free surface is $\eta(x, 0) = 10e^{\frac{-\frac{1}{6}(x-0.2L_x)^2}{\delta^2}}$. The stratified density function for two layers of fluid is given by (4.5) with a small density difference.

The key point of these numerical experiments is that (as we saw in the previous section) waves on the free surface and internal waves on the density interface are not independent. They are locked together in two possible modes. In other words, the two-layer fluid supports two modes of wave motion, namely the Barotropic mode and the Baroclinic mode.

Barotropic mode: In barotropic mode, two surfaces move in phase and the phase speed is the same as the phase speed for single layer shallow water equation, $c = \sqrt{gH}$.

Baroclinic mode: In this mode, two waves has opposite phase. The Baroclinic mode is much slower than barotropic mode and transports less energy.

In this section, we consider the following three numerical experiments to observe the barotropic and baroclinic modes.

1. Perturbation of inertial mass at top layer,

2. Perturbation of inertial mass at interface,

3. Perturbation of density at interface,

Basically, in this section, we are considering stably stratified two-layer scenario for the vertical structure of the ocean, where a layer of water of lower density is above a layer of higher density, separated by a sharp interface. This two layer model is efficient to describe an upper, well mixed oceanic layer. The density gradient layer is unstable and any perturbations to these density gradients are restored by gravity, generating a propagating wave, called internal waves. In addition, internal waves can move in both horizontal and vertical directions, transport energy and trigger vertical mixing of ocean. Since surface waves and internal waves are not independent, the generation of internal waves due to density perturbation influences the surface waves at upper layer and on the other way around. That's why we consider independently perturbations of the inertial mass and density to observe their coupled interactions in terms of barotropic and baroclinic mode. We consider density difference, $\Delta\rho = 0.1$ to see their effect on the modes of wave.

For these test cases, numerically, we calculate

Composite mode of wave i.e., $\eta_{comp} = \sum_{i=1}^{2} \mu_i - H.$

Baroclinic mode of wave $= \eta_{comp} - \eta_{swesloution}.$

Disturbance on two layer, i.e., $\eta_1 = \mu_1 - H_1, \eta_2 = \mu_2 - H_2.$

and the height of two layer, i.e., $h_1 = \mu_1 - \eta_{swesolution}, h_2 = \mu_2 - \eta_{SWEsolution}.$

Also, the the Boussinesq approximation of inertial mass is not the same as buoyancy mass.

4.2.2.1 Internal wave dynamics for two-layer stably stratified flow

In order to understand internal wave dynamics we consider stratified, two layer system as depicted in figure 4.6. Here, ρ_1 is the density of the bottom dense layer and ρ_2 is the density of upper layer. H_1 and H_2 are the height of the lower and upper layer respectively. To find the dispersion relation or the barotropic and baroclinic mode of waves, we solve linearized SWE for two layer fluid with zero mean flow, and for waves traveling in the x-direction only.

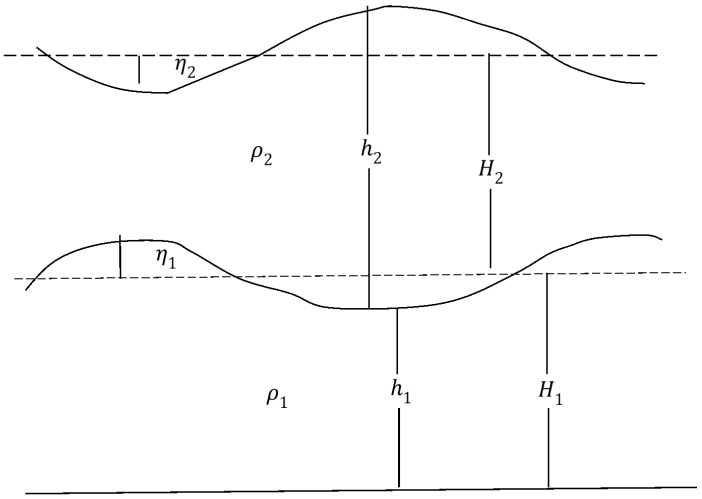

FIGURE 4.6: The physical configuration of two-layer SWE model, where $\frac{\Delta\rho}{\rho} \ll 1$.

Now, the phase speed of the barotropic mode is identical to that of an external gravity wave on the surface of a fluid of depth H, i.e.

$$c_1 = \sqrt{gH} \tag{4.7}$$

A two layer fluid has one barotropic mode and one baroclinic mode. The phase speed for baroclinic mode is

$$c_2 = \sqrt{g' \frac{H_1 H_2}{H}} \tag{4.8}$$

as outlined in [46], here $g' = \frac{g\Delta\rho}{\rho_r}$ is called the reduced gravity which is always less than g. The baroclinic mode is therefore slower than the barotropic mode of wave.

Figure 4.7 shows the phase speeds of the baroclinic and barotropic modes of two-layer fluid. It is clear from the figure that the phase speed of barotropic mode is identical with that of ordinary single layer SWE even if we have different density gradient between two layers of fluid. On the other hand, the phase speed of the baroclinic mode is always less than barotropic mode.

The ratio of the disturbance amplitude on the free surface (B) to that of the interior interface (A) is found in [46];

$$\frac{B}{A} = \frac{c^2}{c^2 - gH_2} \tag{4.9}$$

For the barotropic mode, the ratio of disturbances on the two interfaces can be found by substituting $c^2 = \sqrt{gH}$ in the equation (4.9), i.e.

$$\frac{B}{A} = \frac{c^2}{c^2 - gH_2} = \frac{H}{H_1} \tag{4.10}$$

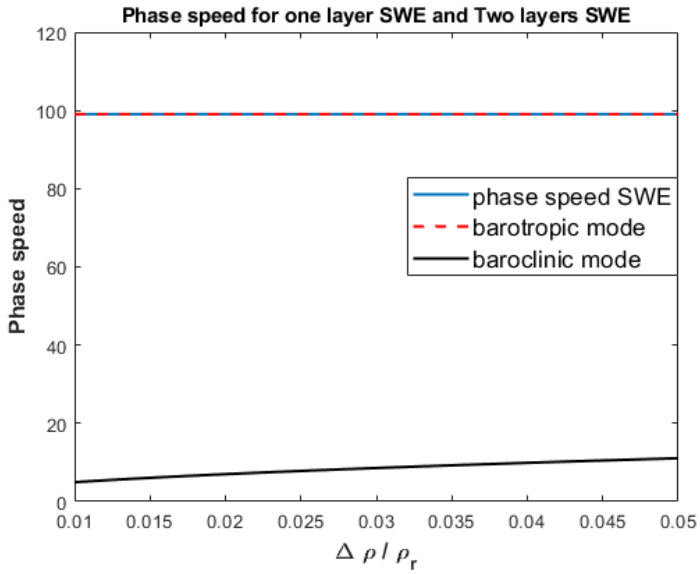

FIGURE 4.7: Comparison of phase speed for ordinary single layer and two layers (Barotropic and Baroclinic mode of wave motions) shallow water equations.

where H_1 and H_2 are the height of the lower and upper layer respectively. This means that, due to the presence of the barotropic mode, the disturbance on the free surface is slightly larger in amplitude than the disturbance on the internal interface. Beside of this, the positive ratio of the disturbance amplitude for barotropic mode confirms that two layers should be in phase.

In contrast, for baroclinic mode, the ratio of disturbances on the two interfaces can be found by substituting $c = \sqrt{g' \frac{H_1 H_2}{H}}$ in the equation (4.9), i.e.

$$\frac{B}{A} = -\frac{g'}{g}\frac{H_1}{H} \tag{4.11}$$

This shows that the disturbance on the free surface is much smaller in amplitude than that on the internal interface, and the two interfaces are out of phase.

4.2.2.2 Perturbation of inertial mass at top layer

We consider two layers of fluid where lower layer is denser than the top layer $\left(\frac{\Delta\rho}{\rho_r} \ll 1\right)$. To study the propagation of internal wave, in this simulation, we consider a small perturbation of inertial mass from free surface. The perturbed η function is;

$$\eta_{perturb} = 10e^{\frac{-\frac{1}{6}(x-0.2L_x)^2}{\delta^2}} \tag{4.12}$$

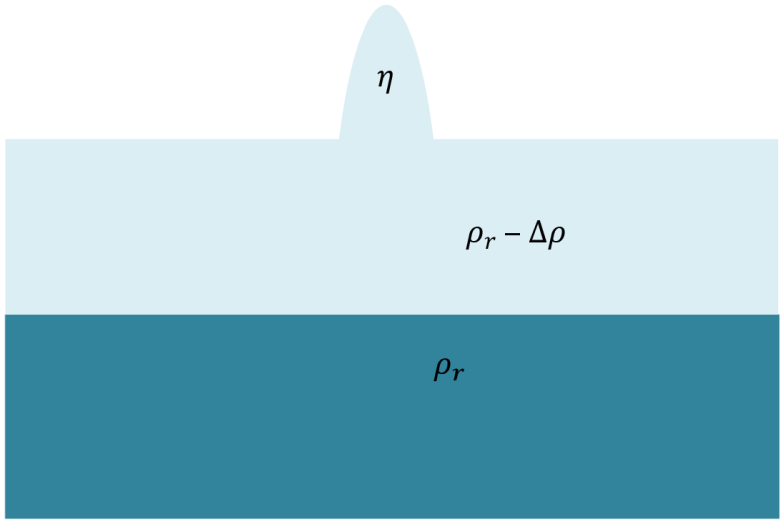

FIGURE 4.8: Two layer of stratified ($\left(\frac{\Delta\rho}{\rho_r} \ll 1\right)$) fluid with a small perturbation to the inertial mass in the top layer.

In the next few figures of this section, we observe how the perturbation of inertial mass (i.e. free surface perturbation) as well as different density differences affect the propagation of the barotropic and baroclinic modes and how the height of two layers change.

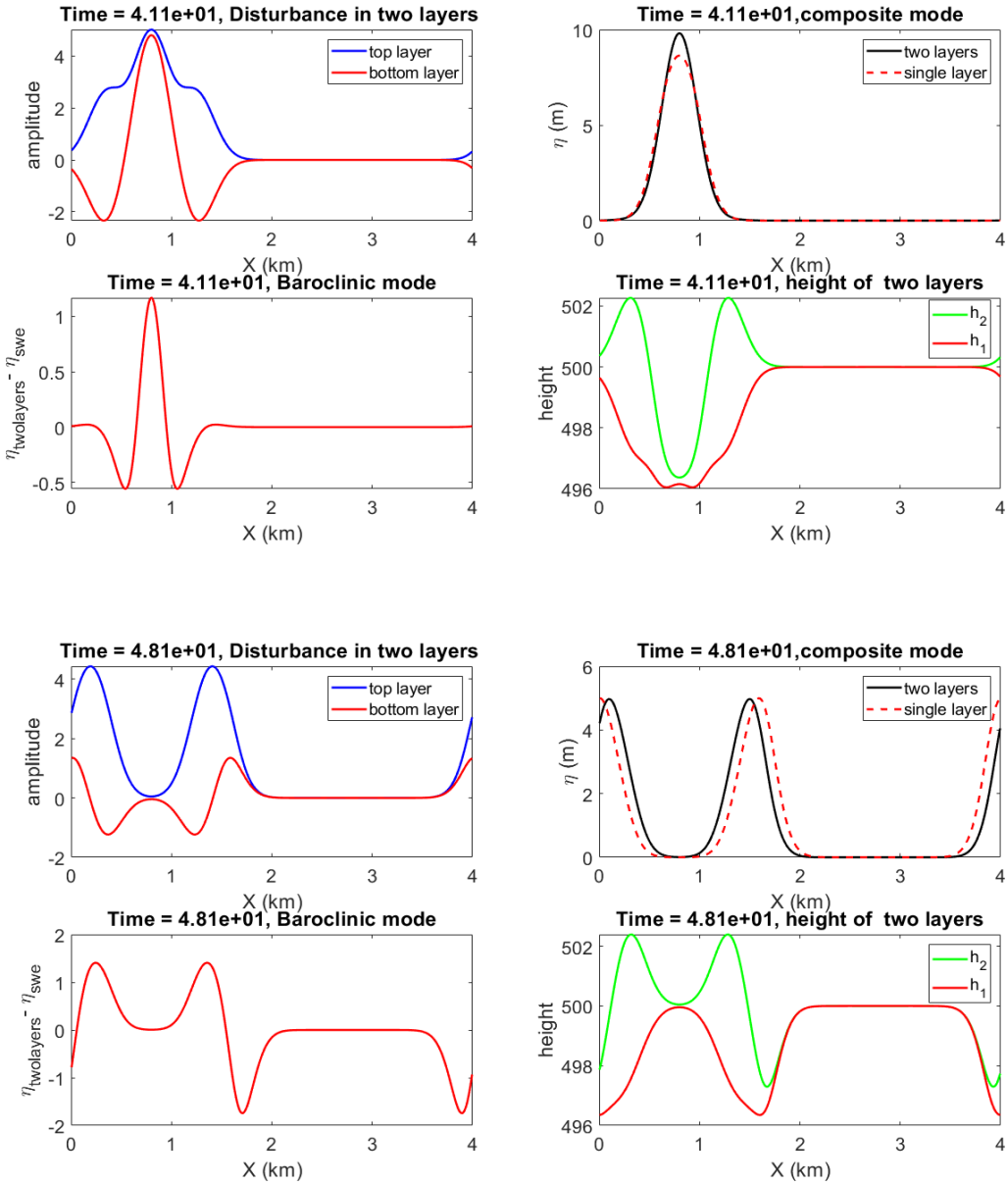

FIGURE 4.9: Propagation of wave at times $t = 41.1$ s and $t = 48.1$ s with $\Delta\rho = 0.1$. Disturbance of two layers, $\eta_1 = \mu_1 - H_1, \eta_2 = \mu_2 - H_2$, Composite mode, $\eta_{comp} = \sum_{i=1}^{2} \mu_i - H$. and Baroclinic mode $= \eta_{comp} - \eta_{swesloution}$.

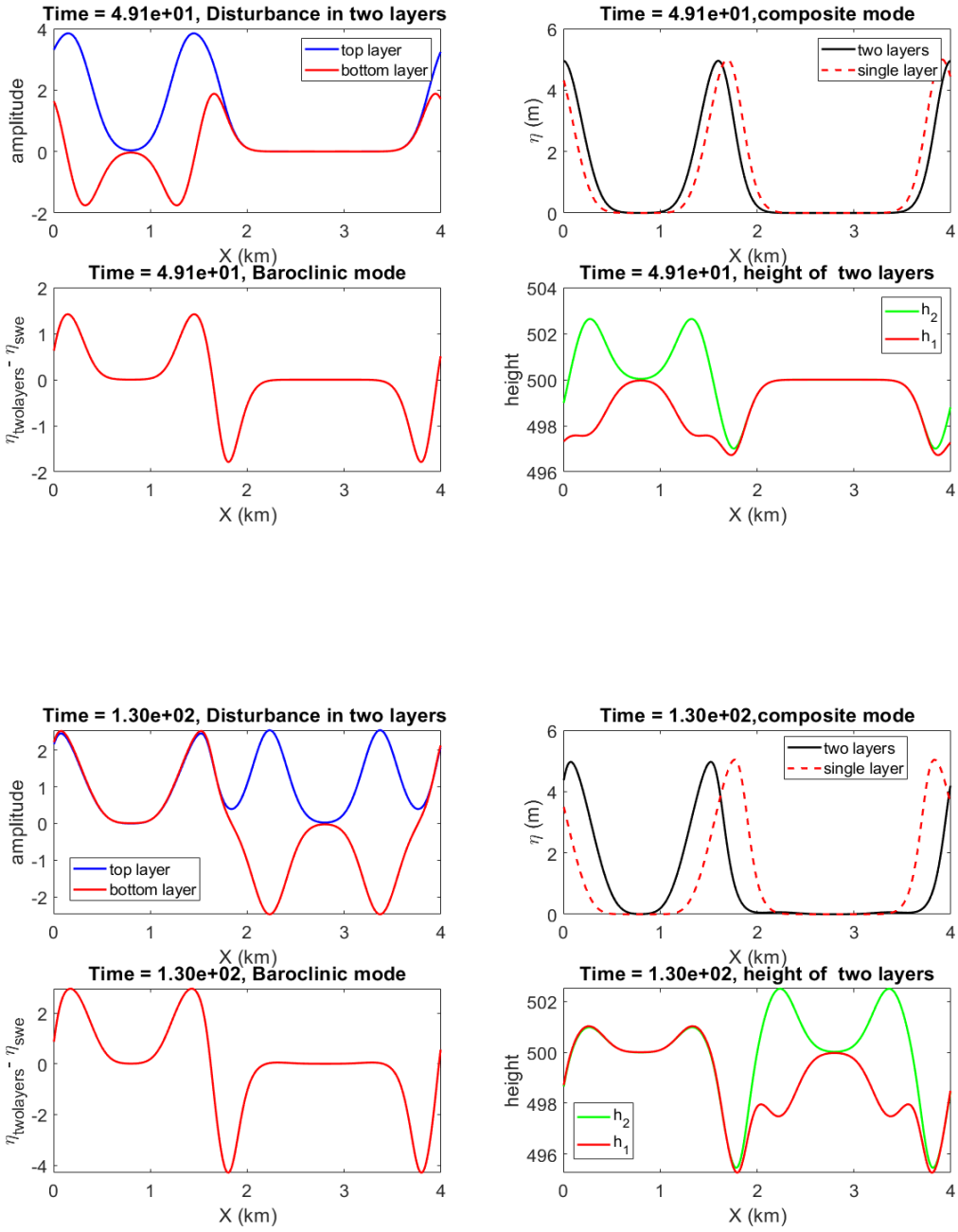

FIGURE 4.10: Propagation of wave at times $t = 49.1$ s and $t = 130$ s with $\Delta\rho = 0.1$. Disturbance of two layer, $\eta_1 = \mu_1 - H_1, \eta_2 = \mu_2 - H_2$, Composite mode, $\eta_{comp} = \sum_{i=1}^{2} \mu_i - H$. and Baroclinic mode $= \eta_{comp} - \eta_{swesloution}$.

4.2.2.3 Perturbation of inertial mass at interface of two layer

To study the propagation of an internal wave, in this simulation, we now consider a small negative perturbation of inertial mass at the interface of two layers . The perturbed function used at the interface is;

$$\text{perturb}_{\text{function}} = -10e^{\frac{-\frac{1}{6}(x-0.2L_x)^2}{\delta^2}} \tag{4.13}$$

And the densities of the two layers are the same as in the previous section.

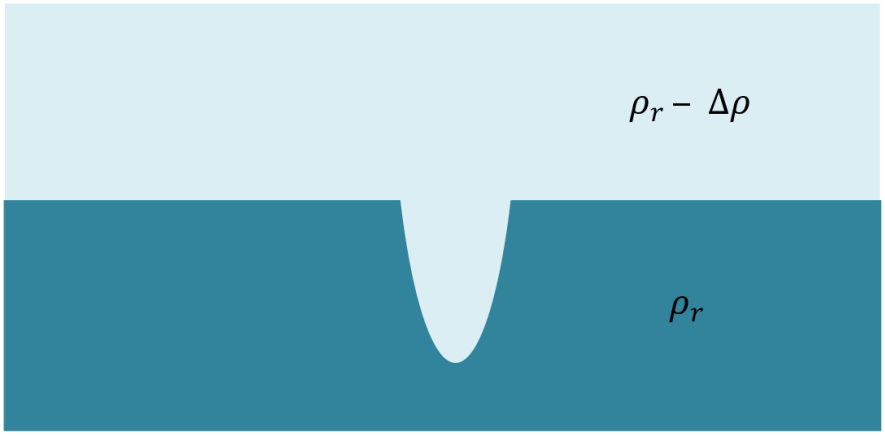

FIGURE 4.11: Two layers of stably stratified $\left(\left(\frac{\Delta\rho}{\rho_r} \ll 1\right)\right)$ fluid with with a negative perturbation to the internal layer.

In the next few figures, we observe how the perturbation of inertial mass at the interfaces as well as different density gradient affects both the free surface and the interface of two layers, propagation of barotropic and baroclinic mode and how the height of two layers changes.

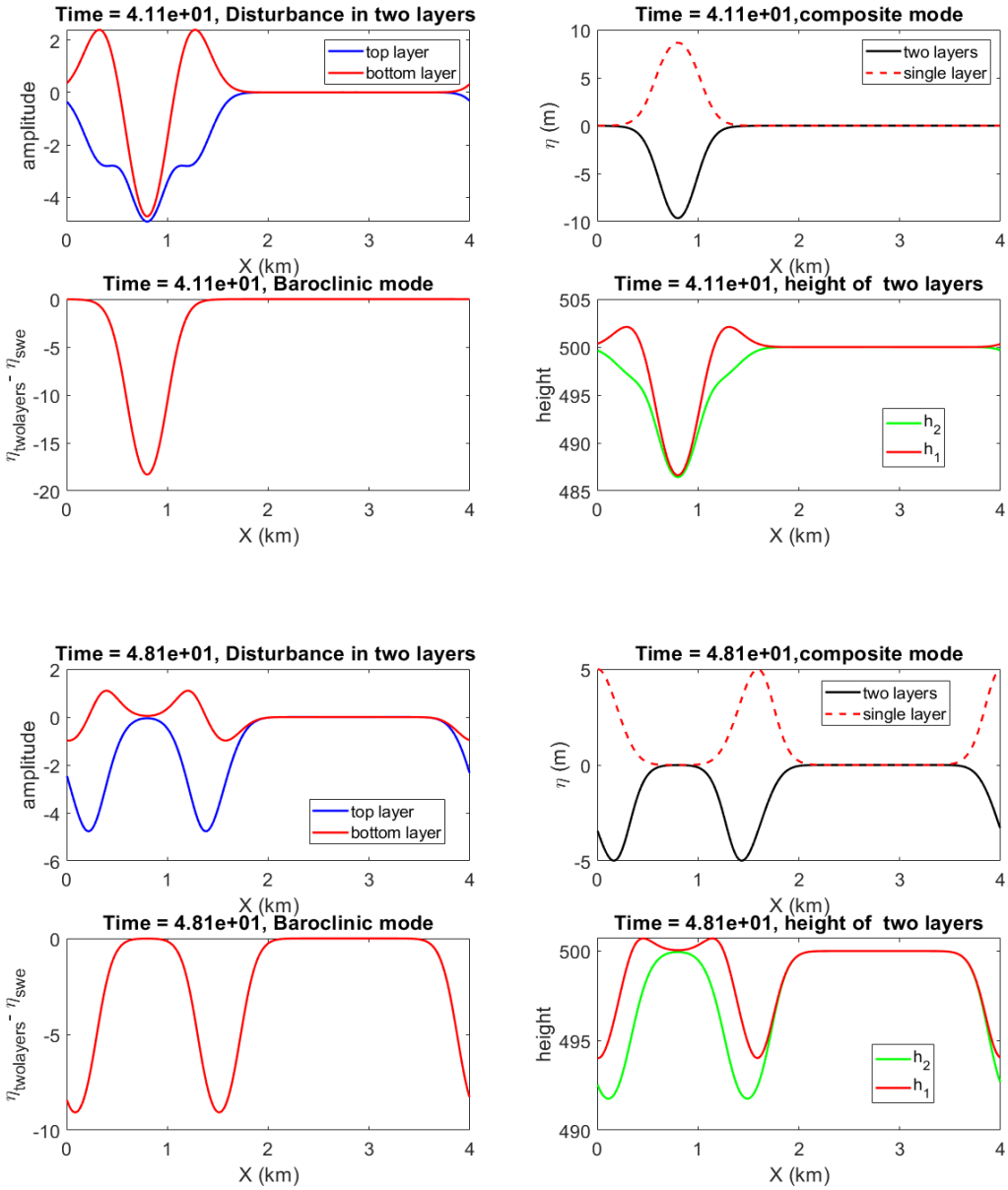

FIGURE 4.12: Propagation of wave at times $t = 41.1$ s and $t = 48.1$ s with $\Delta\rho = 0.1$. Disturbance of two layer, $\eta_1 = \mu_1 - H_1, \eta_2 = \mu_2 - H_2$, Composite mode, $\eta_{comp} = \sum_{i=1}^{2} \mu_i - H$. and Baroclinic mode $= \eta_{comp} - \eta_{swesloution}$.

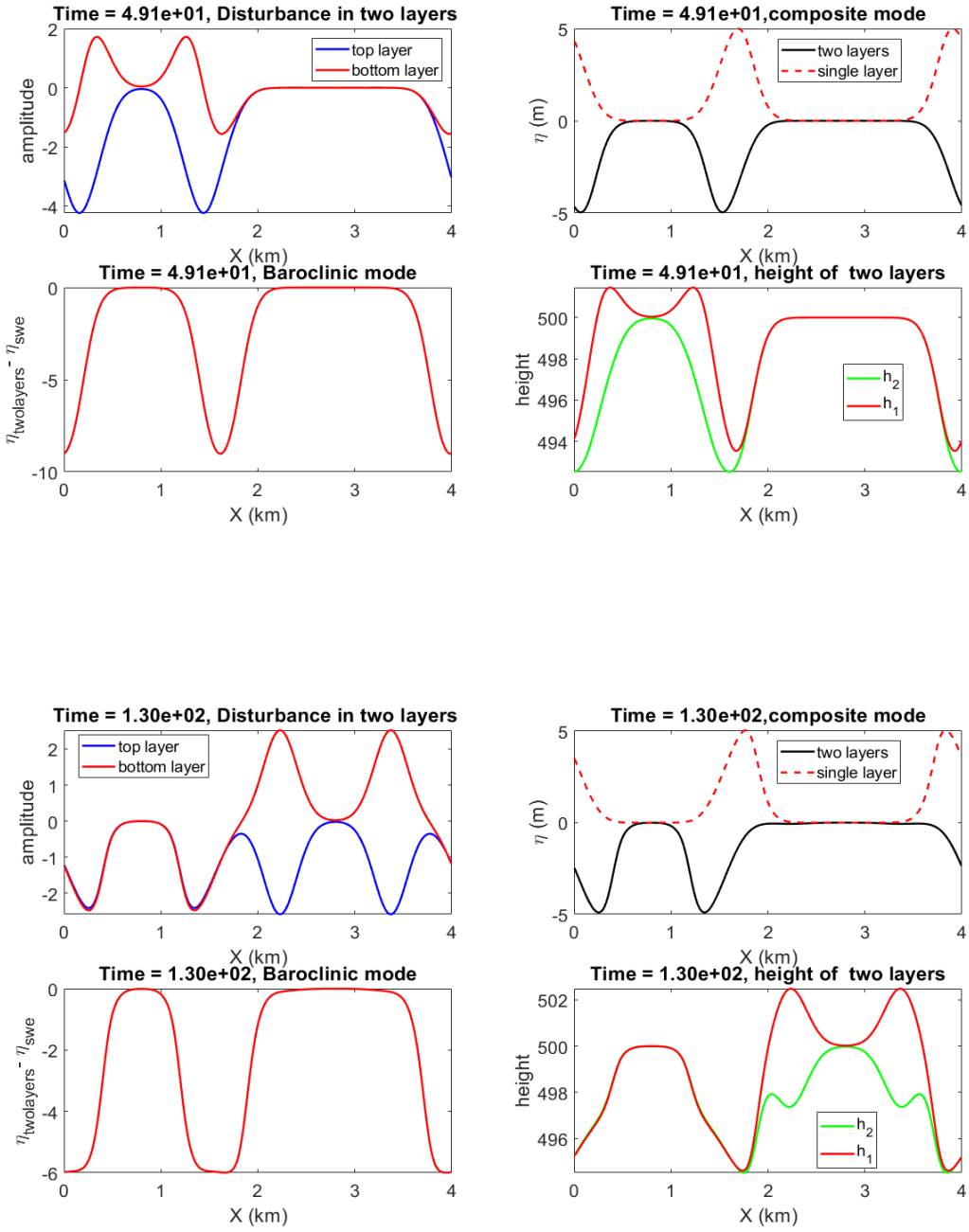

FIGURE 4.13: Propagation of wave at times $t = 49.1$ s and $t = 130.0$ s with $\Delta\rho = 0.1$. Disturbance of two layer, $\eta_1 = \mu_1 - H_1, \eta_2 = \mu_2 - H_2$, Composite mode, $\eta_{comp} = \sum_{i=1}^{2} \mu_i - H$. and Baroclinic mode $= \eta_{comp} - \eta_{swesloution}$.

4.2.2.4 Perturbation of density at interface

In contrast to the previous case, we now add a positive perturbation to the internal layer. The perturbed density function is;

$$\rho_{perturb} = \rho_r \Delta\rho \left(\exp\left(-\left(\left(x - \frac{L_x}{2} \right)^2 + \left(z - \frac{H}{2} \right)^2 \right) / (0.3H)^2 \right) \right) \tag{4.14}$$

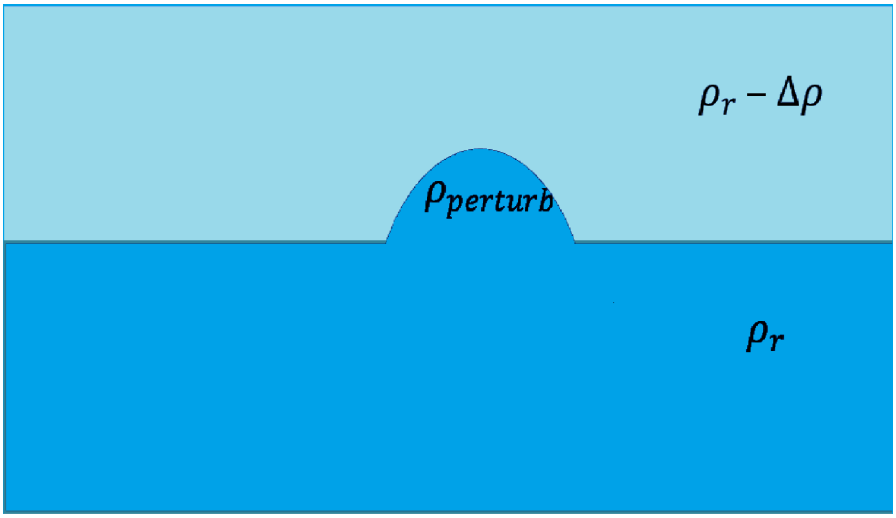

FIGURE 4.14: Two layers of stably stratified fluid with a positive perturbation to the internal layer.

The impact of the perturbation of density on the top layer as well as at the interfaces of two layers have been observed from the following figures. Apart from this, we also observe the changes of water height and the propagation of baroclinc mode for two layers.

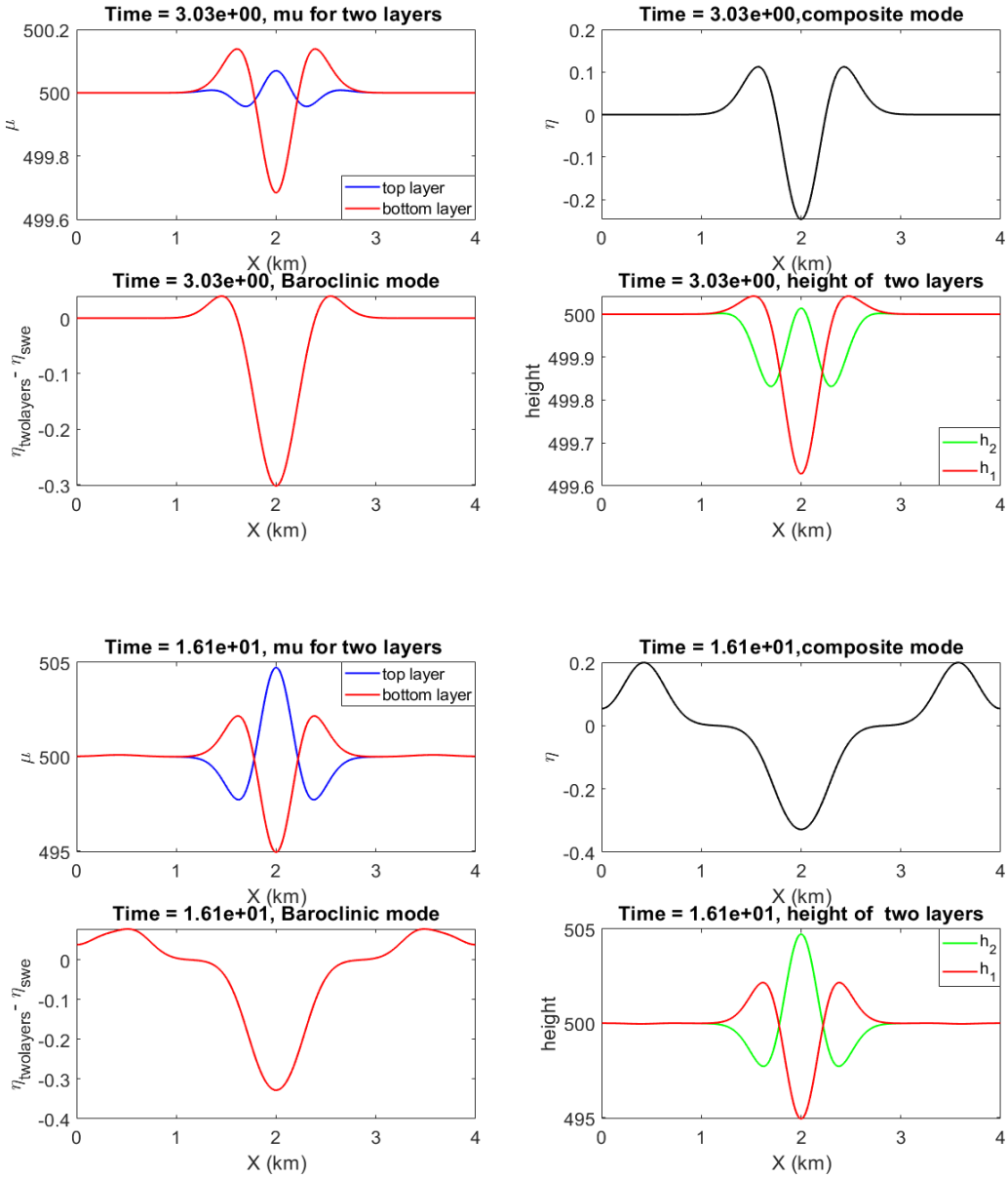

FIGURE 4.15: Propagation of wave at times $t = 3.03$ s and $t = 16.1$ s with $\Delta\rho = 0.1$. Disturbance of two layer, $\eta_1 = \mu_1 - H_1, \eta_2 = \mu_2 - H_2$, Composite mode, $\eta_{comp} = \sum_{i=1}^{2} \mu_i - H$. and Baroclinic mode $= \eta_{comp} - \eta_{swesloution}$.

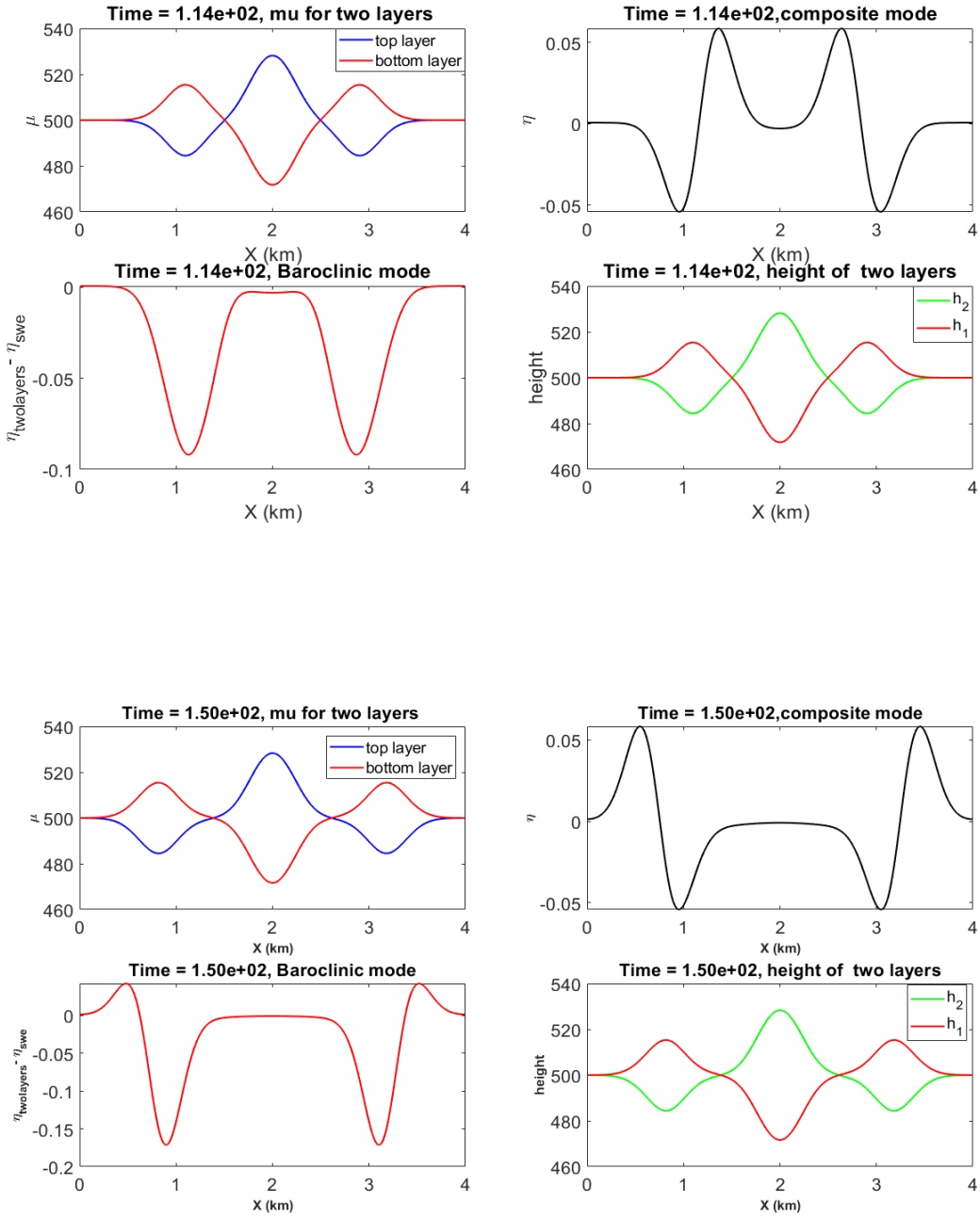

FIGURE 4.16: Propagation of wave at times $t = 114.2$ s and $t = 150.2$ s with $\Delta\rho = 0.1$. Disturbance of two layer, $\eta_1 = \mu_1 - H_1, \eta_2 = \mu_2 - H_2$, Composite mode, $\eta_{comp} = \sum_{i=1}^{2} \mu_i - H$. and Baroclinic mode $= \eta_{comp} - \eta_{swesloution}$.

From all of these above mentioned test cases, the key point that we want to investigate to validate our model is the phase speed and the characteristics of barotropic and baroclinic modes. First of all, it is noted that our choice of initial conditions and parameters ensures that our case satisfies all the validity conditions for the two-layer SWE model (i. e. $\frac{\eta}{H} \ll 1$ and $\frac{Lx}{H} \gg 1, \Delta\rho/\rho_r \ll 1$).

The composite mode of the test case 4.2.2.2 shows that, the waves are very similar, but the phase speed of two-layer SWE model is a bit slower than that of single layer SWE. If we look at the peak of wave both for single and two-layer SWE, we can see that, the peak of single layer SWE reaches to the boundary at $t = 48.1$s, while for two-layer, it reaches at $t = 49.1$s. Here, we observed the phase speed for single layer is $c_{numerical} = \frac{700}{(48.1-41.1)} = 100.0\text{ms}^{-1}$, which is approximately identical to the phase speed of linearized SWE, $c = \sqrt{gH} = \sqrt{9.81 * 1000} \approx 99.0\text{ms}^{-1}$ what we know theoretically. On the other hand, from the composite mode (i.e. perturbation to the free surface) we observed the phase speed for two-layer is $c_{numerical} = \frac{700}{(49.1-41.1)} = 87.5\text{ms}^{-1}$.

Now, if we look back to the equation (4.7) and (4.8) we see that, theoretically, the phase speed for the barotropic and baroclinic mode (for the vertical length H and $\Delta\rho$, we used in our model) is,

$$c_1 = \sqrt{gH} = \sqrt{9.81 * 1000} \approx 99.0\text{ms}^{-1}$$

$$c_2 = \sqrt{g'\frac{H_1 H_2}{H}} = \sqrt{9.81 * 0.1 * (500^2)/1000} \approx 15.7\text{ms}^{-1}$$

and from equation (4.15) and (4.16), the ratio of disturbance on two interfaces for the barotropic and baroclinic mode is,

$$\frac{B}{A} = \frac{H}{H_1} = 2 \tag{4.15}$$

$$\frac{B}{A} = -\frac{g'}{g}\frac{H_1}{H} = 0.1 * (1/2) = 0.05 \tag{4.16}$$

Since the barotropic and baroclinic mode exists on both layers and the direction of propagation of these two modes are relatively opposite to each other, so according to the principle of superposition of wave, the phase speed of their composite mode is, $99.4 - 15.7 = 83.3\text{ms}^{-1}$, which verifies that, our numerical model gives qualitatively accurate result.

In addition, we also found that, at the free surface, the phase speed of the baroclinic wave is slower than the barotropic wave. From the figure, it is seen that, the peak of barotropic wave reaches to the boundary at $t = 49.1$s while the former one reaches to the boundary at $t = 51.1$s.

The behavior of two modes for the dispersion relation with a free surface can be explained by using the following figure.

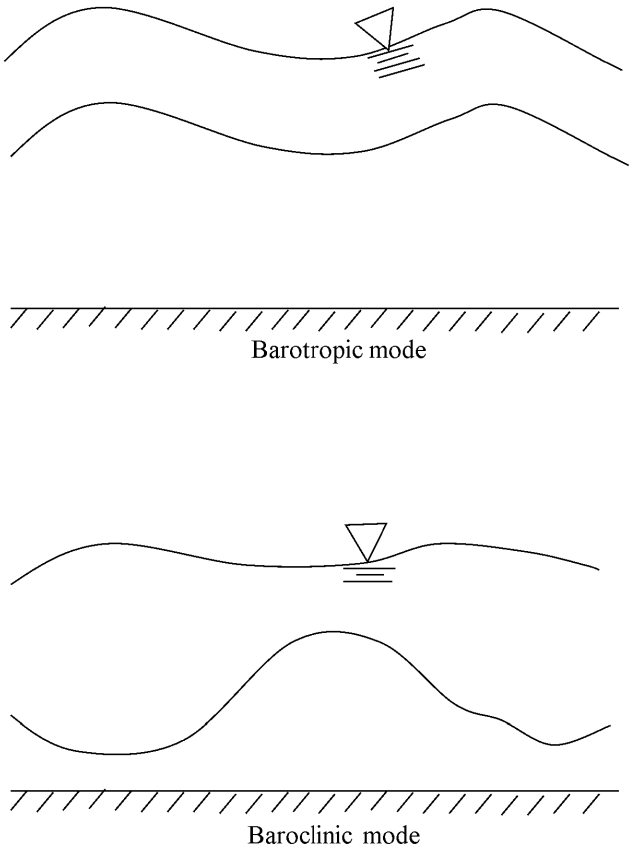

FIGURE 4.17: The behavior of two modes for the dispersion relation with a free surface.

For the barotropic mode, the pressure is constant along the line of constant density and the dominant wave is surface wave. Because this solution is independent of the density differences between layers and the barotropic mode behaves like a way as if the system is unstratified.

In contrast, for baroclinic mode, the pressure varies along the line of constant density and the internal wave motion is much greater than the surface wave and they are 180° out of phase.

Also, when the pycnocline moves down, the total thickness of upper layer increases. Thus in the test case 4.2.2.3, the value of η (perturbation to the internal layer) corresponds to the downward movement of pycnocline, increases the thickness of the upper layer and downwells at pycnocline, i.e. negative vertical velocity has found there.

In test case 4.2.2.4, a positive perturbation of density at the interface of two layer generates internal wave. As we know that, internal waves oscillate in a fluid medium. The water layer don't mix and the interface remain intact. Thus we observe internal wave propagates back and forth along the line of density differences. Since internal waves move both in horizontal and vertical direction, we also observe the generation of waves at the free surface.

Thus the analyzation of these above test cases confirms the validity of two layer shallow water model. For multilayer SWE model, we just subdivided this two-layer into several layers. Thus the validity of two-layer SWE model also confirms the validity of our multilayer SWE model.

4.3 Numerical experiments

In our daily lives, we experience different types of waves and thus waves are all around us. A wave is an immaterial thing and is created by energy passing through a medium. For our numerical experiments we consider the medium is sea water. The ocean is never still and waves in the ocean are most commonly created by the wind. Ocean waves that occurs at the top layer or free surface of ocean is known as surface waves. These waves are created by the stress force between wind and the surface water of ocean. Apart from this, sometimes they also form due to the geological effects (e.g. tsunamis).

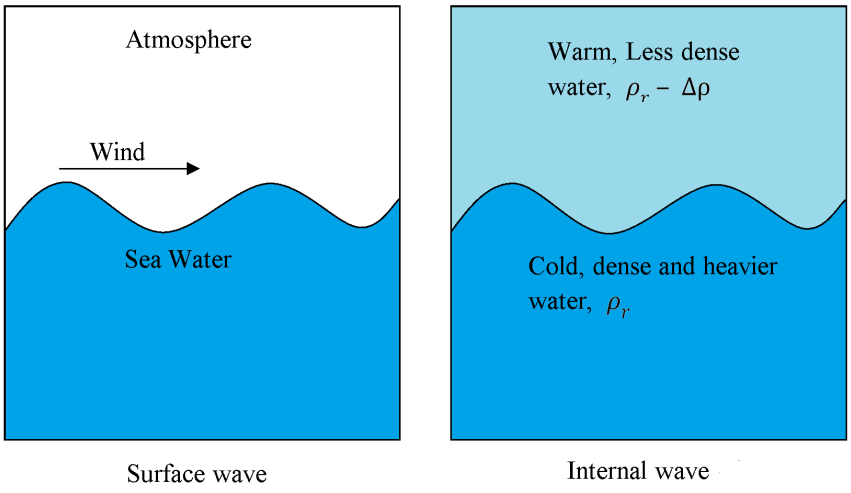

FIGURE 4.18: Comparison between surface waves and an internal wave. Surface waves form at the free surface of ocean due to the stress force between wind and ocean's top layer while Internal waves occur along a boundary of different densities of ocean water.

On the other hand, waves in the interior of the ocean are called internal waves. They can form when the water body consists of layers of different density due to the variation of temperature and salinity. Internal waves also form in the atmosphere

and are visible as periodic bands of clouds, often in the lee of mountains. There are no internal waves in homogeneous fluid where the density doesn't change with depth.

Internal waves transport energy and momentum and they can lead to mixing when they break, thus they play important role in the vertical mixing of ocean. Beside this, surface wave is also important because they interact with internal wave. This section basically deals with the interaction of wave that propagates at the top and underneath of the ocean surface. Regarding this, we consider the following test cases;

1. Perturbation of inertial mass from free surface for flat bottom of ocean with two layered density,

2. Perturbation of inertial mass from free surface with two layered density and bathymetry,

3. Perturbation of inertial mass from free surface for flat bottom of ocean with linearly stratified density,

4. Perturbation of inertial mass from free surface with linearly stratified density and bathymetry,

5. Perturbation of density at the boundary of different density with flat bottom of ocean,

6. Perturbation of density at the boundary of different density with bathymetry of ocean.

4.3.1 Perturbation of free surface for both flat and non-flat bottom of ocean with two-layer density

We are interested to study the generation of internal waves. The domain is $\Omega = [0, 4000]$m.

Flat bottom:

For flat bottom of ocean, the perturbation of the free surface is

$$\eta(x, 0) = 10e^{\frac{-\frac{1}{6}(x-0.2L_x)^2}{\delta^2}}$$

we consider periodic boundary conditions.

Non-flat bottom:

The bathymetry is defined by

$$\beta(x) = 70e^{\frac{-\frac{1}{4}(x-0.7L_x)^2}{\delta^2}}$$

The two-layer stably stratified density is given by,

$$\rho(z) = \rho_r \left(1 - \frac{\Delta\rho}{2}\left(1 - \tanh\left(\frac{-z + H/2}{0.05H}\right)\right)\right)$$

where $\Delta\rho = 0.1$ and $H = 1000$ m. Figure 4.19 shows the initial perturbation of inertial mass and initial density distribution at time $t = 0$ s for flat and non-flat bottom of ocean respectively.

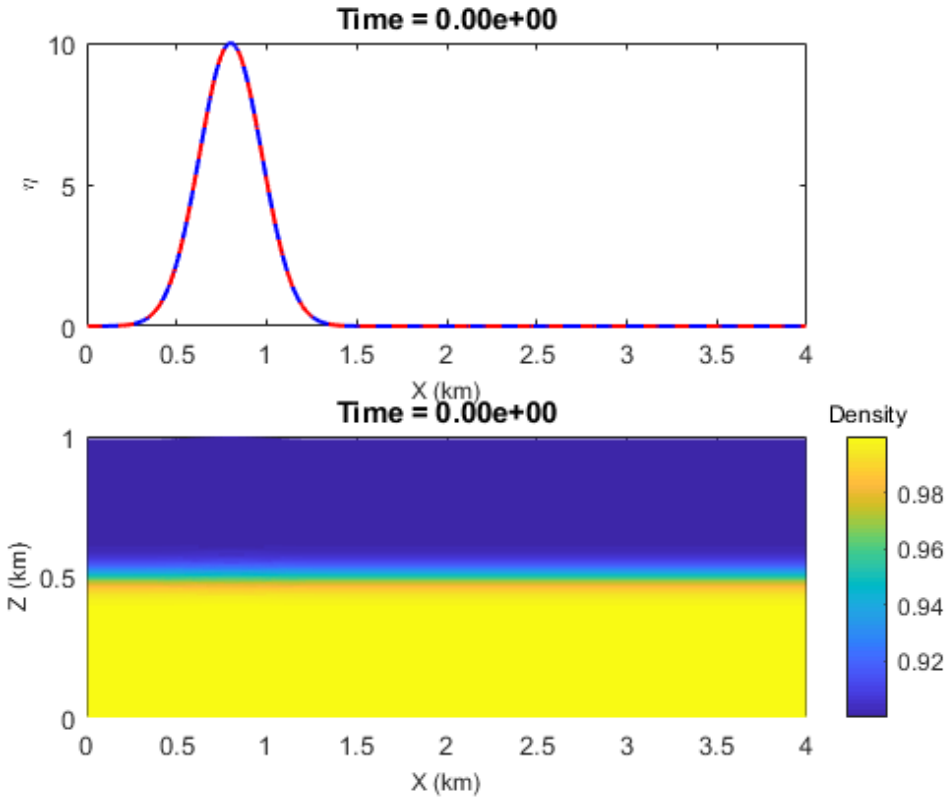

FIGURE 4.19: Initial elevation of water mass from free surface ($\eta(m)$) which is a Gaussian profile of the form $\eta(x,0) = 10e^{\frac{-\frac{1}{6}(x-0.2L_x)^2}{\delta^2}}\ \eta(m)$ and initial distribution of density. The spatial domain X is rescaled as $\frac{L_x}{H}$.

To illustrate the results, we plot the change in inertial mass (μ) as well as the perturbation in normalized density (θ) for different time. To visualize the propagation of internal waves, we subtracted the mean background density stratification from the normalized density function. The propagation of surface waves and internal waves for flat bottom case has been plotted in figures (4.20-4.22). Subfigure.1 of all of these snapshot, represents the comparison of single layer and multilayer SWE for surface wave. Subfigure.2 represents the perturbation in normalized density without mean background density. As we see, due to the perturbation to the

free surface of ocean, both a surface wave and an internal wave are produced and propagate away from the original disturbance. The process at work is easy to apprehend: a positive perturbation causes water to rise above the surface level, then gravity pulls it back down since water is heavier than air and the forces that acquired during the falling movement causes the water to penetrate beneath it's equilibrium level and results a buoyancy motion.

Surface waves can propagate only in horizontal directions. When a water parcel rises somewhere above the surface level, it added some weight on water there. And the weight of this water creates pressure which is locally higher than normal. Eventually, this pressure anomaly pushes the water to move away from that region and generates another surface rise at some distance away. As a result, we get the translation of disturbance, hence a traveling wave, which we call as surface wave.

Both surface waves and internal waves propagate back and forth with time, since we applied periodic boundary conditions. Internal waves are slower since they rely on a weaker density difference and can propagate both vertically and horizontally. Interestingly, at time $t = 270$ s, the vertical mixing of density has been observed. Since the solution is periodic in time, both waves are propagating back to their origin of perturbation at time $t = 500$ s, as seen in Figure 4.22.

The result for non-flat bottom is illustrated in figures (4.23 - 4.25). As we see in the above mentioned case, the disturbance at the free surface generates an internal wave. Apart from that, since this problem simulates flow over a bump, we also observe the creation of another internal wave. This type of internal waves generate when a stably stratified flow is forced over a bump/ an obstacle. This disturbance

lifts the water parcel above their neutral buoyancy level and therefore buoyancy restoring forces act to excite the vertical oscillation of the perturbed water parcel. During this process, a pressure anomaly generates there and that pressure varies along the line of density differences. Thus we can see the propagation of another internal wave.

The another major difference what we observe between flat and non-flat bottom case is the phase speed and the steepness of the wave. For the non-flat bottom case, the wave moves a bit slower and gets steeper than the flat bottom case. As we outlined in 4.2.1.4, when such a wave model approaches progressively in smaller depth (i.e. the area around the bathymetry where the mean height, H is small, compare to that of other area), the longest components of wave which propagate faster, are being slowed down when reaching smaller depth areas. The shorter following wave components, which are still left behind in larger depth, feel less effect of the depth and tries to catch the longest ones. That's how, we see a steeper wave profile.

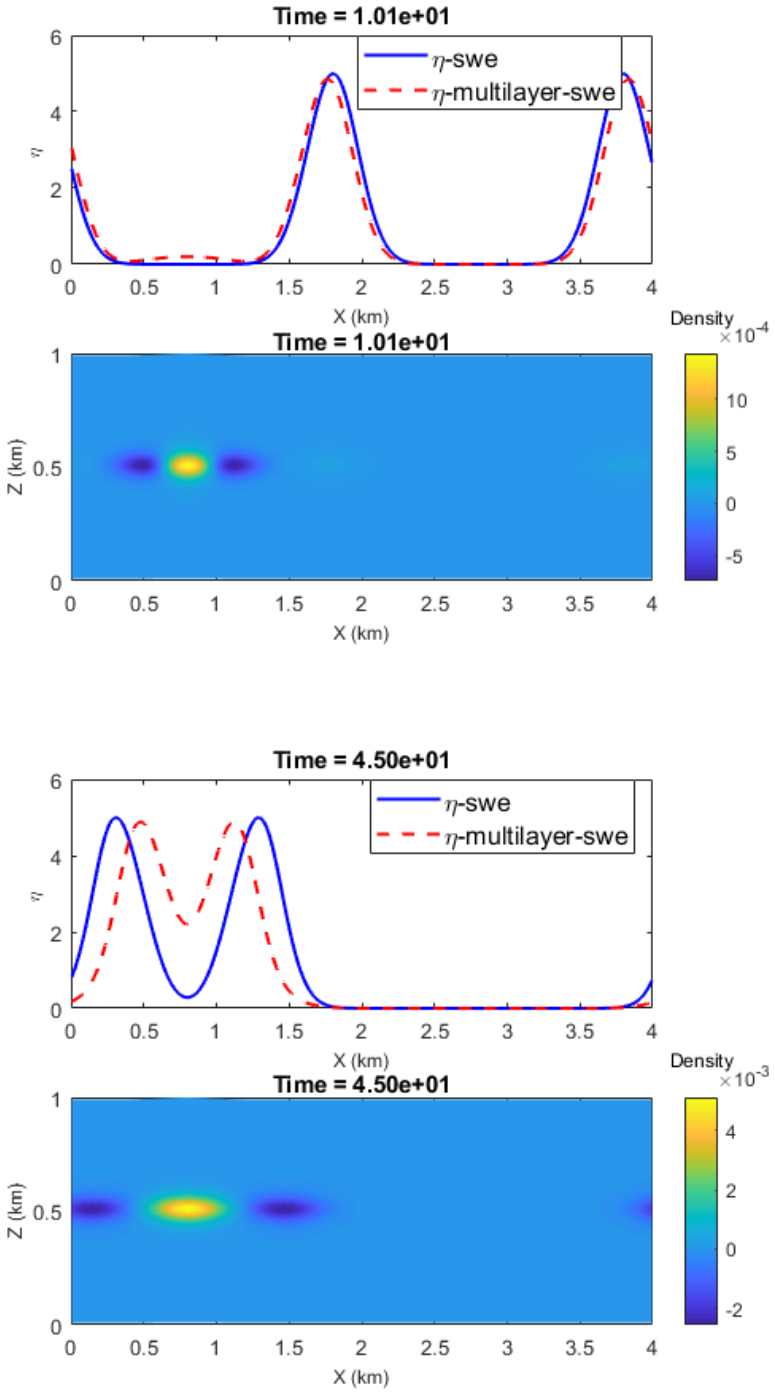

FIGURE 4.20: *Flat bottom:* Surface waves ($\eta(m)$) and Internal waves at $t = 1$ s and $t = 45$ s. Both waves are propagating towards boundary but internal waves are slower than surface wave.

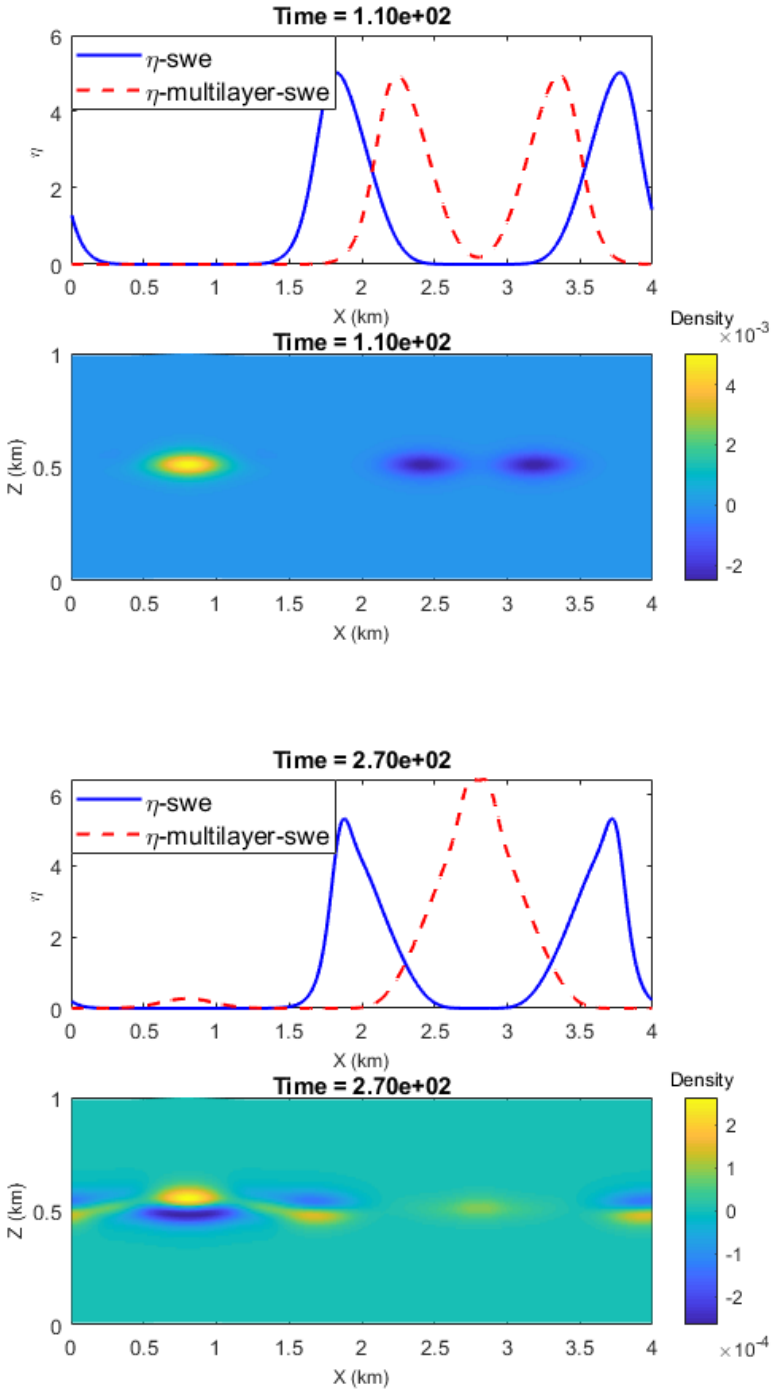

FIGURE 4.21: *Flat bottom:* Surface waves($\eta(m)$) and Internal wave generation at $t = 110$ s and $t = 270$ s. Vertical mixing of density is observed at $t = 270$ s.

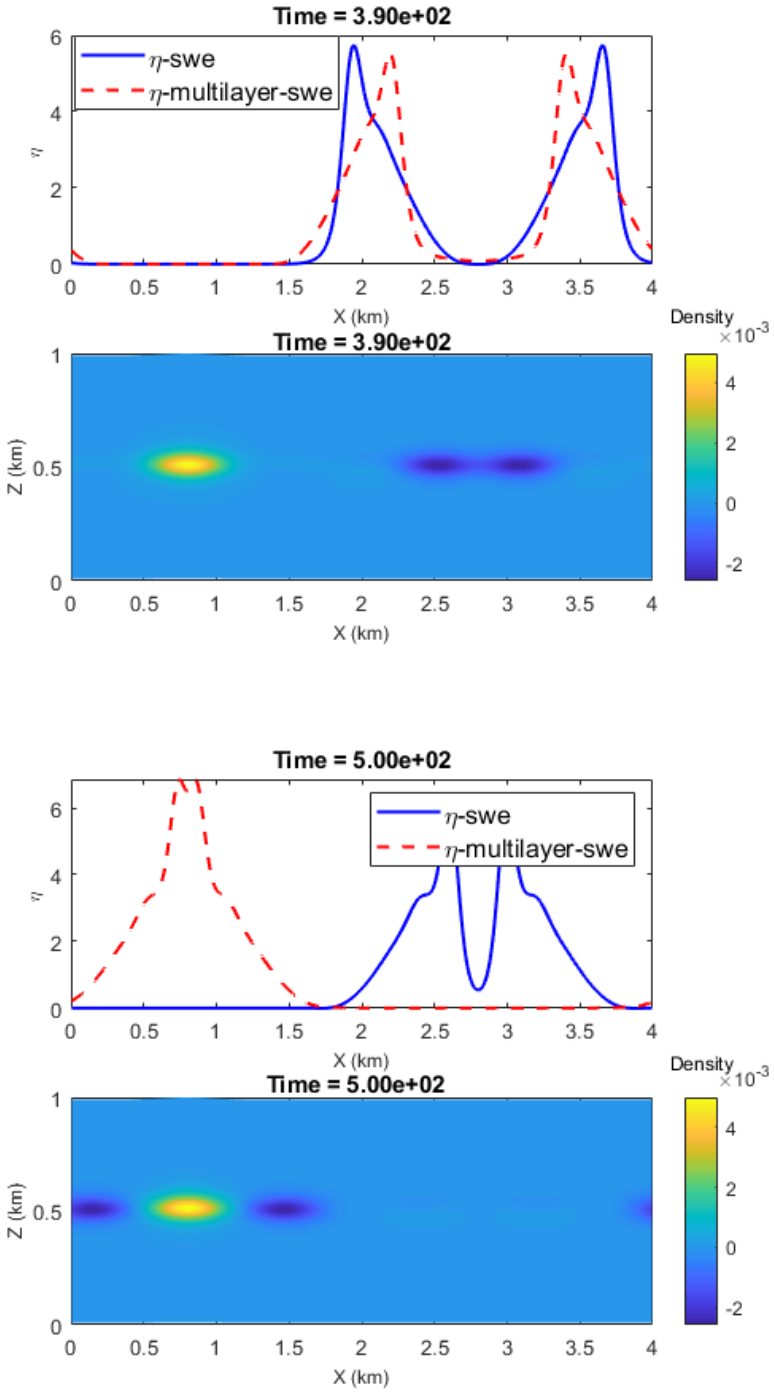

FIGURE 4.22: *Flat bottom:* Surface waves ($\eta(m)$) and Internal wave generation at $t = 390$ s and $t = 500$ s. Both waves propagate back and forth due to the periodic boundary conditions.

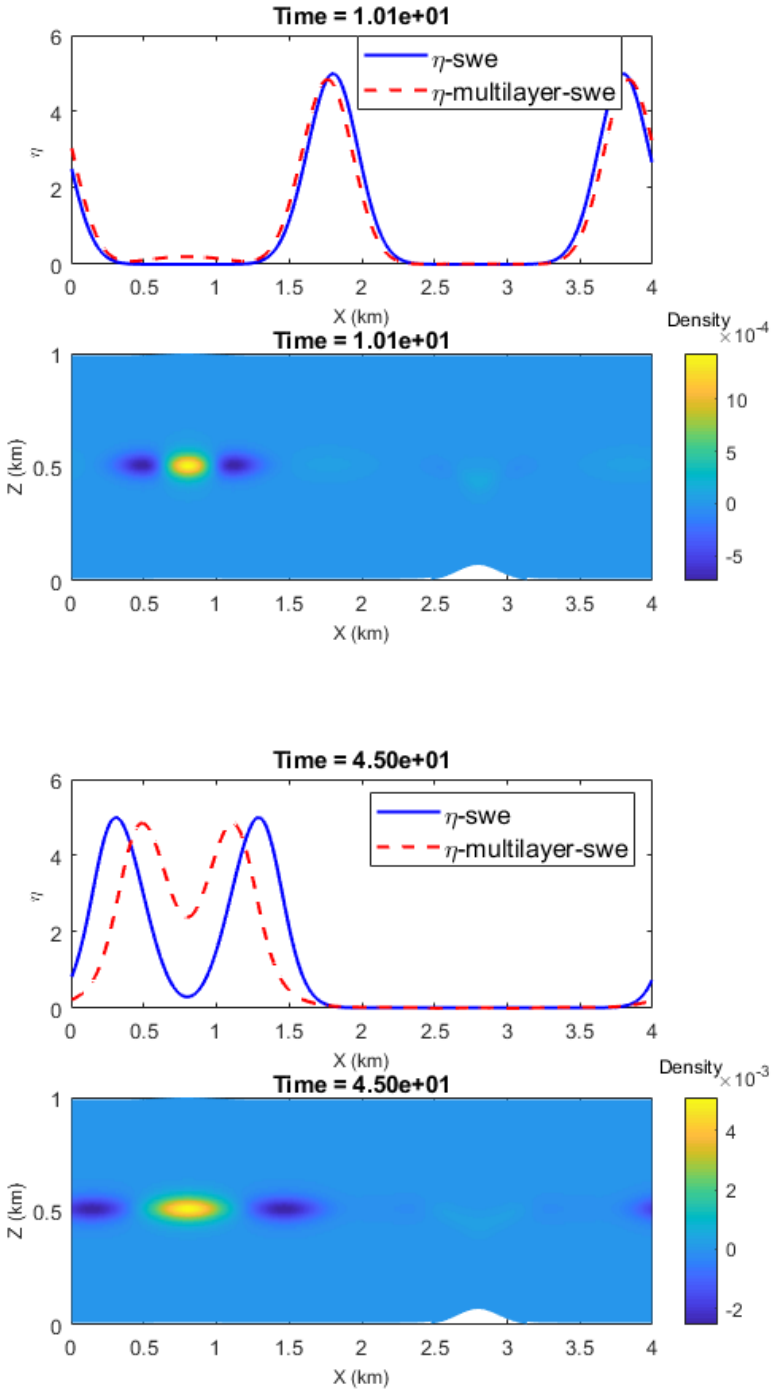

FIGURE 4.23: *Non-flat bottom:* Surface waves ($\eta(m)$) and Internal wave generation at $t = 1$ s and $t = 45$ s. Waves are propagating away from the region of disturbance as well as from topographic region.

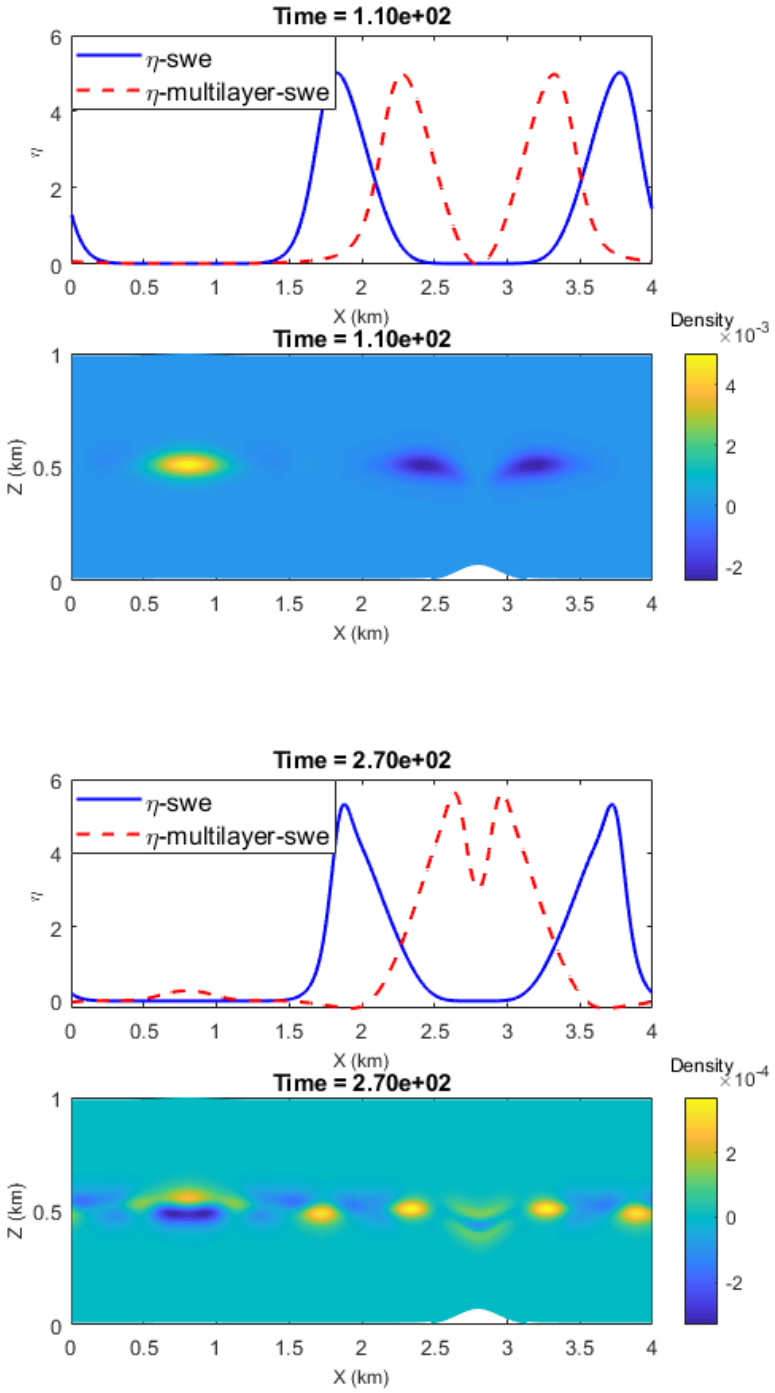

FIGURE 4.24: *Non-flat bottom:* Surface waves ($\eta(m)$) and internal waves at $t = 110$ s and $t = 270$ s. Waves that created due to the disturbance at top layer and vertical mixing is observed at $t = 270$ s.

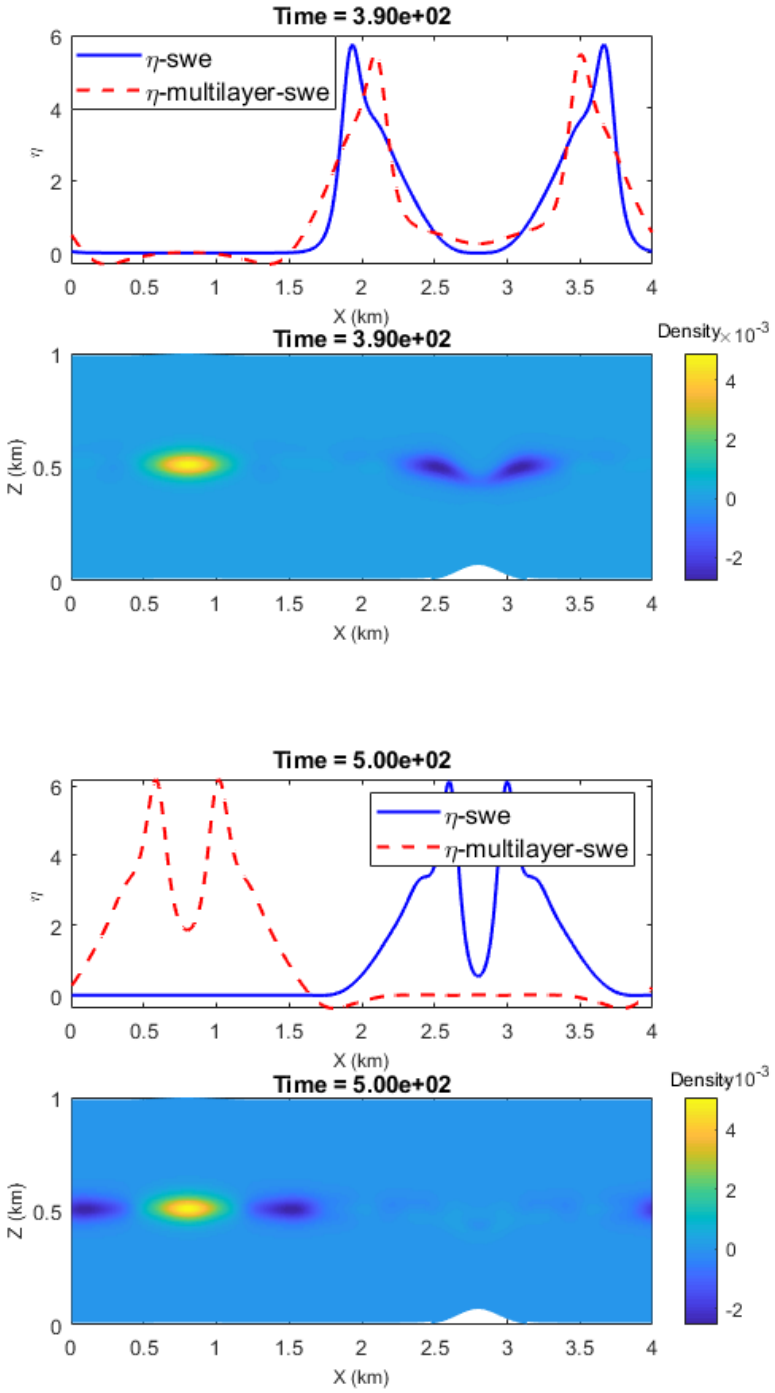

FIGURE 4.25: *Non-flat bottom:* Surface waves ($\eta(m)$) and Internal wave generation at $t = 390$ s and $t = 500$ s. Slicks on the surface is observed when internal waves rebound.

4.3.2 Perturbation of inertial mass from free surface both for flat and non-flat bottom of ocean with linear stratified density

To study the propagation of internal wave in a linear stratified ocean, we chose the same function for the perturbation of inertial mass, as introduced in section 4.3.1, both for flat and non-flat bottom case. Also the horizontal and vertical domain as well as the bathymetry function we consider for this test case is similar to the case 4.3.1.

But for the density stratification, a linear stratified density function is given as,

$$\rho = \rho_r \left(1 - \Delta\rho \frac{z}{H}\right)$$

where $\Delta\rho = 0.1$ and $H = 1000$ m. Figure 4.26 shows the initial perturbation of inertial mass and initial density distribution at time $t = 0$ s.

Just as the test case 4.3.1, to visualize the propagation of surface wave and internal wave, we plot the change in free surface height as well as the perturbation in normalized density (θ) for different times. As in two layer density case, we observe that both surface waves and internal waves propagate in a similar pattern. However, in this case, the internal waves propagate away from the region of disturbance in an angle to the vertical. Furthermore, for internal waves, energy propagates in the direction of group velocity. This means that, internal wave which is generated by a localized source, could never have the appearance of concentric circular crest as surface waves does [47], instead of having it, the crests and other surfaces of

constant phase propagate radially outward from the source. Because waves energy propagates in the direction of group velocity, which is parallel to the surface of constant phase.

For $\omega \leq N$, all these surfaces move at an angle $\theta = \cos^{-1}(\omega/N)$ to the vertical and therefore, all the wave energy travels from the source region in an angle to the vertical. In addition, the direction of the propagation of wave can be determined by the fact that, the phase velocity is perpendicular to the group velocity. This means, if the group velocity has positive vertical component then the phase velocity has negative vertical component and the other way around.

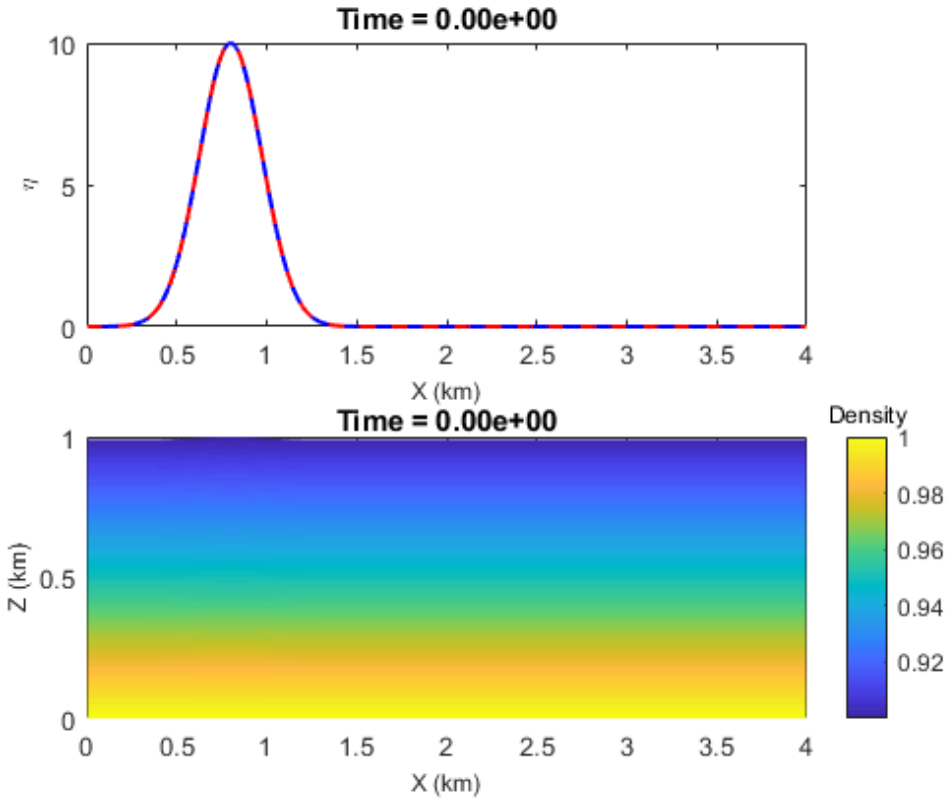

FIGURE 4.26: Initial elevation of water mass from free surface ($\eta(m)$) and initial distribution of density. The spatial domain X is rescaled as $\frac{L_x}{H}$.

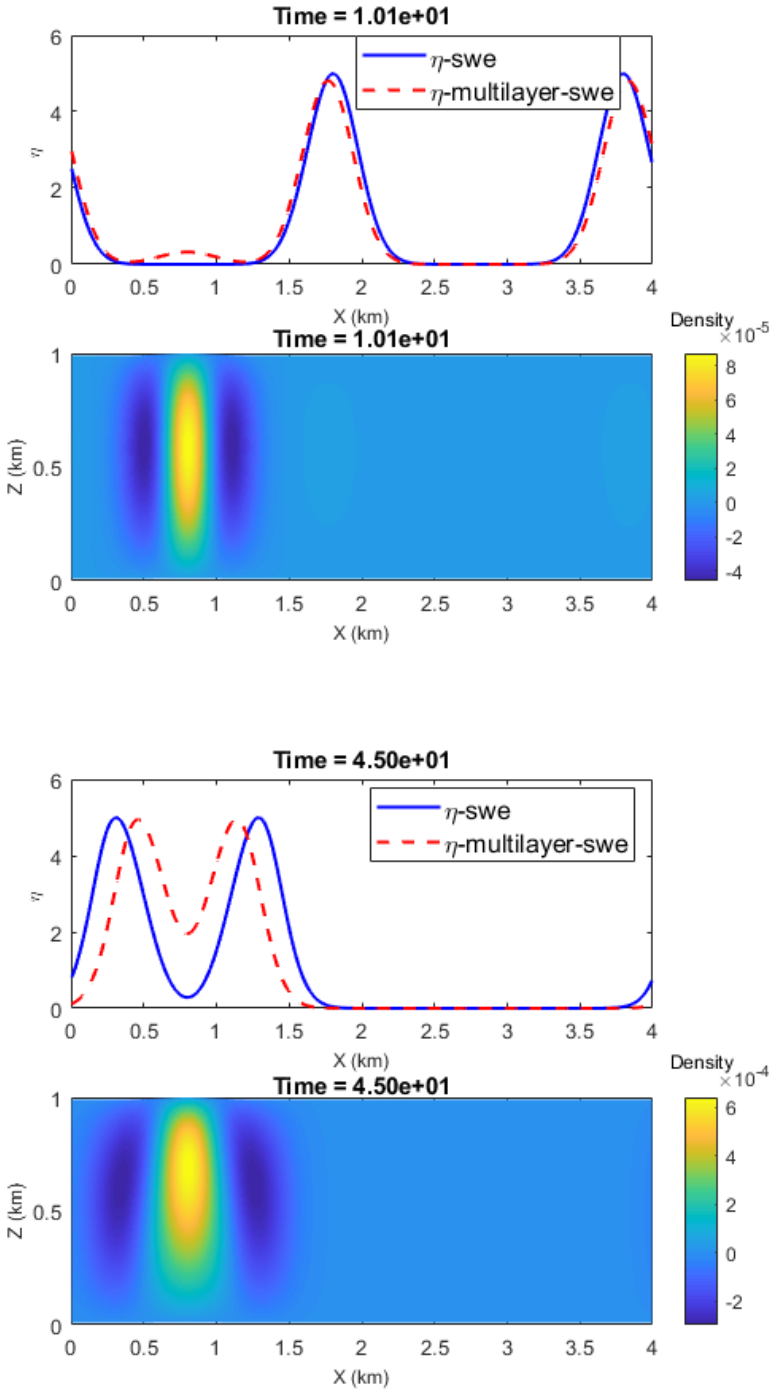

FIGURE 4.27: *Flat bottom:* Surface waves ($\eta(m)$) and Internal wave generation at $t = 1$ s and $t = 120$ s. Waves are propagating away from the region of disturbance.

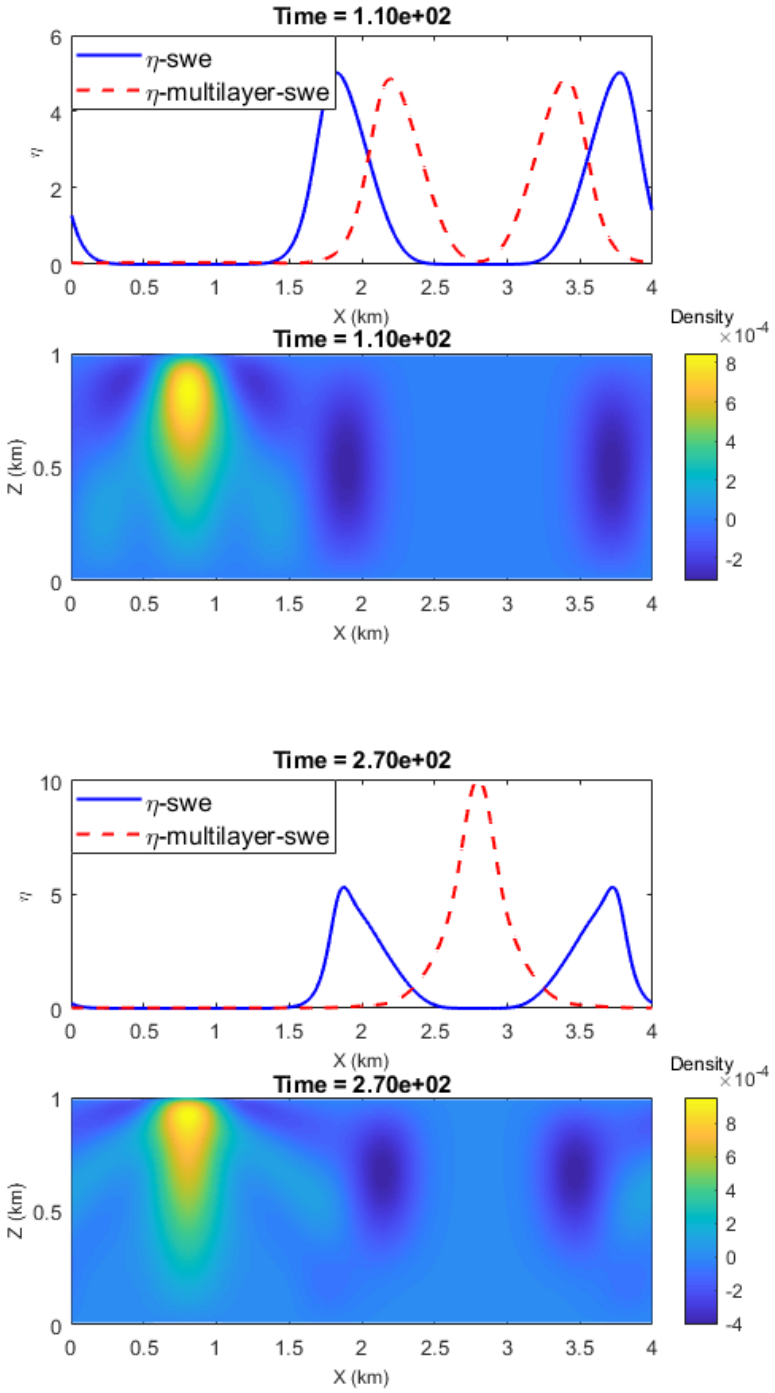

FIGURE 4.28: *Flat bottom:* Surface waves ($\eta(m)$) and Internal wave generation at $t = 245$ s and $t = 300$ s. Waves are propagating towards boundary under an angle with vertical.

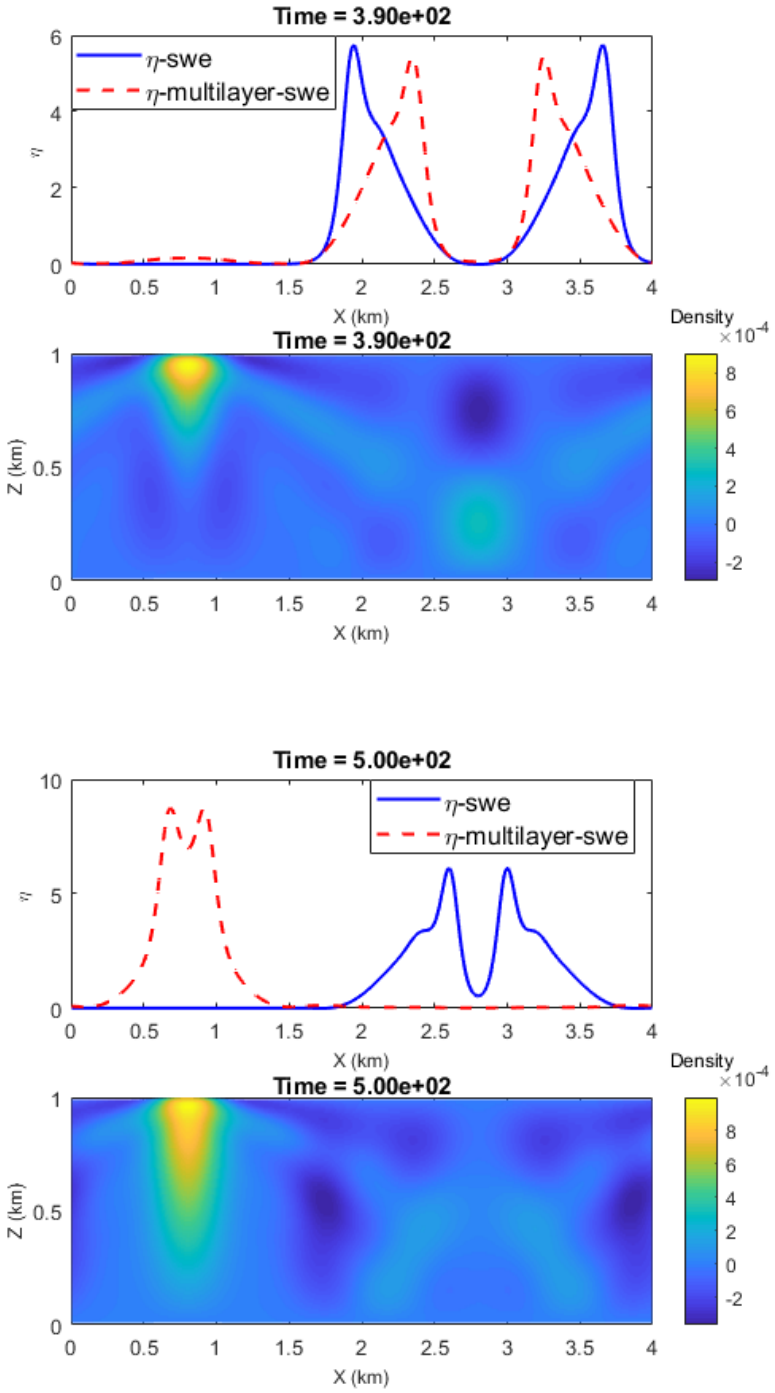

FIGURE 4.29: *Flat bottom:* Surface waves ($\eta(m)$) and Internal wave generation at $t = 365$ s and $t = 500$ s. Vertical mixing in the interior ocean has been observed.

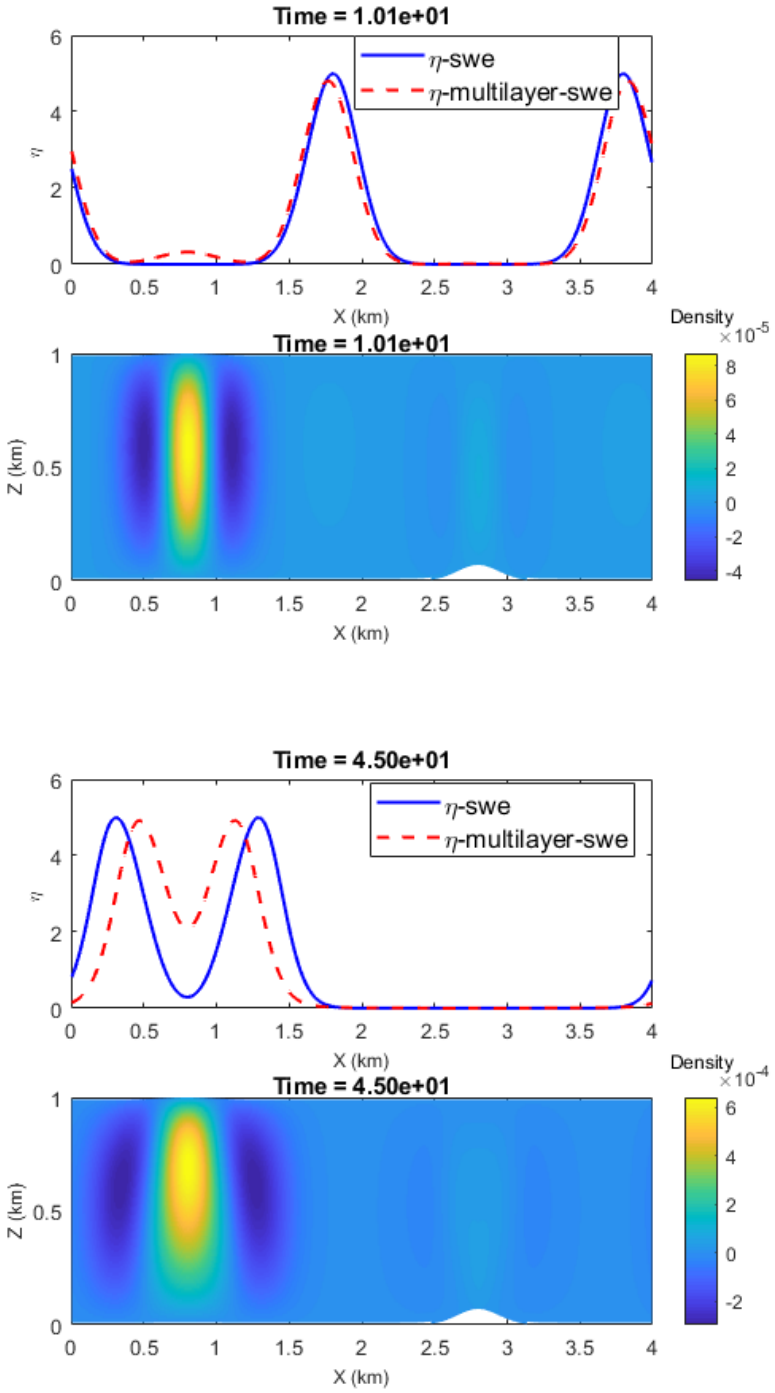

FIGURE 4.30: *Non-flat bottom:* Surface waves ($\eta(m)$) and Internal wave generation at $t = 1$ s and $t = 45$ s. Waves are propagating away from the region of disturbance as well as from topographic region.

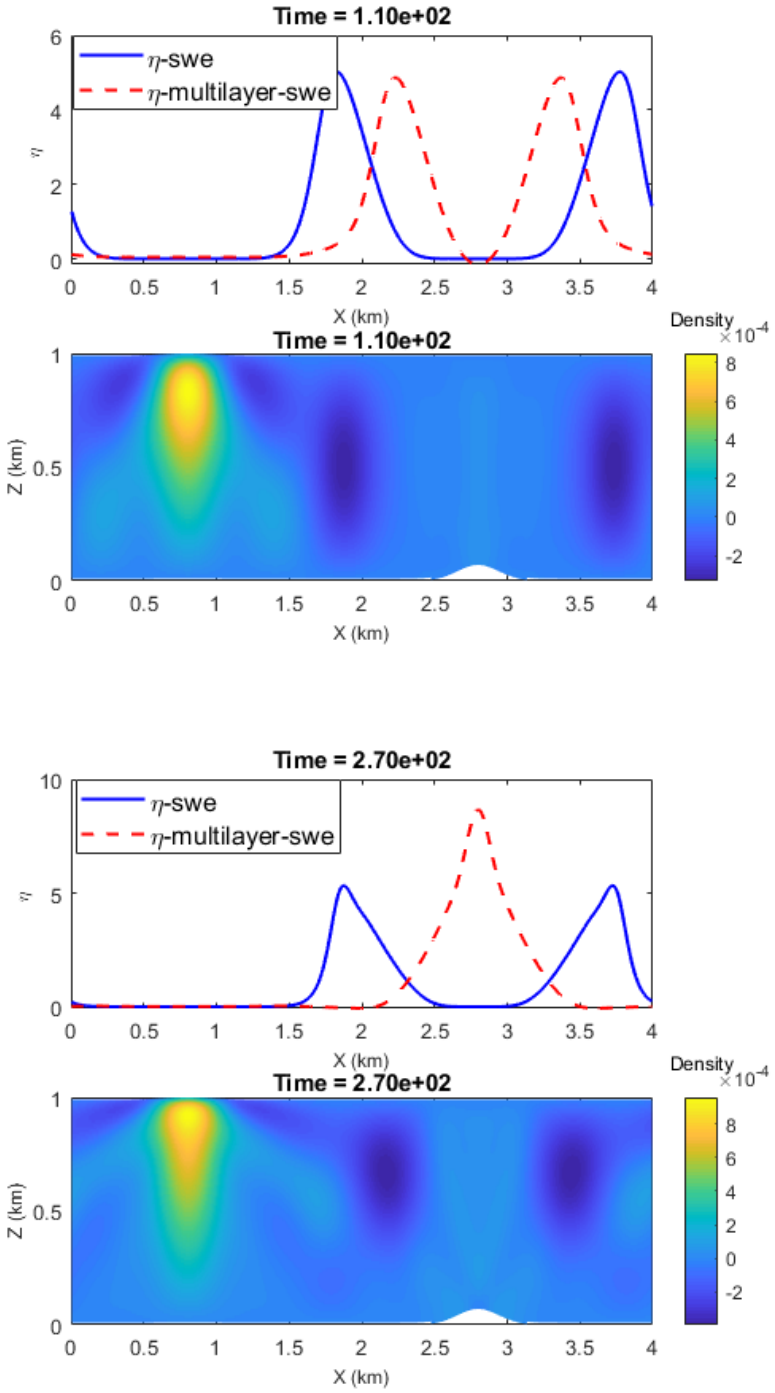

FIGURE 4.31: *Non-flat bottom:* Surface waves ($\eta(m)$) and internal waves at $t = 110$ s and $t = 270$ s. Waves that created due to the disturbance at top layer, propagates towards boundary and merge with the waves propagating away from the topographic region.

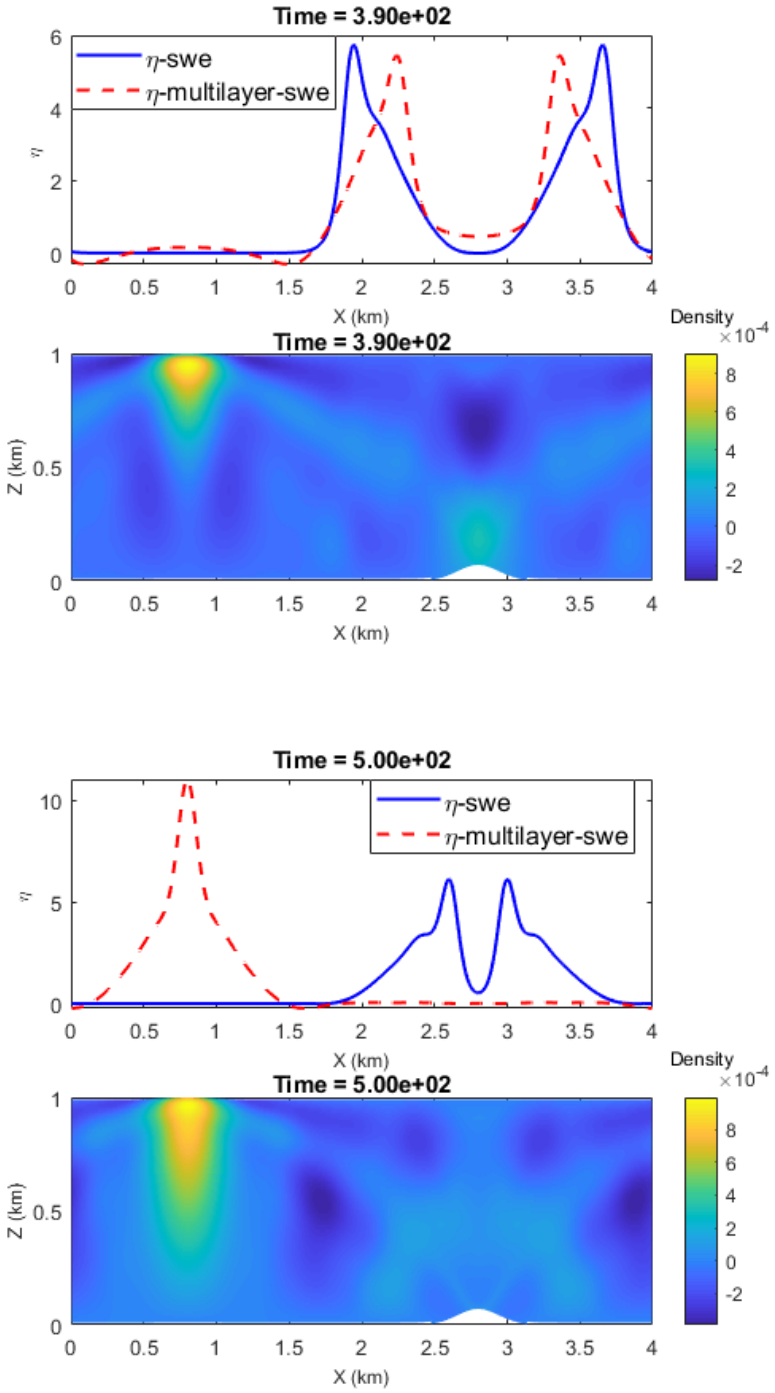

FIGURE 4.32: *Non-flat bottom:* Surface waves ($\eta(m)$) and Internal wave generation at $t = 390$ s and $t = 500$ s. Waves are propagating back and forth and vertical mixing of density has been observed.

4.3.3 Perturbation at the density interface with flat and non-flat bottom of ocean

In this test case, we consider two layer of density where the lower layer is denser than the upper layer. The density function is given by;

$$\rho = \rho_r \left(1 - \frac{\Delta\rho}{2}\left(1 - \tanh\left(\frac{-z + H/2}{0.05H}\right)\right)\right)$$

where $\Delta\rho = 0.1$ and $H = 1000$ m.

We consider the inertial mass at free surface is in rest. The goal of this numerical test case is to observe how a small perturbation of density at the interior interface of ocean generates oceanic wave. For the perturbation of density we consider the following function;

$$\rho_{perturb} = \rho_r \Delta\rho \left(\exp\left(-\left(\left(x - \frac{L_x}{2}\right)^2 + \left(z - \frac{H}{2}\right)^2\right) / (0.3H)^2\right)\right)$$

For non-flat bottom of ocean, the bottom bathymetry is defined by the following Gaussian function

$$\beta(x) = 70e^{\frac{-\frac{1}{4}(x-0.7L_x)^2}{\delta^2}}$$

Figure 4.33 shows the initial state inertial mass at free surface and initial density distribution at time $t = 0$ s.

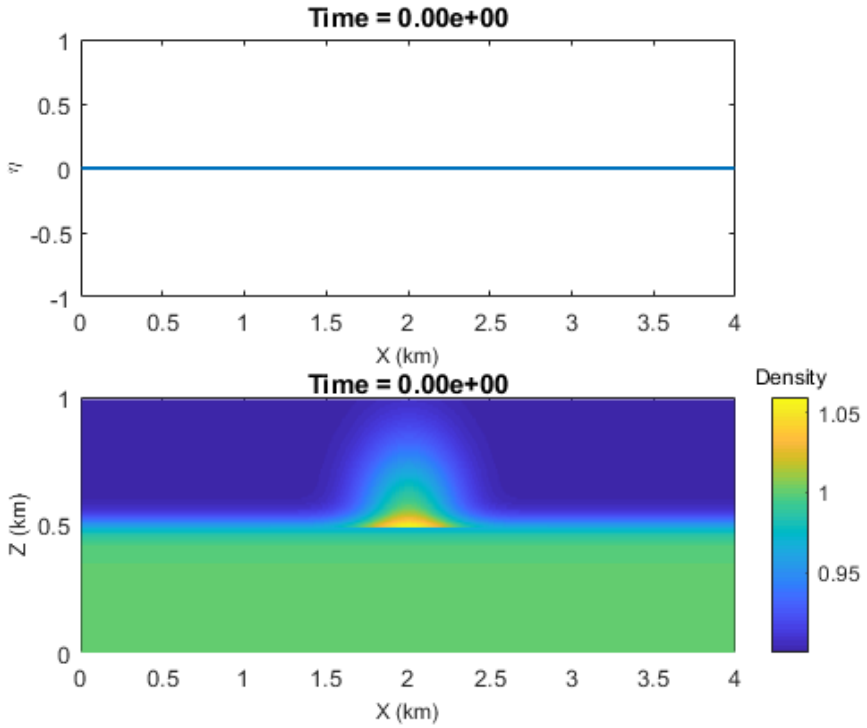

FIGURE 4.33: *Flat bottom:* Inertial mass at free surface ($\eta(m)$) and initial distribution of density with a small perturbation to the density gradients. Initially, there is no change in inertial mass at free surface.

To illustrate the results, we plot the change in inertial mass (η) as well as the perturbation in normalized density (θ) for different time. The propagation of surface waves and internal waves for flat bottom case has been plotted in figures (4.34-4.39).

The boundary conditions at left and right boundaries of our domain are set to be periodic. Internal waves are generated when energy is applied to the interface of water layers with steep density gradients. The layer don't mix and the interface remain intact. These waves propagate back and forth with time, as we see from figures. For surface wave, atmospheric wind mainly apply the triggers to lift water

from the equilibrium level of surface and then gravity pushes it downwards again and thus creates a rippling wave. While for internal wave, most of the cases, the trigger can be the propulsion of energy from a ship or could be due to tidal motions. Internal waves are much larger than the surface waves, because the density differences between two layers is much smaller than that between air and water. So less energy is required to displace the interface from it's equilibrium position and oscillation is more easily set up at the internal interface than that at the surface. On the other hand, the wave at the surface become rougher when the internal wave dropped down. And when it rebounded up, the surface water form a smooth slick [28]. Some particular snapshot after 20 periods of forcing is sufficient to visualize all these scenarios, as presented in figures (4.34-4.39).

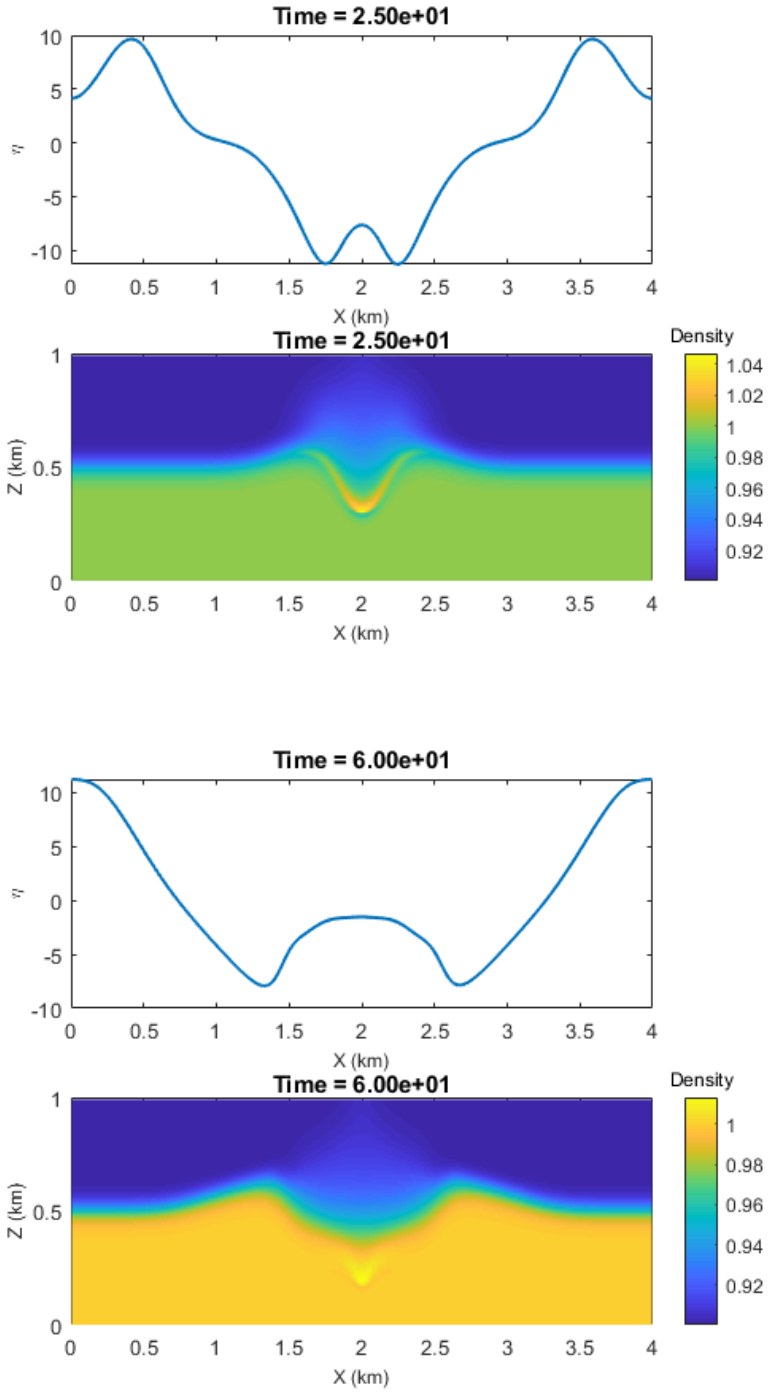

FIGURE 4.34: *Flat bottom:* Change in inertial mass at free surface ($\eta(m)$) and propagation of internal wave at the interior ocean at $t = 25$ s and $t = 60$ s.

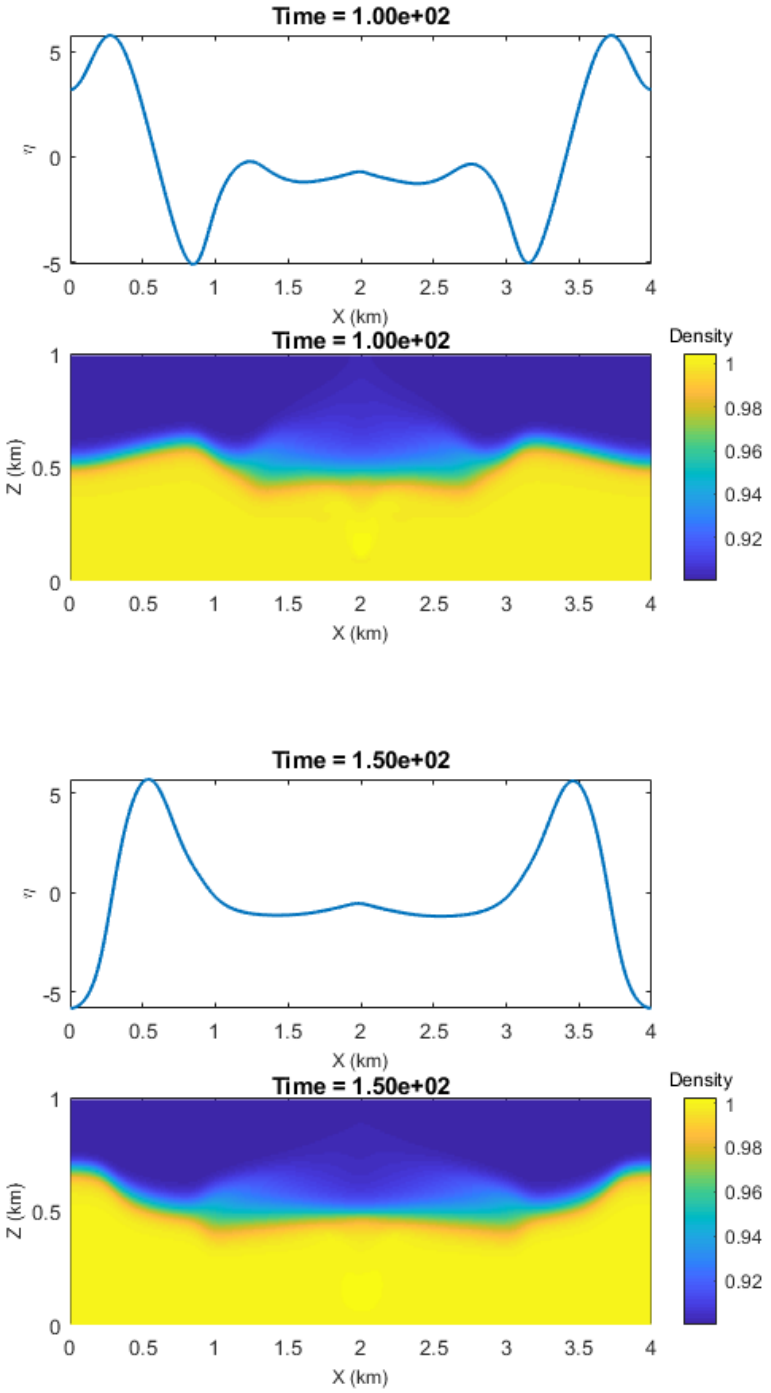

FIGURE 4.35: *Flat bottom:* Change in inertial mass at free surface ($\eta(m)$) and propagation of internal wave at the interior ocean at $t = 100$ s and $t = 150$ s.

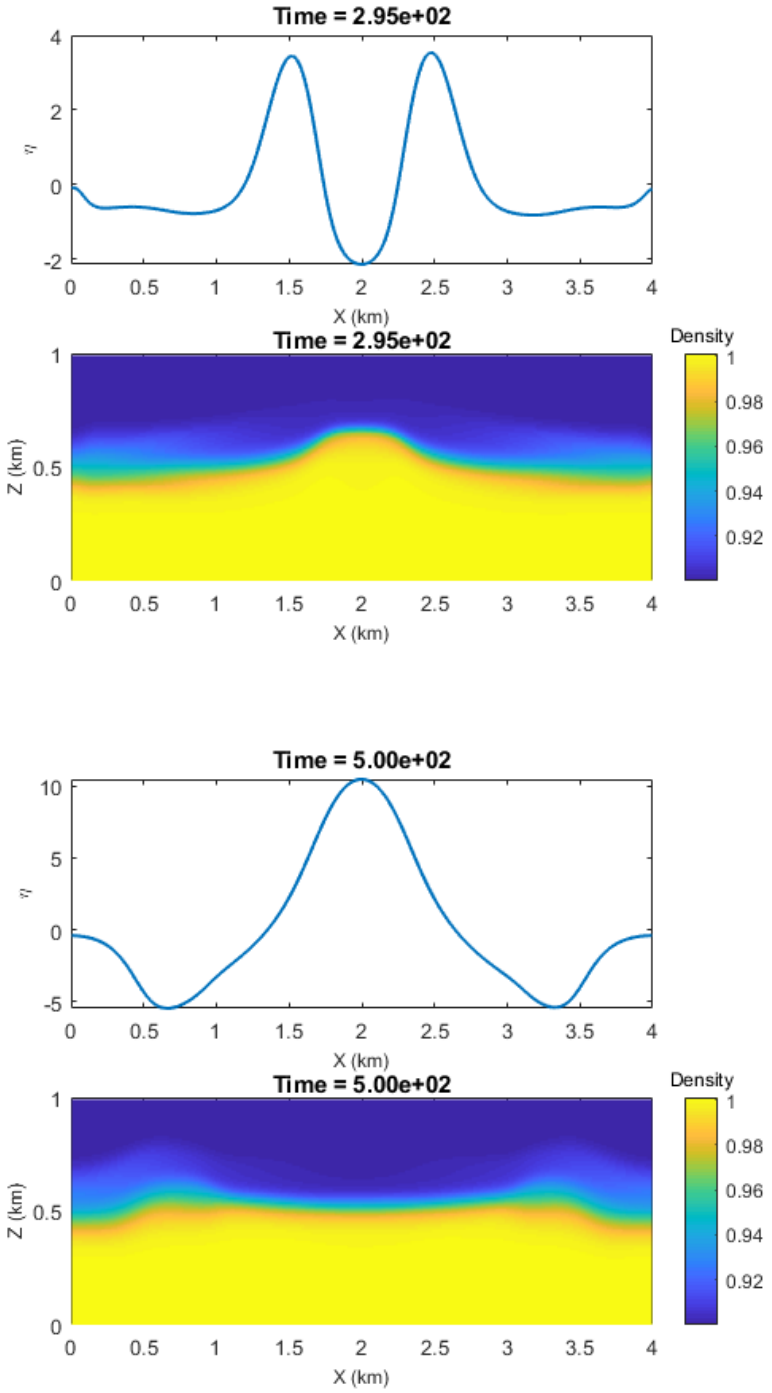

FIGURE 4.36: *Flat bottom:* Change in inertial mass at free surface ($\eta(m)$) and propagation of internal wave at the interior ocean at $t = 295$ s and $t = 500$ s.

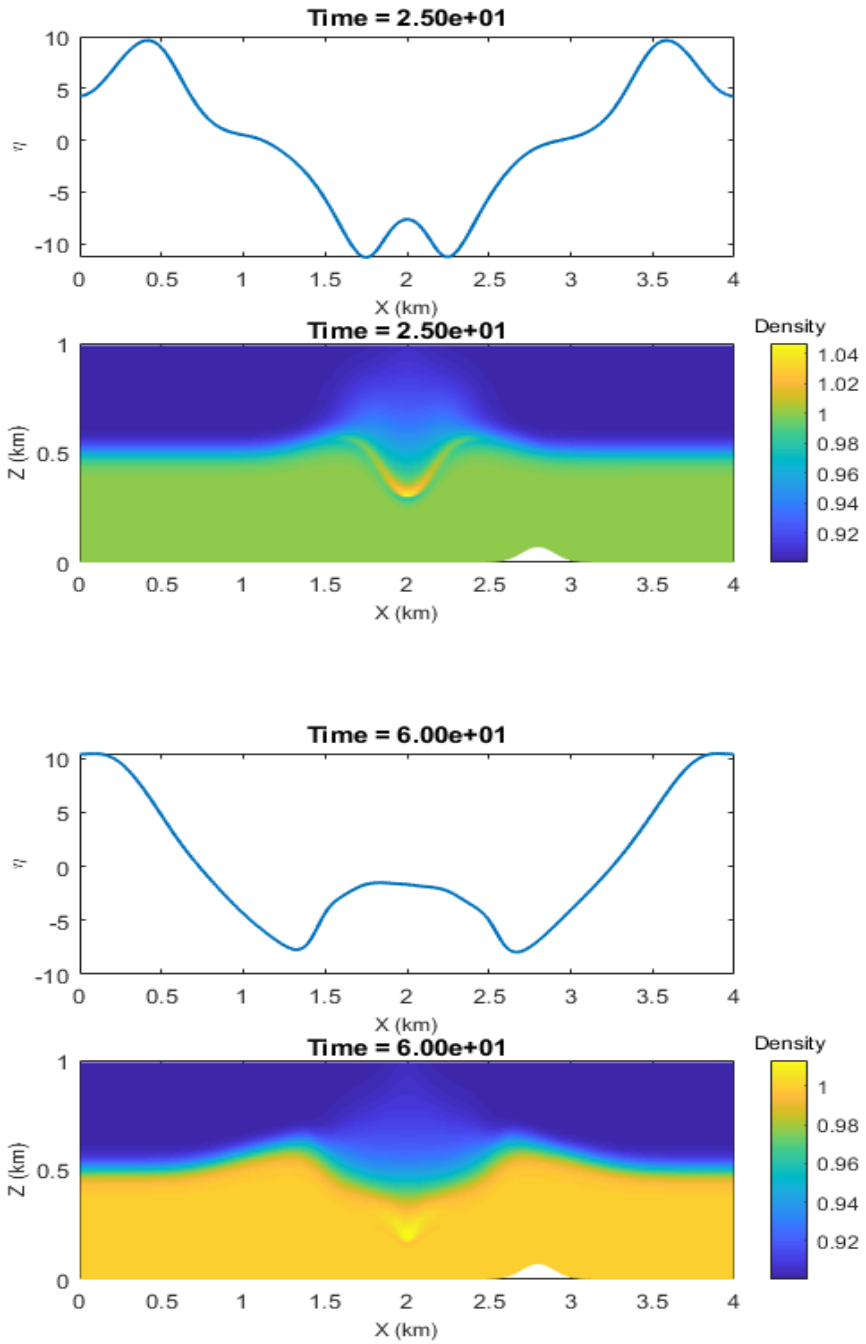

FIGURE 4.37: *Non-flat bottom:* Change in inertial mass at free surface ($\eta(m)$) and propagation of internal wave at the interior ocean at $t = 20$ s and $t = 65$ s.

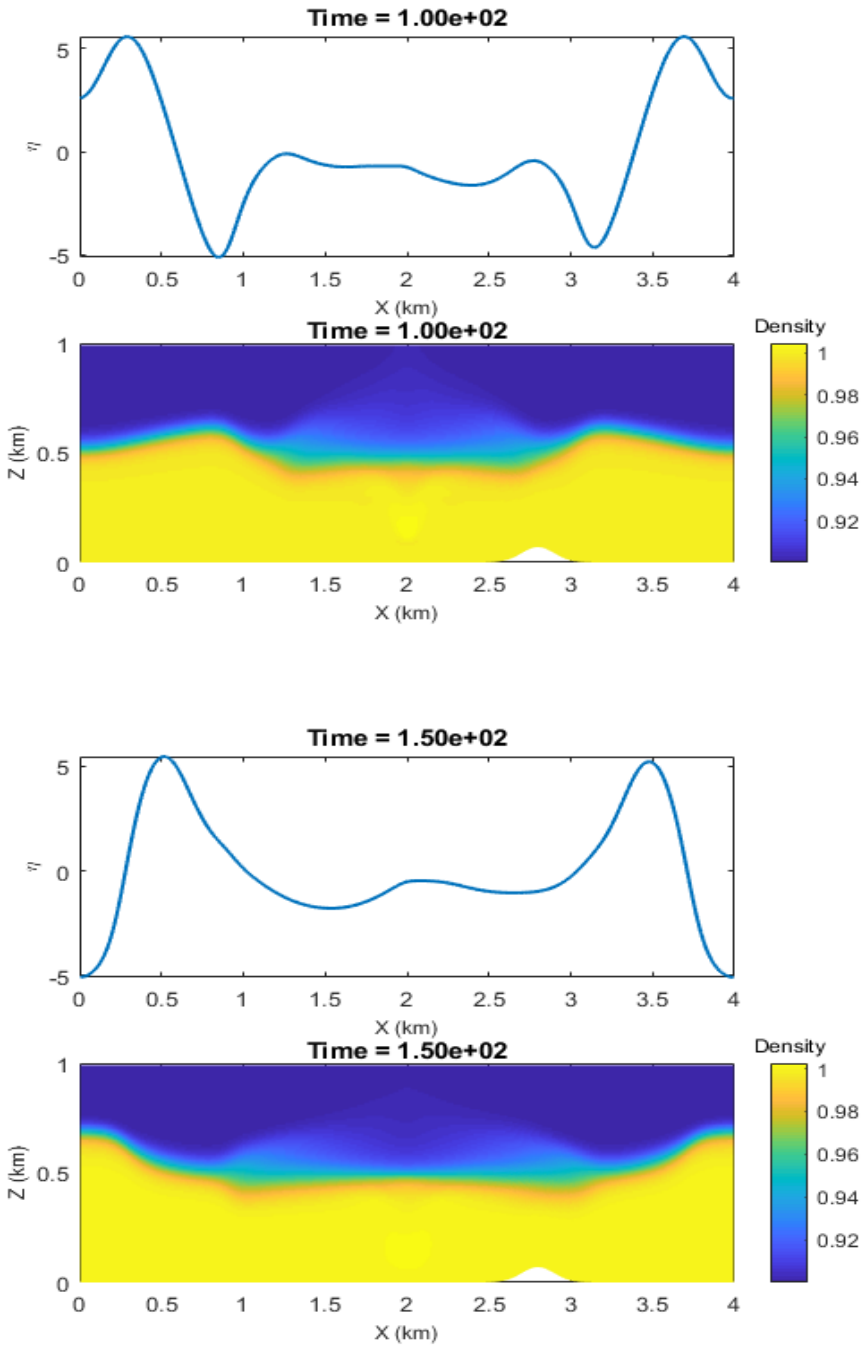

FIGURE 4.38: *Non-flat bottom:* Change in inertial mass at free surface ($\eta(m)$) and propagation of internal wave at the interior ocean at $t = 105$ s and $t = 205$ s.

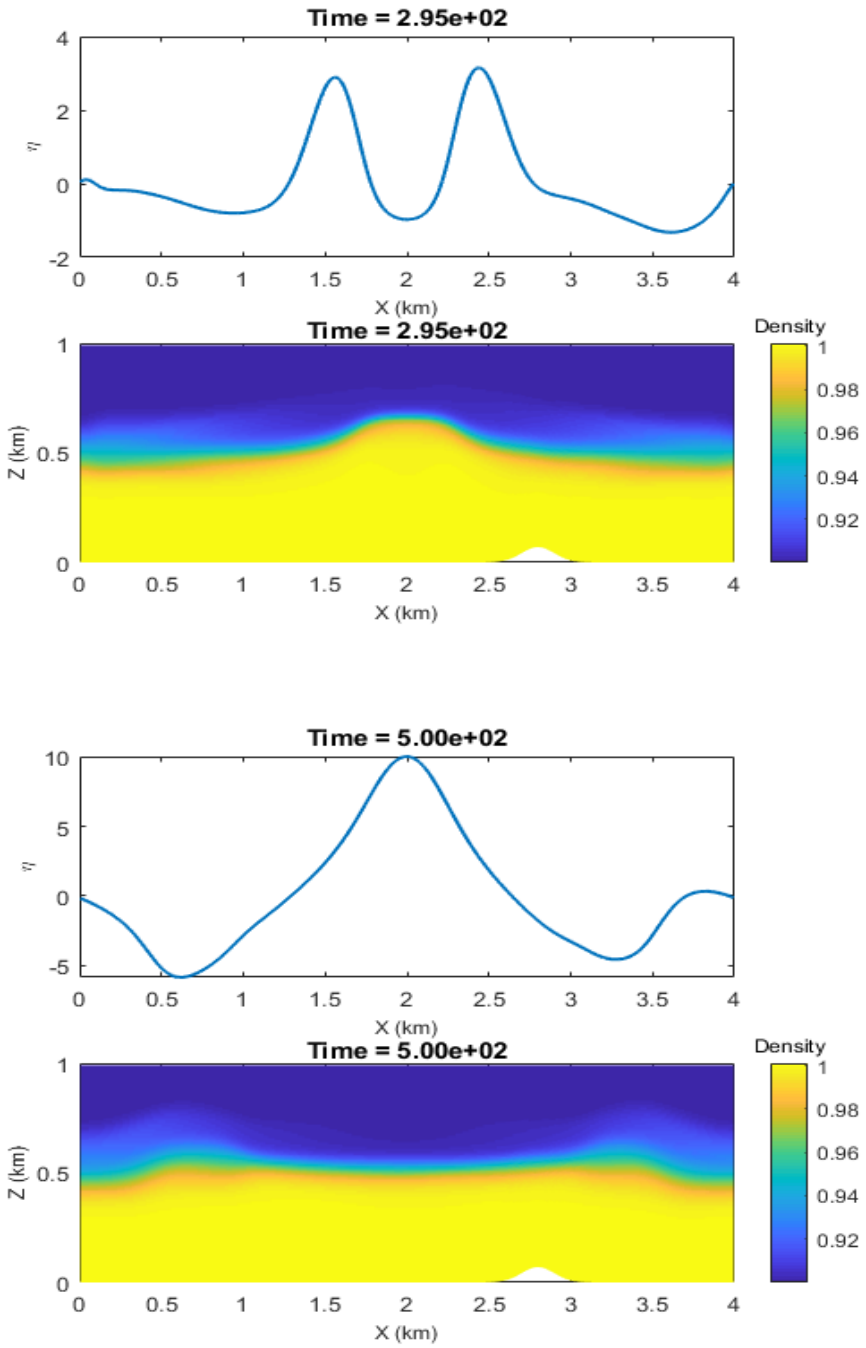

FIGURE 4.39: *Non-flat bottom:* Change in inertial mass at free surface ($\eta(m)$) and propagation of internal wave at the interior ocean at $t = 250$ s and $t = 350$ s.

Chapter 5

Conclusions and Future work

5.1 Conclusions

The ocean is stratified due to the dynamics of temperature, salinity, position and pressure. These changes in the ocean often lead to strong variation of density in the vertical direction. Consequently, the density stratification (either at an interface between ocean and atmosphere or an interface between two layers of ocean water) allows oscillation of fluid. The wave phenomena associated with these oscillation are called surface waves (i.e. waves at free surface of ocean) and internal waves (i.e. waves in the interior of ocean). Buoyancy force generates this oscillation. This study presents the dynamic and interaction between surface waves and internal waves, with and without bathymetry of ocean.

Multilayer SWE has been solved by using an explicit staggered finite volume method to understand the behavior of internal waves. In the multilayer model

we consider a stratified fluid with small density differences, consistent with the Boussinesq approximation. Boussinesq approximation for buoyancy, what we use for multilayer model is not the same as the Boussinesq approximation for surface waves. Here we include density variations in terms when multiplied by gravity. Due to the use of a Lagrangian vertical coordinate, vertical layers change from their original positions as the flow evolves. Therefore, conservative remapping is required periodically to keep the layers from collapsing or spreading too far apart.

To validate our numerical model, we compare the phase speed and the wave characteristics of multilayer surface wave with that of single layer SWE with and without density stratification. As seen in the results, without any density differences, as expected, the wave speed is the same for both models. But in the presence of density differences, surface waves for the multilayer case move slowly due to the generation of internal waves in the interior of the ocean. For 1D SWE, the steepening as seen in the results, is just the usual nonlinear wave steepening. Moreover, 2-D multilayer model shows the expected nonlinear wave steepening in the presence of bathymetry. In addition, the numerical analysis of the barotropic and baroclinic mode for linearized two-layer SWE confirms that the phase speed of barotropic mode is faster than baroclinic mode.

The interaction between internal waves and surface waves have been investigated in a series of numerical experiments. It shows that, free surface waves perturb the density isopycnals and that generates mixed layers in the interior of the flow. The adjustment to gravitational equilibrium then generates internal waves. During this adjustment process, internal waves are generated and emitted. Apart from this, when fluid flows over bathymetry, a vertical components of wave

arise and it oscillates at a frequency as like as the horizontal component of wave. This vertical component of wave brings isopycnal surfaces into oscillation and thus propagate energy both in horizontally and vertically. Moreover, surface waves are created in the zone where density changes very sharply between air and water and restricted their movement and energy propagation just in the surface. On the contrary, internal waves are formed at density gradients in the interior ocean, which is smoothly stratified over the vertical and thus transports energy from one depth level to the other.

Surface waves and internal waves are definitely an interesting topic to study. Beside them, there are many types of ocean waves and they can all co-exist with different wave speeds and wavelengths. In addition, they can also influence and affect each other. Internal wave dynamics, and their interaction with wind-driven surface waves, are an essential part of ocean climate models.

5.2 Future work

A brief sketch of possible future work is given below:

1. Extend multilayer incompressible SWE to three dimensions on the sphere. This project will develop an ocean version of the dynamically adaptive climate model being developed by Dubos and Kevlahan and will build on earlier work by Aechtner et al (2015) for the 2-D SWE.

2. In the present study, we used a sigma-type Lagrangian vertical coordinate which doesn't allow mass to flow across the vertical layer. In the future work, we will investigate and compare with a mass-based coordinate system which explicitly includes a vertical velocity.

3. For the vertical discretization, we used sigma type $(\sigma - z)$ coordinate systems. Apart from this, we can also consider other vertical coordinate system such as isopycnal coordinates.

4. For ocean's bathymetry, we assumed that $\beta(x)$ depends on horizontal position x only. We could also include dynamic bathymetry, as occurs in earthquakes, by allowing β to be a function of both x and t.

Bibliography

[1] Stephen M. Griffies. *Fundamentals of ocean climate models*. Princeton University Press, Princeton, USA, 2004.

[2] Couderc et al. An explicit asymptotic preserving low Froude scheme for the multilayer shallow water model with density stratification. *Journal of Computational Physics* 343 (2017), 235–270.

[3] Shiue et al. Boundary value problems for the shallow water equations with topography. *Journal of Geophysical Research* 116 (2011), CO2015.

[4] Andreas Bollermann et al. A well-balanced reconstruction of wet/dry fronts for the shallow water equations. *Journal of Scientific Computing* 198 (2013), 3723–3750.

[5] I. K. Nikolos and A. I. Delis. An unstructured node-centered finite volume scheme for shallow water flows with wet/dry fronts over complex topography. *Computer Methods in Applied Mechanics and Engineering* 343 (2009), 235–270.

[6] J. Burguete et al. Friction term discretization and limitation to preserve stability and conservation in the 1d shallow-water model: Application to unsteady irrigation and river flow. *International Journal for Numerical Methods in Fluids* 58 (2008), 403–425.

[7] L. Cea and M. E. Vázquez-Cendón. Unstructured finite volume discretization of bed friction and convective flux in solute transport models linked to the shallow water equations. *Journal of Computational Physics* 231 (2012), 3317–3339.

[8] Yulong Xing and Xiangxiong Zhang. Positivity-Preserving Well-Balanced Discontinuous Galerkin Methods for the Shallow Water Equations on Unstructured Tria ngular Meshes. *Journal of Scientific Computing* 57(1) (2013), 19–41.

[9] Audusse et al. A fast and stable well-balanced scheme with hydrostatic reconstruction for shallow water flows. *SIAM Journal of Scientific Computing* 25 (2004), 2050–2065.

[10] N. Kevlahan and T. Dubos. A conservative adaptive wavelet method for the shallow-water equations on staggered grids. *Quarterly Journal of the Royal Meteorological Society* 139 (2013), 1997–2020.

[11] N. Kevlahan et al. A conservative adaptive wavelet method for the shallow-water equations on the sphere. *Quarterly Journal of the Royal Meteorological Society* 140(690) (2015), 1712–1726.

[12] Manuel Castro et al. A Q-scheme for a class of systems of coupled conservation laws with source term. Application to a two-layer 1-D shallow water

system. *Mathematical Modelling and Numerical Analysis* 35(1) (2001), 107–127.

[13] Rémi Abgrall and Smadar Karni. Two-layer shallow water system: a relaxation approach. *SIAM Journal on Scientific Computing* 31(3) (2009), 1603–1627.

[14] A. Kurganov and G. Petrova. Central-Upwind Schemes for Two-Layer Shallow Water Equations. *SIAM Journal on Scientific Computing* 31(3) (2009), 1742–1773.

[15] Kyle T Mandli. A numerical method for the two layer shallow water equations with dry states. *Ocean Modelling* 72 (2013), 80–91.

[16] Audusse et al. Approximation of the hydrostatic Navier–Stokes system for density stratified flows by a multilayer model: Kinetic interpretation and numerical solution. *Journal of Computational Physics* 230(9) (2011), 3453–3478.

[17] Emmanuel Audusse et al. A fast finite volume solver for multi-layered shallow water flows with mass exchange. *Journal of Computational Physics* 272 (2014), 23–45.

[18] François Bouchut and Vladimir Zeitlin. A robust well-balanced scheme for multi-layer shallow water equations. *American Institute of Mathematical Sciences* 13(4) (2010), 739–758.

[19] M. Parisot and JP Vila. Numerical scheme for multilayer shallow-water model in the low-Froude number regime. 352(11) (2014), 953–957.

[20] AL Stewart and PJ Dellar. Multilayer shallow water equations with complete Coriolis force. Part I. Derivation on a non-traditional beta-plane. *Journal of Fluid Mechanics* 651 (2010), 387–413.

[21] Dubos et al. DYNAMICO-1.0, an icosahedral hydrostatic dynamical core designed for consistency and versatility. *Geoscientific Model Development* 8 (2015), 3131–3150.

[22] Phillips N. The general circulation of the atmosphere: A numerical experiment. *Quarterly Journal of the Royal Meteorological Society* 82(352) (1956), 123–164.

[23] Smagorinsky J. General circulation experiments with the primitive equations: I. The basic experiment. *Quarterly Journal of the Royal Meteorological Society* 91 (1963), 99–164.

[24] Kasahara A. Various vertical coordinate systems used for numerical weather prediction. *Mon. Wea. Rev.* 102 (1974), 509–522.

[25] Juang H. A spectral fully compressible nonhydrostatic mesoscale model in hydrostatic sigma coordinates: Formulation and preliminary results. *Meteorology and Atmospheric Physics* 50(1) (1974), 75–88.

[26] Starr and V.P. *A quasi-Lagrangian system of hydrodynamical equations.* 2. 1945, 227–237.

[27] S. J. and Lin. A vertically Lagrangian finite-volume dynamical core for global models. *Mon. Wea. Rev.* 132 (2004), 2293–2307.

[28] https://www.whoi.edu/oceanus/feature/the-waves-within-the-waves.

[29] https://en.wikipedia.org/wiki/Internal_wave.

[30] G. Whitham. *Linear and Nonlinear Waves*. Wiley-Interscience, New York, 1974.

[31] M.J. Boussinesq. Linear solution to the problem of the propagation of the solitary wave to through a permeable submerged structure. *C.R. Acad. Sci. Paris* 72 (1871), 755–9.

[32] D.H. Peregrine. Long waves on a beach. *J. Fluid Mech.* 27 (1967), 815–27.

[33] S. Beji and K. Nadaoka. A formal derivation and numerical modelling of the improved Boussinesq equations for varying depth. *Ocean Engineering* 32(8) (1996), 691–704.

[34] P.A. Madsen and O.R. Sorensen. A new form of the Boussinesq equations with improved linear dispersion characteristics. Part 2. A slowly varying bathymetry. *Coastal Engineering* 18 (1992), 183–204.

[35] M.A. Walkley. A Numerical Method for Extended Boussinesq Shallow-Water Wave Equations (1999).

[36] J. T. Kirby. Boussinesq models and applications to nearshore wave propagation, surfzone processes and wave-induced currents. *in Advances in Coastal Modeling* (2003), 1–41.

[37] S. Vitousek and O. B. Fringer. Physical vs. numerical dispersion in nonhydrostatic ocean modeling. *Ocean Modelling* 40(1) (2011), 72–86.

[38] L. Dongfang et al. Comparison between boussinesq and shallow-water models in predicting solitary wave runup on plane beaches. *Coastal Engineering* 18 (1992), 183–204.

[39] Wang et al. *Nat Hazards*. https://doi.org/10.1007/s11069-016-2317-x.. 2016.

[40] Anna von der Heydt. *Rossby and Kelvin waves*. Institute for Marine and Atmospheric research Utrecht Utrecht University, Utrecht, The Netherlands, 2016.

[41] http://oceanservice.noaa.gov/facts/rossby-wave.html.

[42] A. V. Fedorov and J. N. *EQUATORIAL WAVES Yale University*. New Haven, CT, USA.

[43] https://earthobservatory.nasa.gov/IOTD/view.php?id=87519.

[44] https://ceprofs.civil.tamu.edu/kchang/ocen689/ocen689ch10.pdf.

[45] Harry Putu Gunawan. Numerical simulation of shallow water equations and related models. *General Mathematics* ().

[46] http://snowball.millersville.edu/~adecaria/ESCI343/esci343_lesson07_two_layer_gravity_waves.pdf.

[47] https://ocw.mit.edu/courses/mechanical-engineering/2-062j-wave-propagation-spring-2017/lecture-notes/MIT2_062J_S17_Chap7.pdf.